PROPERTIES OF SUPERCONDUCTING CU-RICH COMPOSITES CONTAINING V_3SI OR V_3GA

Thesis by

Wilkie Yung-Kee Chen

In Partial Fulfillment of the Requirements

for the Degree of

Doctor of Philosophy

California Institute of Technology

Pasadena, California

1975

(Submitted June 24, 1974)

To Mei and My Parents

ACKNOWLEDGMENTS

The author wishes to express his deepest gratitude to Dr. C. C. Tsuei and Professor Pol Duwez for their constant advice and encouragement extended throughout this work. He is also indebted to S. Kotake, J. Wysocki, C. Geremia, F. Youngkin, and K. Evans (of the Jet Propulsion Laboratory) for their technical assistance; to H. So, K. Karasek, and M. Yung for their help in the measurements of electrical resistivities and critical current densities. He owes his special thanks to H. So, who delivered most of the help and assisted in developing the computer software connected with this study. The author is also thankful to Mrs. Angela Bressan for typing the rough draft, to J. Wysocki for proof reading of the text, and to Mrs. Roberta Duffy for the final typing of the thesis.

Financial support was gratefully received from the U. S. Atomic Energy Commission.

To his wife, Mei-yu, and his parents for their continuing encouragement throughout the course of the work, the author wishes to acknowledge his sincere appreciation.

ABSTRACT

Superconducting Cu-rich composites containing the A-15 compounds V_3Si or V_3Ga have been made by the "Tsuei" process, which consists of melting the constituent elements into ingots followed by subsequent cold working and heat treatment. The superconducting transition temperatures of the resulting composites have been measured. X-ray diffraction analyses have been performed to identify the phases in the alloys. The microstructures have been studied using both the optical metallograph and the scanning electron-microscope. For some composites containing V_3Ga, the critical current densities as functions of transverse magnetic field up to 60 kG, and as functions of temperature from 4.2°K to 12°K have been measured. It was found that the Tsuei process does not work for the composites containing V_3Si, but works satisfactorily for the composites containing V_3Ga. The reasons are discussed based on the results of microstructure studies, electrical resistivity measurements, and also the relevant binary phase diagrams. The relations between the measured properties and the various metallurgical factors such as the alloy compositions, the cross-section reduction ratios of the materials, and the heat treatment are discussed. The basic mechanism for the observed superconductivity in the materials is also discussed. In addition, it was found that the Tsuei composites are expected to have high inherent magneto-thermal stability based on the stability theory of superconducting composites.

TABLE OF CONTENTS

section		page
I.	INTRODUCTION	1
II.	EXPERIMENTAL PROCEDURES	3
	A. Preparation of Alloys	3
	B. Preparation of Composites	3
	C. Heat Treatment	6
	D. X-Ray Diffraction	7
	E. Electrical Resistivity	7
	F. Critical Current Measurements	10
	G. Metallographic Studies	18
	H. Magnetization	19
III.	EXPERIMENTAL RESULTS	21
	A. Electrical Resistivity and Superconducting Transition Temperature Measurements	21
	1. Cu-V-Si Specimens	21
	1.1 Alloys containing 8 at. % and 10 at. % of V_3Si	21
	1.2 Alloys containing 15 at. % and 17.5 at. % of V_3Si	28
	1.3 Alloys containing 20 at. % of V_3Si	33
	1.4 Alloys with other compositions	38
	2. Cu-V-Ga Specimens	40
	2.1 Alloys containing 5 at. % vanadium	40
	2.2 Alloys containing 8 at. % vanadium	40
	2.3 Alloys containing 10 at. % vanadium	46
	2.4 Alloys containing 15 at. % and 20 at. % vanadium	54
	B. X-Ray Diffraction	59
	1. Cu-V-Si Alloys	59
	2. Cu-V-Ga Alloys	62
	C. Metallographic Studies	64
	1. Cu-V-Si Alloys	64
	2. Cu-V-Ga Alloys	68

section		page
	D. Critical Current Density Measurements	88
	1. Critical Current Densities at Zero Field and Liquid Helium Temperature	88
	2. Critical Current Densities at Liquid Helium Temperature between 0 and 60 kG	96
	3. Critical Current Densities as a Function of Temperature	97
	E. Magnetization Measurements	106
IV.	DISCUSSION	109
	A. The Cu-V-Si Alloys	109
	1. Phases Present in the Alloys	109
	2. Superconducting Transitions in $Cu_{80}(V_3Si)_{20}$ Specimens	114
	3. Optimum Conditions for Heat Treatment	114
	B. The Cu-V-Ga Alloys	118
	1. Phases Present in the Alloys	118
	2. The Role of the Cu-Phase in the V_3Ga Formation Process	122
	3. Optimum Composition and Optimum Heat Treatment	124
	C. Effect of Discontinuity in the Superconducting Filaments	130
	D. Critical Current Densities	133
	1. Review of Relevant Theories	133
	2. Stability of Cu-V-Ga Composites	140
	3. Optimum Composition and Heat Treatment	143
	E. Suggestions for Further Studies	146
	1. Ternary Phase Diagrams	146
	2. Optimum Fabrication Procedures	146
	3. Further Studies of Critical Current Densities	147
	4. Effect of Additional Elements	147
	5. Studies of AC Properties	147
	6. Other Studies	148

section	page
V. SUMMARY AND CONCLUSIONS	149
References	153

I. INTRODUCTION

Intermetallic A-15 "β-tungsten" compounds such as Nb_3Sn, V_3Ga, V_3Si, and the recently obtained Nb_3Ge are superconductors with the highest superconducting transition temperatures and critical fields among all superconducting materials known by far. Thus, these materials are expected to be most useful for engineering applications such as magnets, power transmission lines, motors, and generators. But these materials are accompanied with the common property - brittleness, thus making the fabrication of these materials into usable form, for example wires, very difficult.

At present, several methods for fabricating superconducting composites containing A-15 compounds have been developed; among these are surface diffusion process[1, 4, 5], vapor deposition process[2], and composite process[3, 6-8]. These processes are complex and costly; thus, their commercial usefulness is limited. Also, it is difficult to achieve optimum conductor configuration in these composites.

A new kind of process for fabricating ductile superconducting composites containing elements such as Nb has been proposed by Tsuei[9]. The process consists of first casting a ductile matrix metal such as Cu with the superconducting element into ingots. Due to the small solubility of Nb in Cu, the added Nb appears as precipitates of an average size of a few microns[11]. Subsequent drawing of these ingots into wires elongates these Nb precipitates into filaments, the size of which depends on the degree of drawing. These wires have been found to be superconducting with transition temperatures close to that of Nb, and reasonably high critical current densities.

It has been found that by melting appropriate amounts of Sn with Nb in Cu, then fabricating the ingot into wires, and then applying suitable heat treatment, these wires can have superconducting transition temperatures as high as 16°K, indicating the formation of Nb_3Sn in the Cu matrix[9]. This new process is expected to be applicable in fabricating composites containing other β-W compounds.

Since V_3Ga has higher critical current density than Nb_3Sn at fields above 100 kG[7], and thus seems to be the better candidate for generating magnetic fields above this strength, investigations have been made to find out if V_3Ga filaments can be formed in a Cu matrix by a similar process. Furthermore, it is desirable to study some of the superconducting properties of the resulting composite, for instance, the transition temperature, the critical field, and the critical current density, etc., in order to determine the applicational value of the new material. Meanwhile, since V_3Si is also a good A-15 superconducting compound, it is also desirable to explore the possibility of applying the process to V_3Si - Cu composites.

The present study involves preparation of composites containing both V_3Si - Cu and V_3Ga - Cu, measurements of superconducting properties including transition temperature, critical current density as a function of temperature and transverse magnetic field, x-ray analysis and identification of phases, microstructure studies using both optical and scanning electron microscopes, magnetization measurements, and some analysis of parameters based on existing theory on superconducting composites.

II. EXPERIMENTAL PROCEDURES

A. Preparation of Alloys

Two classes of alloys have been studied. Their compositions are of the form $Cu_{100-x-y}V_xSi_y$ and $Cu_{100-x-y}V_xGa_y$, where x and y fall in appropriate ranges. Values for x and y for these two classes of alloys which have been studied are given in Tables 1 and 2, respectively. The purities of the various elements used for preparing these alloys are: 99.99% pure Cu, 99.99999% pure Ga, 99.999% pure Si, 99.5% pure V. Some alloys are prepared with slight amounts of impurity, such as Al (99.99% pure) or P (99.9% pure) added.

Because of the high melting point of V (1900°C) which is present in alloys studied, the silver-boat technique[12] has been used for making all the alloy ingots. Appropriate quantities of constituent elements were melted by induction melting in an argon atmosphere on a silver boat cooled by running water. The temperature reached is estimated to be near 2000°C. The melting processes were repeated several times, and then the ingots, averaging 3 grams in weight, were cooled at a rate of about 100°C/sec. Extra amounts of the more volatile element such as Cu were added to compensate for the loss during the melting process in order to ensure that the compositions were close to the nominal one.

B. Preparation of Composites

The as-cast ingots obtained by the induction melting process described above were then cold-worked into various forms. First, they were rolled with a Stanat Model CX 100 Rolling Mill into rods of cross section of about 1 mm × 1 mm. Some specimens were further

TABLE 1. Composition $Cu_{100-x-y}V_xSi_y$ of Alloys Studied.

x	y	Composition[63]
3.75	1.25	$Cu_{95}(V_3Si)_5$
6	2	$Cu_{92}(V_3Si)_8$
7.5	2.5	$Cu_{90}(V_3Si)_{10}$
11.25	3.75	$Cu_{85}(V_3Si)_{15}$
7.5	7.5	$Cu_{85}V_{7.5}Si_{7.5}$
13.125	4.375	$Cu_{82.5}(V_3Si)_{17.5}$
15	5	$Cu_{80}(V_3Si)_{20}$
16.875	5.625	$Cu_{77.5}(V_3Si)_{22.5}$
3.75	1.25	$Cu_{93.5}(V_3Si)_5Al_{1.5}$
7.5	2.5	$Cu_{88.5}(V_3Si)_{10}Al_{1.5}$
11.25	3.75	$Cu_{83.5}(V_3Si)_{15}Al_{1.5}$
15	5	$Cu_{78.5}(V_3Si)_{20}Al_{1.5}$
11.25	3.75	$Cu_{84.9}(V_3Si)_{15}P_{0.1}$

TABLE 2. Composition $Cu_{100-x-y}V_xGa_y$ of Alloys Studied.

x	y	Composition
5	2	$Cu_{93}V_5Ga_2$
8	10	$Cu_{82}V_8Ga_{10}$
8	12.5	$Cu_{79.5}V_8Ga_{12.5}$
10	5	$Cu_{85}V_{10}Ga_5$
10	8	$Cu_{82}V_{10}Ga_8$
10	10	$Cu_{80}V_{10}Ga_{10}$
10	12.5	$Cu_{77.5}V_{10}Ga_{12.5}$
15	10	$Cu_{75}V_{15}Ga_{10}$
20	10	$Cu_{70}V_{20}Ga_{10}$

rolled on the same rolling mill into sheets of cross section of about 0.25 mm × 3 mm. To obtain a higher degree of cold working, some specimens in rod form containing V, Ga, and Cu were sent to Sigmund Cohn Corp., which specialize in wire drawing of metals, to be made into wires of diameters of ~0.4 mm, ~0.3 mm, and ~0.13 mm.

During the rolling process, it was sometimes necessary to anneal the specimens at 400°C for about 2 days for stress relieving in order to prevent the specimens from cracking. It was found that alloys containing more than 12.5 at.% of Ga and those containing more than 7.5 at.% of Si were very difficult to cold work. They cracked easily in spite of frequent intermediate annealing.

In the early stage of the work, powder metallurgy technique was used to make alloys containing V, Si, and Cu. Fine powders of Cu and V_3Si (made by grinding V_3Si crystals) were thoroughly mixed together and then pressed into pellets of dimensions of about 0.6 cm × 0.6 cm × 2.5 cm. The pellets were then melted on the silver boat, hoping that V_3Si could stay undissociated in the melting process. The resulting ingots were then rolled into rods, and their electrical resistivities were measured. However, the result turned out to be unsuccessful, and the effort was discontinued.

C. Heat Treatment

After being fabricated into rods, sheets, or wires, specimens were cut into segments of about 3 cm in length and sealed in quartz tubes under vacuum. They were heat treated in furnaces for various lengths of time at several temperatures. For Cu-V-Si specimens, the temperatures used for annealing were 400°C, 500°C, 600°C,

700°C, 800°C, and 900°C. For Cu-V-Ga specimens, the temperatures used were 600°C, 650°C, and 800°C. The annealing time ranged from a few hours to a few days.

D. X-Ray Diffraction

The Debye-Scherrer method[13] was used to identify the alloy structure and sometimes to determine the lattice parameters of the phases. The specimens were filed into powders and passed through a 325-mesh screen, then loaded into thin-walled quartz capillaries of 0.3 mm or 0.5 mm diameter. The capillaries were then mounted on the rotating specimen holder of a 114.6 mm diameter Debye-Scherrer camera. Care was taken in centering the specimen capillary in the incoming x-ray beam. Typical exposure time was about 4 to 6 hours at 45 kV and 20 ma with Ni filtered Cu $K\alpha$ radiation. In general, between 12 to 18 diffraction lines were visible on the film. Each line was then identified to determine the lattice structure, and thus the phase, which gave rise to the observed diffraction. Lattice parameters were corrected for film shrinkage, camera radius error, and specimen centering error by extrapolating against the Nelson-Riley function.

E. Electrical Resistivity

A standard four-probe method was used to measure the electrical resistivities of specimens. Specimens in rod form were etched in dilute nitric acid to reduce the cross section to about 0.5 mm × 0.5 mm. Specimens in sheet form were cut to cross sections of about 0.25 mm × 1 mm. All specimens were then cut to a length of about 3 cm, and two potential leads were attached to the speci-

mens by spot welding. The distance between the two potential leads was about 1 cm. The two ends of the specimens served as current leads.

The superconducting transition temperature (T_c) for a specimen was determined from the measured electrical resistivity as a function of temperature between 4.2°K and 25°K. The criterion for superconductivity was that the potential drop across the two potential leads of a specimen was less than 0.01 μV at a current of 0.1 A. This corresponds to an upper bound electrical resistivity of the order of 10^{-11} Ω cm.

Due to the large number of specimens that require electrical resistivity measurements, an automatic data acquisition system has been assembled to handle the large number of measurements. As shown in Figure 1, the data acquisition system consists of a micro-processor which will be described later, a relay array, an ASR-33 teletype, and a digital voltmeter. The relay array, which is controlled by the micro-processor through one of its four output ports (one port consists of four bits of binary data), is used for analog channel selection. The selected analog signal, which is either the DC potential drop across the two potential leads of one of the three specimens or the DC potential delivered by the temperature sensor, is sent to the digital voltmeter, which digitizes the analog signal into parallel BCD data, which are then fed back to the micro-processor which then encodes the BCD data into ASCII characters and transmits them serially to the teletype unit where data are recorded on punched paper tapes.

The micro-processor consists of an Intel-4004 Central Proc-

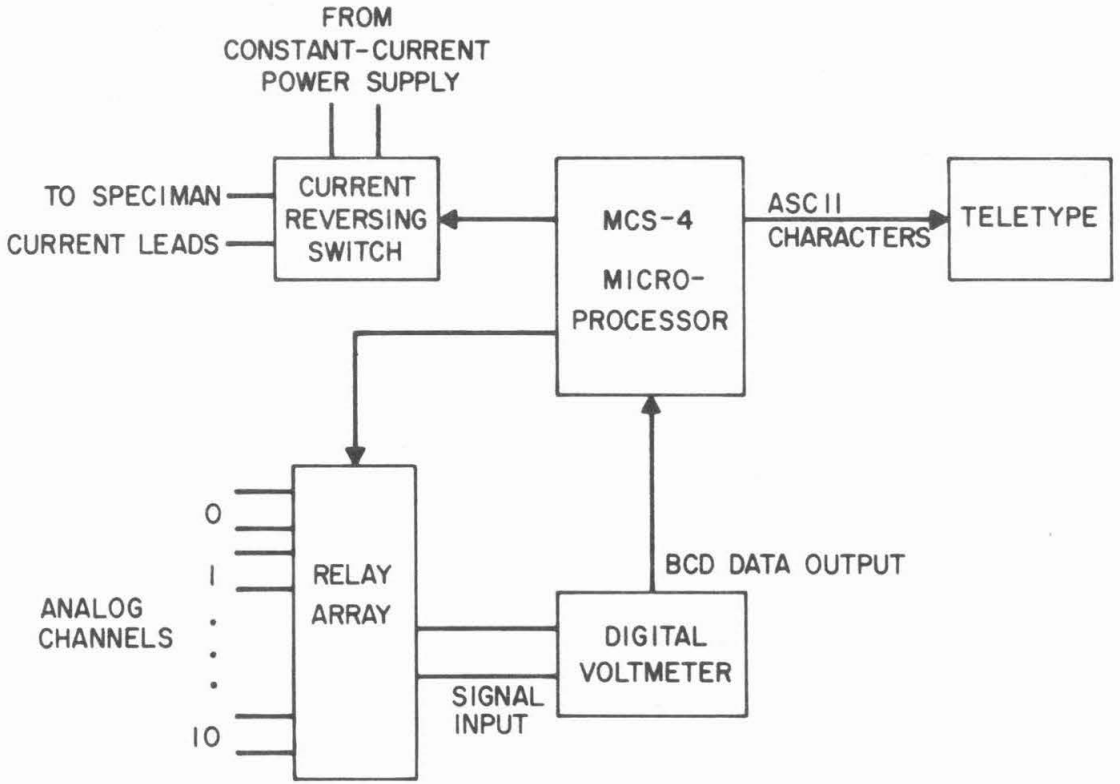

Figure 1. Block diagram for the MCS-4 Data Acquisition System used for the electrical resistivity measurements.

essor Unit, an Intel 4008 Address Interface, an Intel 4009 I/O Interface, a Random Access Memory (RAM) Array consisting of four Intel 4002 RAM, and a Programmable Read Only Memory (PROM) Array consisting of four Intel 1702A PROM. Some TTL devices are used for data multiplexing and logic level shifting. The programs are stored on the PROM Array. Figure 2 shows the block diagram of the microprocessor unit. The programs were written in machine codes. An assembler was written with FORTRAN to assemble the machine codes. The programs' execution was simulated on the Caltech PDD-10 Time Sharing System and debugged before they were loaded on the PROM.

The digital voltmeter used in the data acquisition system is a $7\frac{1}{2}$ digit Hewlett Packard 3462A digital voltmeter. The analog signal was amplified by a Keithley 150AR Micro-Ammeter/Amplifier before it was fed to the digital voltmeter. The constant current source used is a North Hills Model TC-1002 BR Voltage/Current Reference Source.

F. Critical Current Measurements

Critical current measurements were made on Cu-V-Ga specimens only. For some specimens, only the critical current densities at 4.2°K and zero transverse magnetic field were measured. The apparatus used for the measurement is similar to that described in Ref. 1. The critical current was defined as the value of the current which produced a potential difference of 1 μV. The potential difference was measured as the average potential difference with the current flowing in both forward and reverse directions through the specimen. This was done in order to eliminate the thermal drift in the measuring circuit. The potential difference was measured with a Dana 5800 digi-

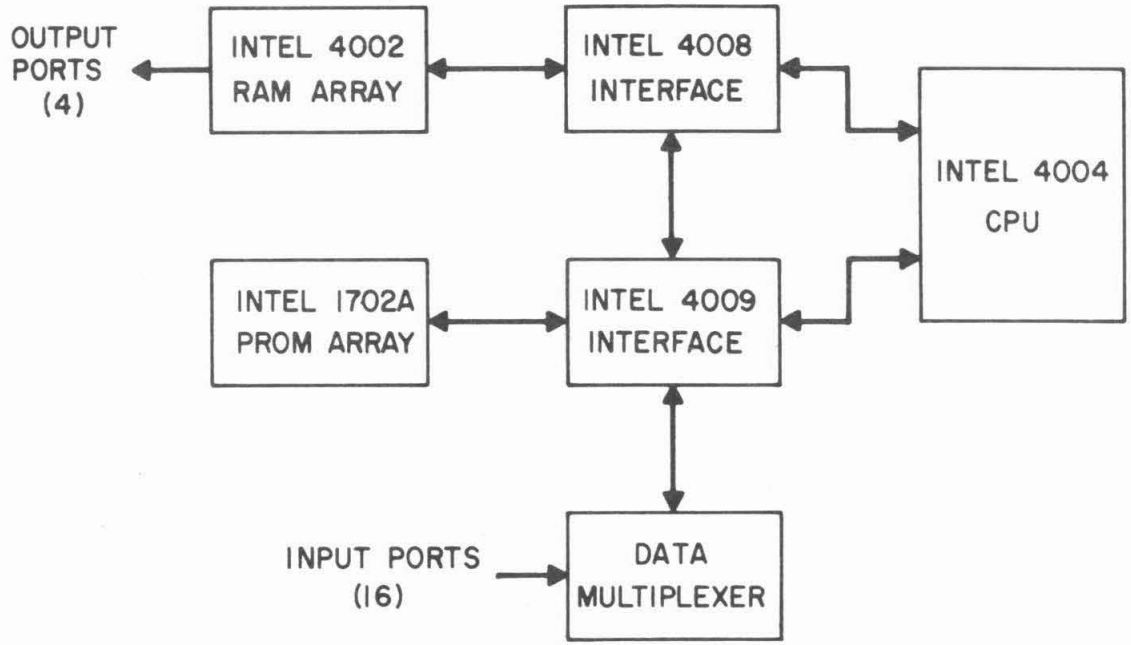

Figure 2. Block diagram for the MCS-4 micro-processor.

tal voltmeter. The critical current density was defined as the value of the critical current divided by the total cross-sectional area of the specimen.

For some selected specimens, the critical current densities at 4.2°K as a function of transverse magnetic field between 0 to 60 kG were measured. The specimens were mounted on an apparatus for measuring critical current densities, and the apparatus was inserted in the bore of a Westinghouse Nb-Zr superconducting solenoid capable of generating a field of 65 kG at the center of its bore. The specimen and the superconducting solenoid were immersed in the same liquid He bath during the measurement.

For measuring critical current densities as a function of temperature, the pulsed current method was used. The specimen was mounted in a probe similar to the apparatus for critical current measurement except that the specimen and the current leads were mounted in between two copper heaters which were hemi-circular in cross section. The heater wires were wound non-inductively on the copper pieces. A calibrated GaAs temperature sensor made by Lake Shore Cryogenics was placed under the specimen. The entire heater - specimen assembly was sealed in a cylindrical canister with Wood's metal used for sealing. The probe was pumped, and then a few centimeters of Hg pressure of He gas were led into the canister to improve the heat exchange. A temperature controller was used to control the temperature of the heater - specimen assembly to within 0.1°K resolution. Figure 3 shows the design of the probe used in the measurement.

Figure 4 shows the circuit used to derive the current pulse and

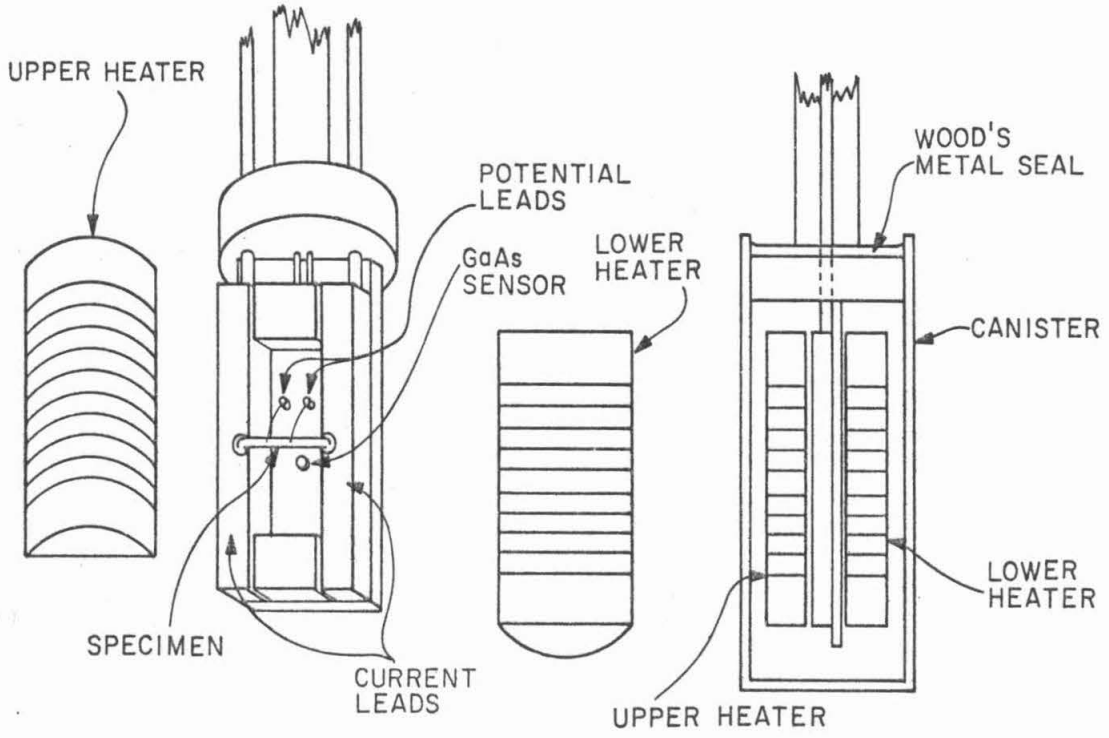

Figure 3. Schematic diagram of the probe used for measuring the critical current density as functions of both field and temperature using the pulsed current method.

to record the waveform of signals. The current pulse passing through the specimen was obtained from a Hewlett Packard HP 6260B power supply operating in the remote voltage programming mode. The shape of the current pulse was approximately triangular. The duration of the pulse was about 5 msec. The programming voltage signal, which was triangular in shape, was obtained from a Hewlett Packard HP-3300A Function Generator equipped with a HP-3302A Trigger Plug In unit. The function generator was in turn triggered by a timer with delay time variable between 0 and 99 seconds.

The voltage signal developed across the potential leads of the specimen was amplified with a Princeton Applied Research Type-113 Low Noise Preamplifier, and then recorded with a Tektronics Type 536 Oscilloscope. The current pulse passing through the specimen was also recorded through the same circuit. The typical shapes of the current and voltage pulses are shown in Figures 5 and 6.

It has been found that the duration of 5 msec for the current pulse was close to optimum. If the duration exceeds 15 msec, the specimens tend to burn out after they go through the superconducting - normal transition. On the other hand, the drop in frequency response in the programming circuit of the HP-6260B power supply for frequencies exceeding 120 Hz limited the magnitude of the current available in the circuit if a shorter duration was used. Since the duty cycle of the pulsing was low (about 1 pulse per 30 seconds on the average), the heating effect caused by the current at the solder joints between the specimen ends and the current leads was negligible. In fact, that was the main reason the pulsed current method was used to measure

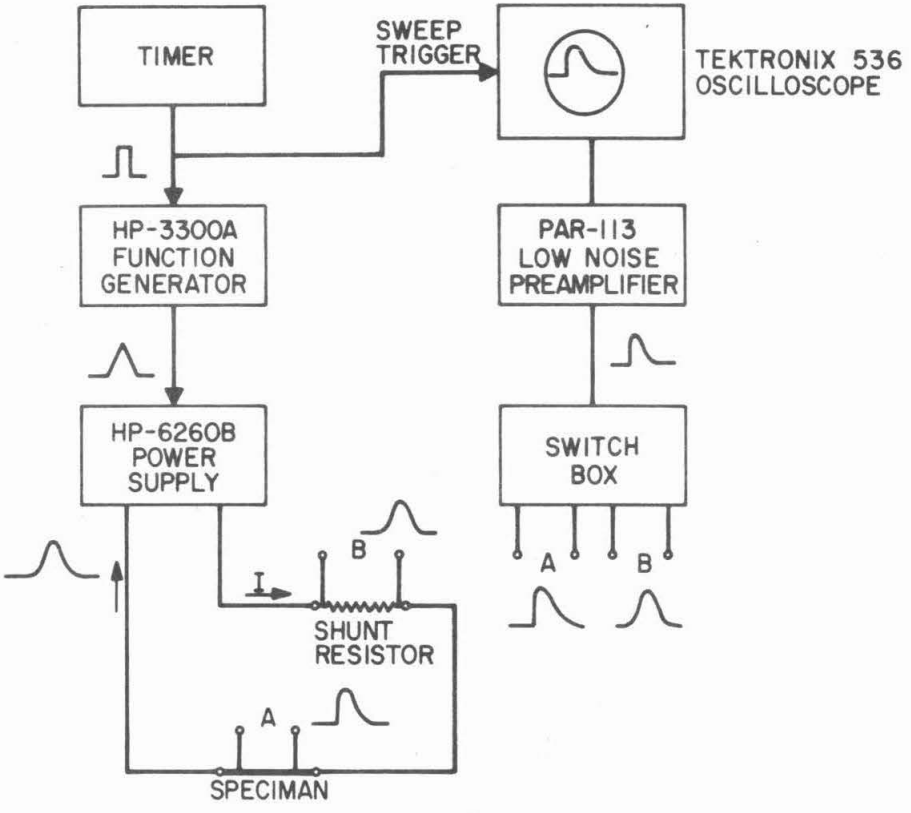

Figure 4. Block diagram of the circuit used for measuring the critical current density as function of field and temperature using the pulsed current method.

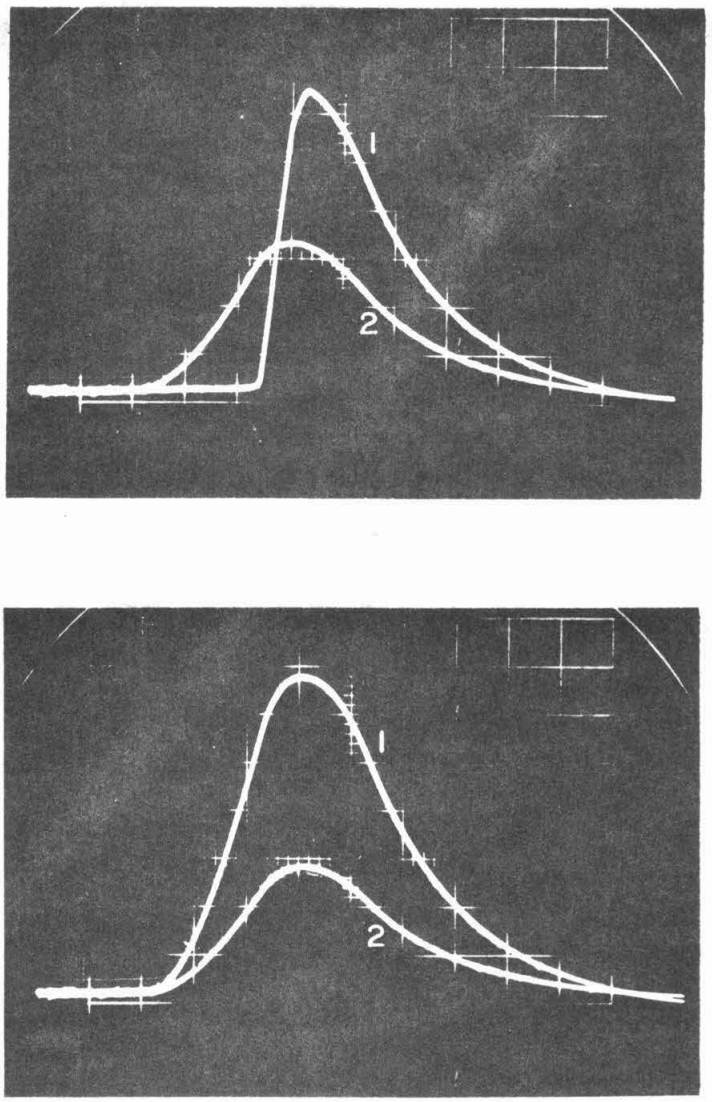

Figure 5. Potential and current waveforms for a 0.25 mm $Cu_{80}V_{10}Ga_{10}$ sheet, heat treated at 650°C for 2 days. A) T = 9.1°K, H = 0 kG. Curve 1: potential, 4.0 mV/div; Curve 2: current, 3.2 A/div. B) T = 12.5°K, H = 0 kG. Curve 1: potential, 1.6 mV/div; Curve 2: current 1.6 A/div. Horizontal: 1.6 msec/div.

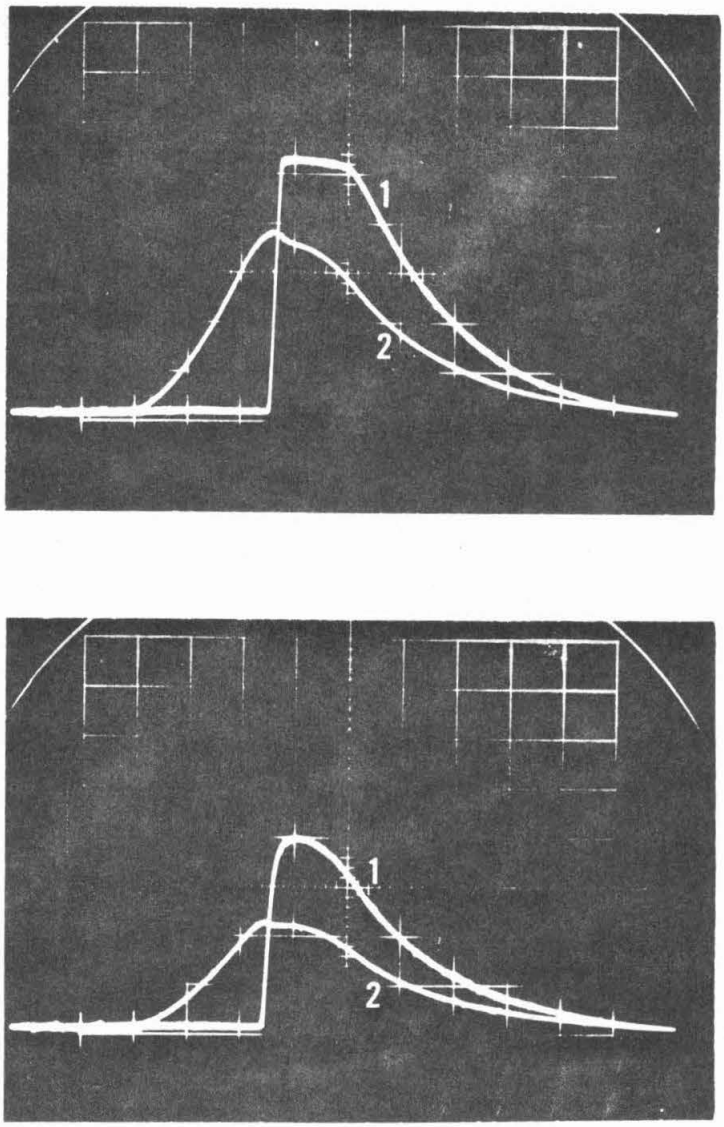

Figure 6. Potential and current waveforms for a 0.4 mm $Cu_{80}V_{10}Ga_{10}$ wire, heat treated at 650°C for 2 days. A) T = 4.2°K, H = 7.0 kG. Curve 1: potential 16 mV/div, Curve 2: current, 3.2 A/div. B) T = 9.1°K, H = 1.0 kG. Curve 1: potential, 16 mV/div, Curve 2: current, 3.2 A/div. Horizontal: 1.6 msec/div.

the critical current as a function of temperature; otherwise, if DC current was used, the heating effect would make the temperature measurement entirely unreliable, since current as high as 60 amps was sometimes required to cause the specimen to go normal.

The value of the current at which the potential across the specimen jumped from zero was taken as the critical current. It was found that the measured critical current at 4.2°K was in reasonable agreement with the result obtained by DC measurements where the specimens were immersed in liquid He during the measurement.

The same apparatus can be modified to make AC loss measurements. All that is required is to replace the power supply by a power amplifier coupled with a linear low-impedance transformer such as a UTC LS-34 High Level Matching Transformer made by United Transformer Co., and operating the function generator in free run mode with sinusoidal wave output.

G. Metallographic Studies

Some of the specimens were prepared for metallographic examination. A number of Cu-V-Ga specimens have been further examined with a scanning electron microscope. The specimens were prepared in the following manner. A piece of wire or rod specimen was placed in a Buehler 1 1/4" bakelite ring mold and then vacuum cast in Buehler plastic epoxide resin. Specimens in sheet form required special mounting. They were firmly clamped between two 1/8" × 1/2" × 3/4" 316 stainless steel blocks, and then placed in the bakelite ring mold so that the specimen appeared on the edge before casting.

The mounted specimens were then wet ground on No. 400 wet-

or-dry sand paper followed by No. 600 paper. Rough polishing was done on an 8" wheel, covered with nylon cloth, and charged with 6 μm diamond paste. Intermediate polishing was done on an 8" wheel covered with Buehler microcloth, and charged with 1 μm diamond paste. Final polishing was done on an 8" wheel covered with microcloth, and charged with a distilled-water suspension of 0.05 μm gamma alumina.

Etching was done by swabbing with an etching solution containing 1/3 of 3% H_2O_2, 1/3 of 5% NH_4OH, and 1/3 of distilled water. Etching time was 20 to 30 seconds, depending on the individual specimen. Each specimen was alternately polished and etched at least three times to assure removal of the disturbed layer. The specimens were then examined with a Bausch and Lomb Metallograph. Typical magnification used was 750X. Some Cu-V-Ga specimens were also examined with a Cambridge Scanning Electron Microscope equipped with EDAX (Energy Dispersive Analysis of Secondary X-ray Emission Spectrum) in order to get higher resolution and also to better identify the phases. Typical magnification used ranged between 200X to 5000X.

Some of the Cu-V-Ga specimens were also examined with an electron microprobe to investigate the distribution of various elements in the specimen.

H. Magnetization

The magnetization as a function of field in the range of ±6 kG for a few Cu-V-Ga specimens has been measured. A standard Faraday Magnetometer was used to do the measurement. The magnetic field was generated by a 6" Varian electromagnet equipped with a constant force pole cap. The force gradient was 10.25 kG^2/cm for

0.4 inches under a pole piece gap of 1 inch. An RG Cahn electrobalance was used to measure the force exerted on the specimen. The output of the electrobalance was measured with a digital voltmeter; typically a 5 microvolt signal corresponds to a force of 0.1 microgram.

The specimen was chopped into fine pieces and loaded in a gelatine capsule, which was then suspended from the measuring arm of the electrobalance with an 0.003-inch quartz fiber. The balance was housed in a bell jar, with a stainless steel tube extending downwards from the bell jar. The quartz fiber, gelatine capsule, and a heater-thermometer assembly were suspended in the stainless steel tube. Care has been taken to make sure that the capsule was hanging freely from the balance only. The magnetic field was measured with a Bell incremental gaussmeter. The accuracy of the magnetization measurement is estimated to be about 2 per cent, decreasing to about 7 per cent for a field below 1 kG.

III. EXPERIMENTAL RESULTS

A. Electrical Resistivity and Superconducting Transition Temperature Measurements

The electrical resistivities of specimens have been measured for both Cu-V-Si and Cu-V-Ga specimens in various forms. Furthermore, different annealing temperatures and annealing times have been chosen to heat treat the specimens, and the electrical resistivities were again measured after the heat treatment. About 400 separate electrical resistivity measurents were made, and the results are summarized in this section.

1. Cu-V-Si Specimens. Most of the specimens studied have fixed atomic per cent ratios of vanadium to silicon, namely, 3 to 1. Thus, we can classify the Cu-V-Si alloys studied according to their V_3Si content.[63] In order to study the effect of varying the relative atomic percentages of vanadium and silicon, some alloys of other compositions were also studied, for example, $Cu_{85}V_{7.5}Si_{7.5}$.

1.1 Alloys containing 8 at. % and 10 at. % of V_3Si. Figure 7 shows the measured electrical resistivities as a function of temperature between 4.2°K and 25°K for $Cu_{92}(V_3Si)_8$ rods annealed at 400°C for various lengths of time. As can be seen from Figure 7, all specimens regardless of their annealing time showed the onset of a superconducting transition at ~17°K, which is the superconducting transition temperature for V_3Si (16.9°K).[18] This agrees with the results of x-ray diffraction analysis which will be described in the next section. The specimens with annealing time less than 4 days were not superconducting. Specimens which were annealed for 4

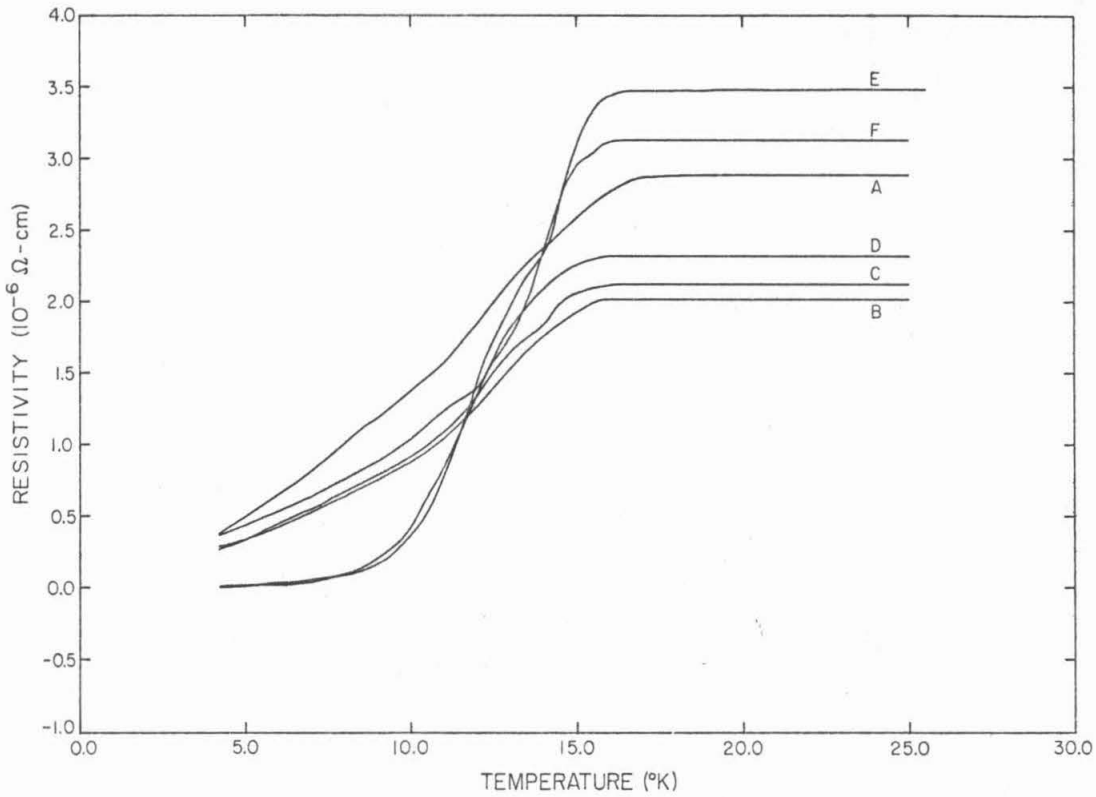

Figure 7. Electrical resistivities for $Cu_{92}(V_3Si)_8$ specimens. A: as rolled. B, C, D, E, F: heat treated at 400°C for 1, 2, 3, 4, 6 days, respectively.

days and 6 days showed complete superconducting transitions at temperatures slightly above $5^{\circ}K$.

Figure 8 shows the measured electrical resistivities as a function of temperature for $Cu_{92}(V_3Si)_8$ rods annealed at $600^{\circ}C$ for 1 day, 2 days, and 3 days. All specimens showed the onset of superconductivity at $\sim 17^{\circ}K$, but none of them had a complete superconducting transition above $4.2^{\circ}K$.

Figure 9 shows the measured electrical resistivities as a function of temperatures for $Cu_{90}(V_3Si)_{10}$ rods annealed at $400^{\circ}C$ for various lengths of time. As can be seen, none of the specimens were completely superconducting above $4.2^{\circ}K$, although they all showed the onset of the transition at about $17^{\circ}K$. Annealing at $600^{\circ}C$ did not improve the superconducting properties of $Cu_{90}(V_3Si)_{10}$ rods, as can be seen from Figure 10, on which the electrical resistivities of rod specimens annealed at $600^{\circ}C$ for various periods of time are shown. High-temperature annealing tends to deteriorate the properties of $Cu_{90}(V_3Si)_{10}$ specimens, as can be seen from Figure 11, which shows the measured electrical resistivities of specimens annealed at $900^{\circ}C$ for various periods of time.

Thus, we can see that for Cu-V-Si specimens containing 10 at. % of (V_3Si) or less, annealing did not improve the superconducting properties of the specimens. There is evidence of formation of V_3Si in the Cu matrix during the process of melting the ingots, but further annealing did not cause the reaction to go any further. Measurements made on specimens containing 5 at. % of V_3Si showed similar results. This is quite in contrast with the results

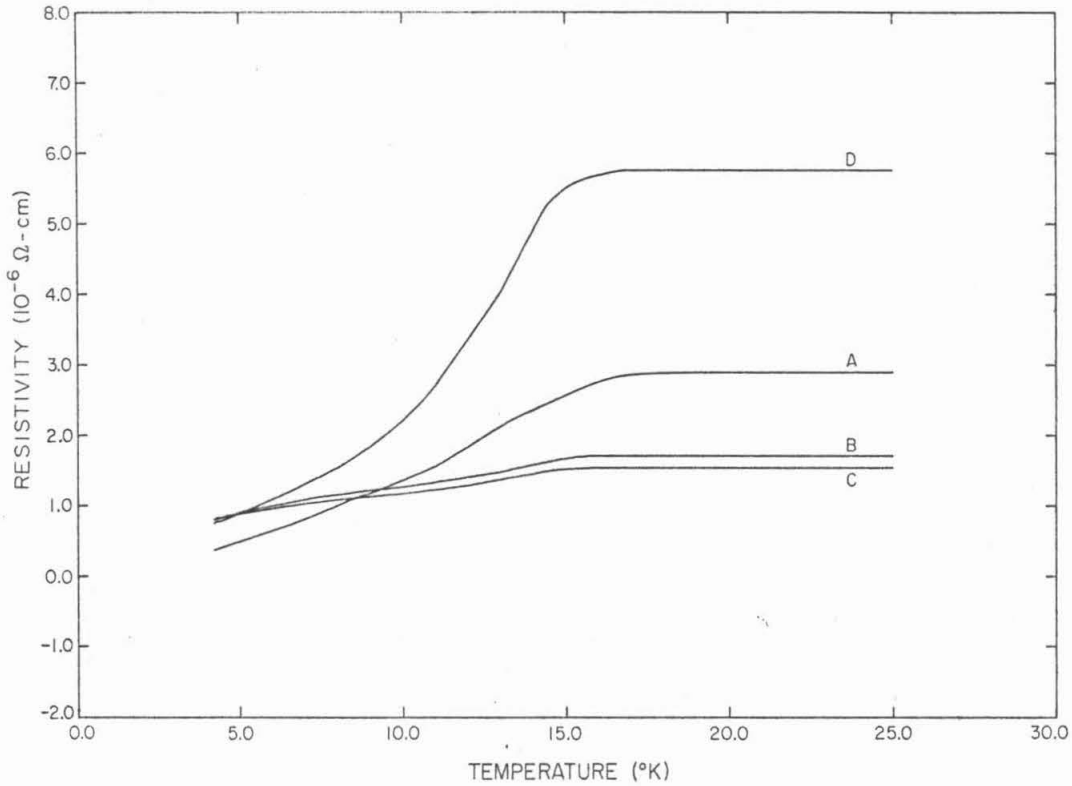

Figure 8. Electrical resistivities for $Cu_{92}(V_3Si)_8$ specimens. A: as rolled. B, C, D: heat treated as 600°C for 1, 2, 3 days, respectively.

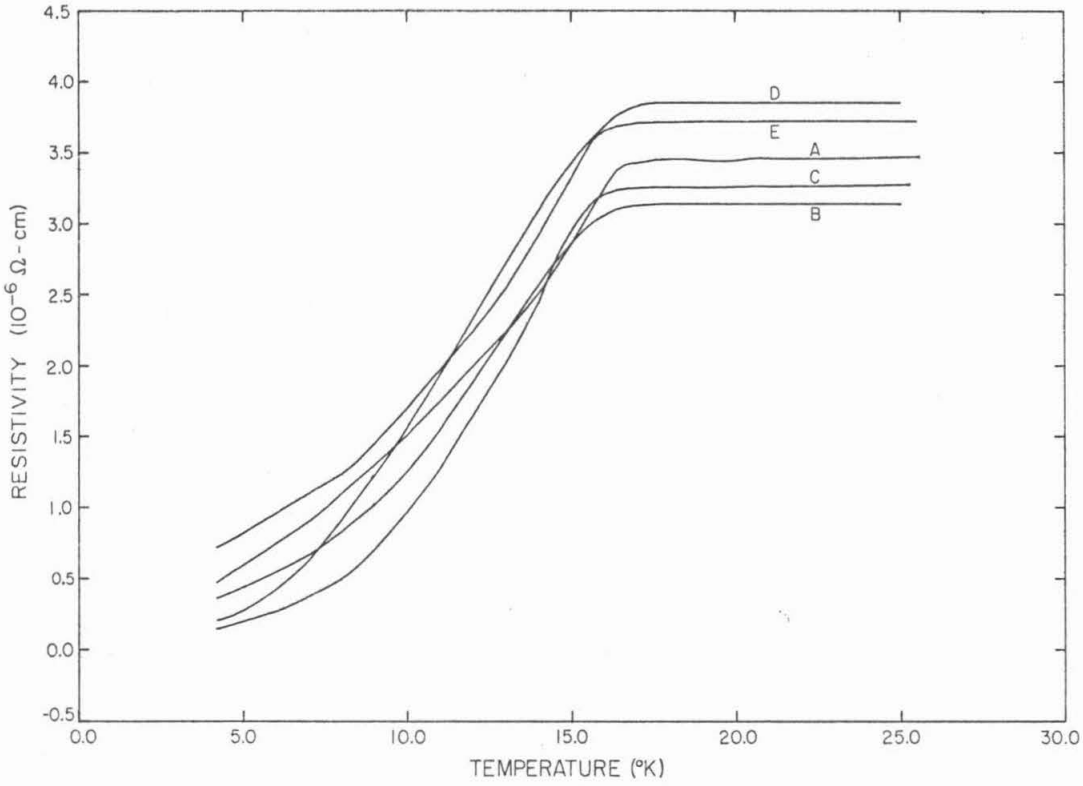

Figure 9. Electrical resistivities for $Cu_{90}(V_3Si)_{10}$ specimens. A: as rolled. B, C, D, E: heat treated at 400°C for 1, 2, 3, 4 days, respectively.

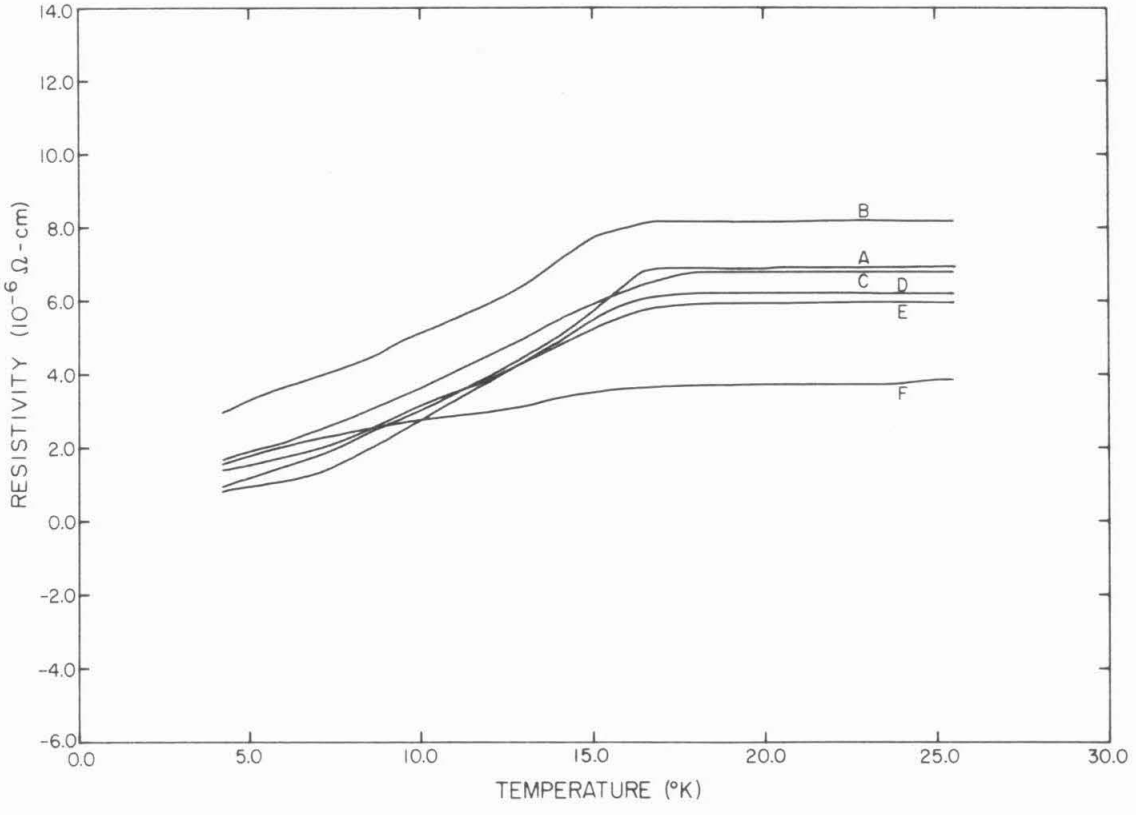

Figure 10. Electrical resistivities for $Cu_{90}(V_3Si)_{10}$ specimens. A: as rolled. B, C, D, E, F: heat treated at 600°C for 1, 2, 3, 4, 6 days, respectively.

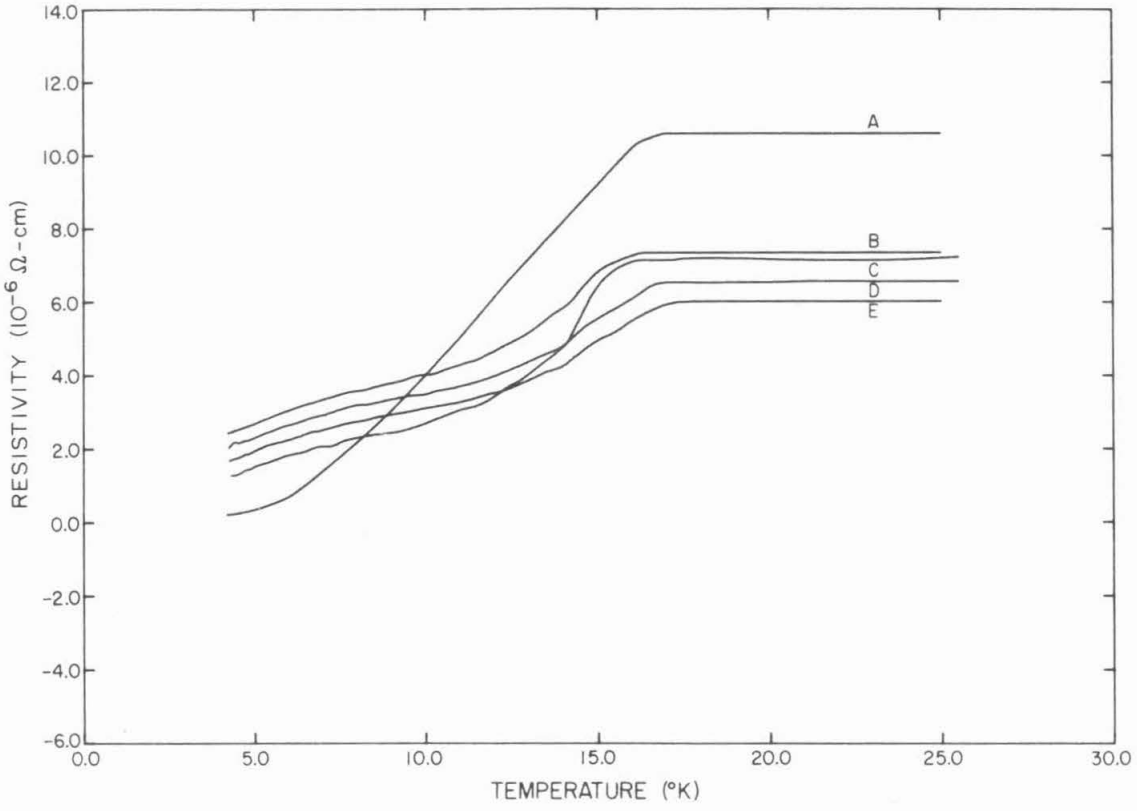

Figure 11. Electrical resistivities for $Cu_{90}(V_3Si)_{10}$ specimens. A: as rolled. B, C, D, E: heat treated at 900°C for 4, 14, 41, 69 hours, respectively.

obtained on Cu-V-Ga specimens, which will be discussed later in this section.

1.2 Alloys Containing 15 at. % and 17.5 at. % of V_3Si. Figure 12 shows the measured electrical resistivities for $Cu_{85}(V_3Si)_{15}$ rods annealed at 600°C for various lengths of time. As can be seen, the as-rolled specimen was nearly superconducting at about 5.0°K, and showed two onsets of transitions at ~ 17°K and ~ 10°K, respectively. But the annealed specimens seemed to have lost this behavior after heat treatment. Figure 13 shows the measured electrical resistivities for $Cu_{85}(V_3Si)_{15}$ rods which have been annealed at 800°C for various lengths of time. As in the case of the specimens annealed at 600°C, the superconducting properties of the as-rolled specimens deteriorated after annealing at 800°C. Annealing at 900°C seems to have improved the superconducting properties, as can be seen from Figure 14. The specimen annealed at 900°C for 3 hours was nearly superconducting at ~ 7°K.

Thus, it seems that in order to obtain specimens which can have complete superconducting transitions above 4.2°K, the specimens must contain more of V_3Si than a certain minimum. Furthermore, the annealing temperature has to be high, as all indications show that the reaction for formation of V_3Si proceeds only at high temperatures near or above 900°C.

Results obtained from measurements made on $Cu_{82.5}(V_3Si)_{17.5}$ specimens also showed this trend. Figure 15 shows the measured electrical resistivities for $Cu_{82.5}(V_3Si)_{17.5}$ rods annealed at 700°C for various lengths of time. It can be seen that the specimen annealed

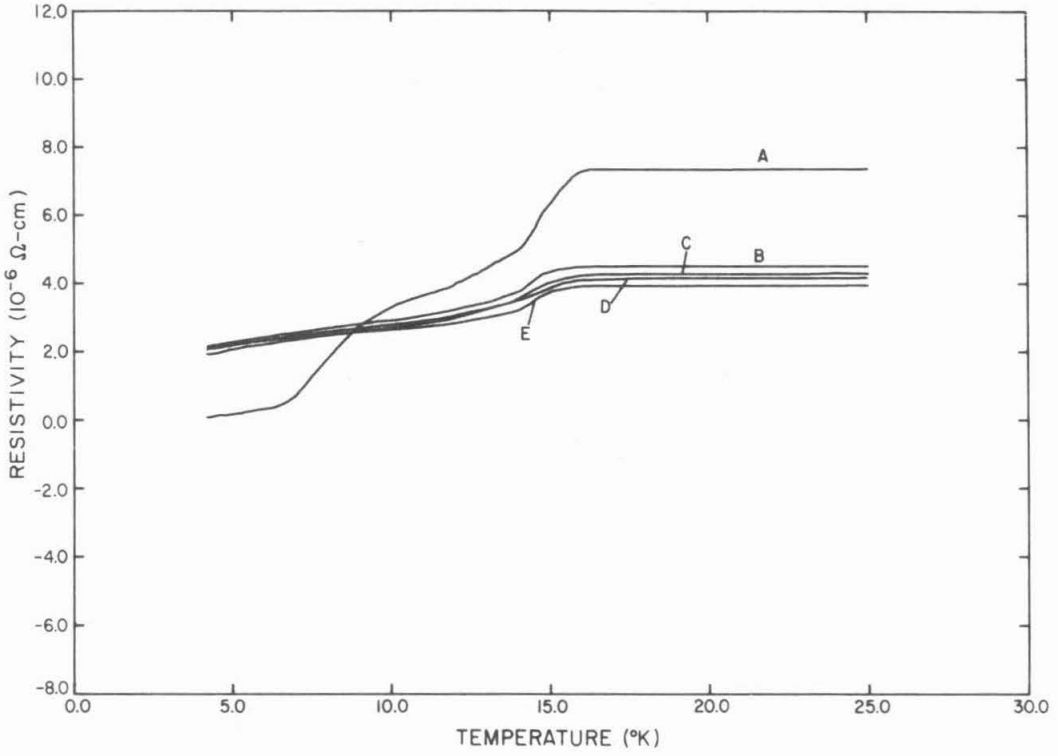

Figure 12. Electrical resistivities for $Cu_{85}(V_3Si)_{15}$ specimens. A: as rolled. B, C, D, E: heat treated at 600°C for 1, 2, 3, 4 days, respectively.

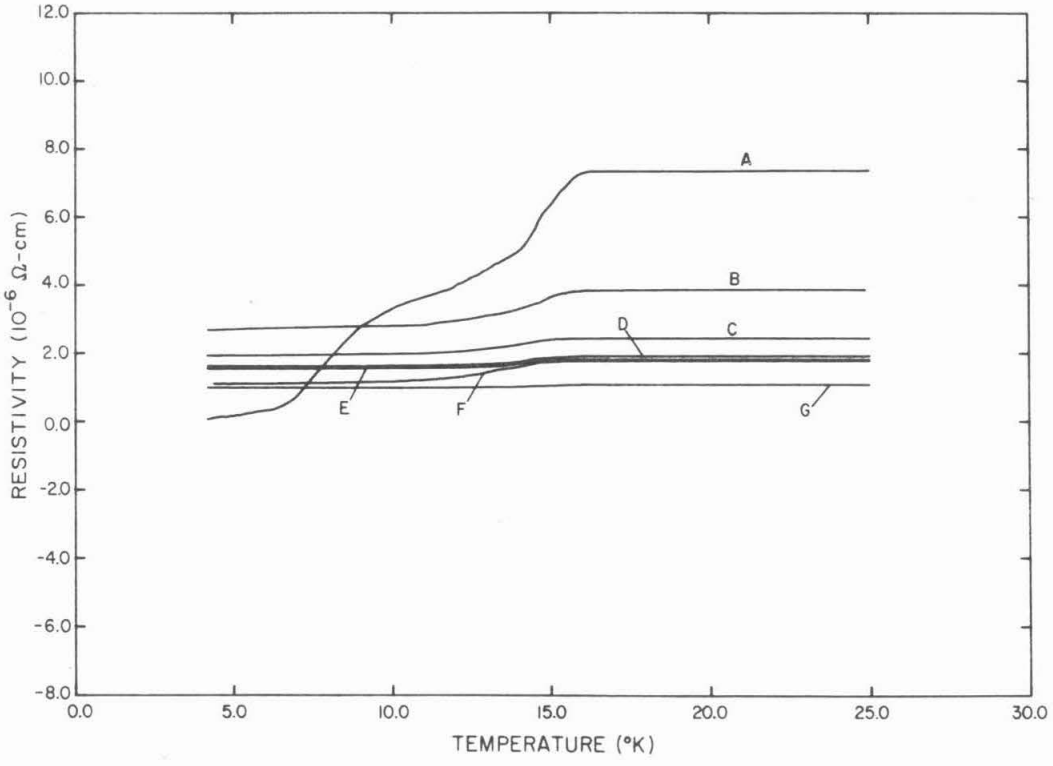

Figure 13. Electrical resistivities for $Cu_{85}(V_3Si)_{15}$ specimens. A: as rolled. B, C, D, E, F, G: heat treated at 800°C for 4, 17, 28, 39, 72, and 144 hours, respectively.

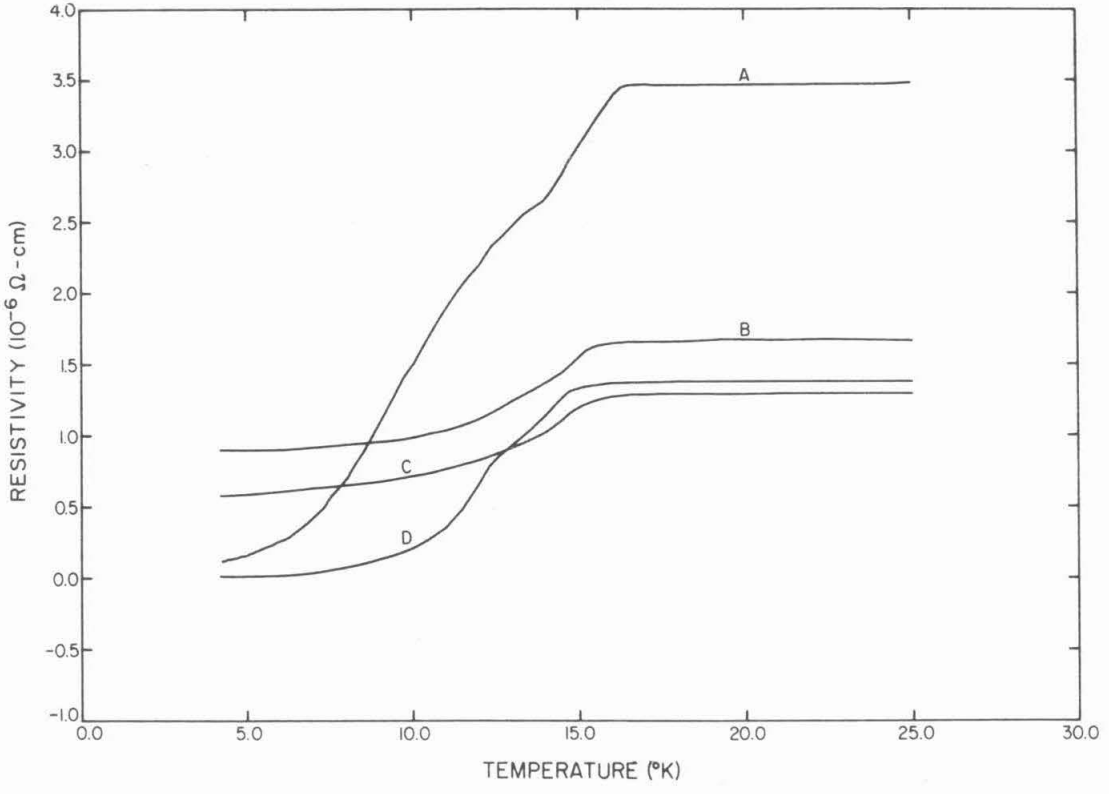

Figure 14. Electrical resistivities for $Cu_{85}(V_3Si)_{15}$ specimens. A: as rolled. B, C, D: heat treated at 900°C for 1, 2, 3 hours, respectively.

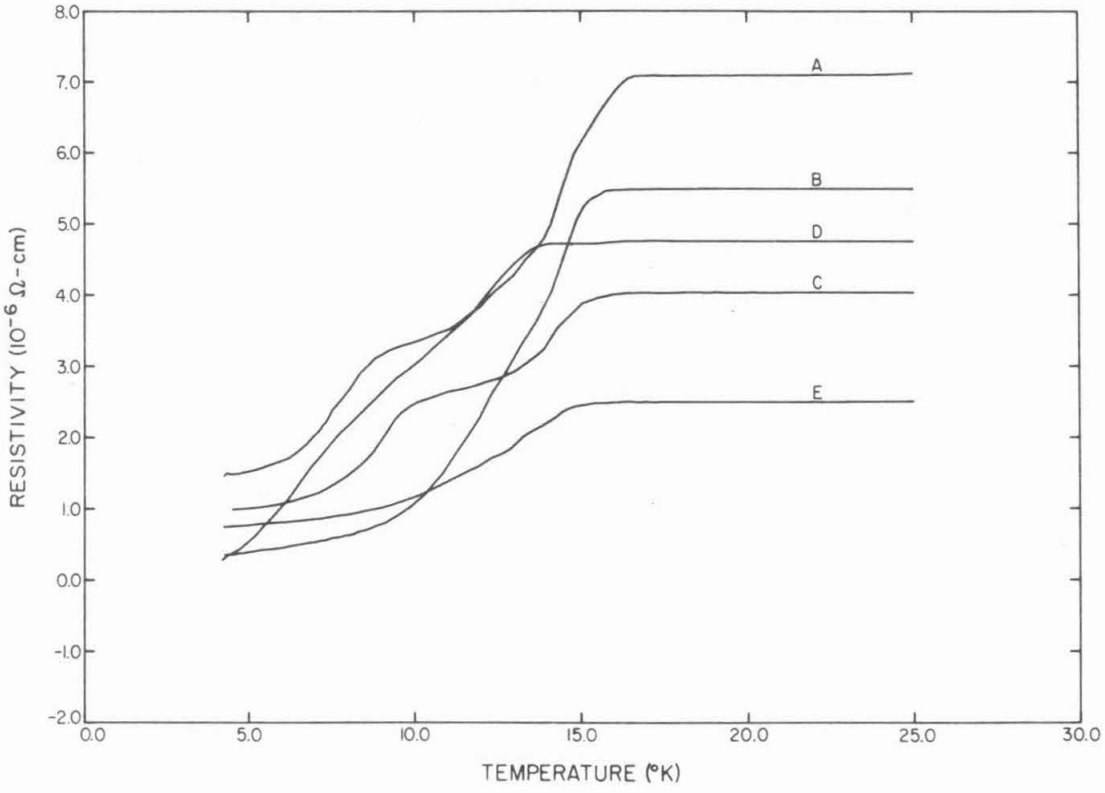

Figure 15. Electrical resistivities for $Cu_{82.5}(V_3Si)_{17.5}$ specimens. A: as rolled. B, C, D, E: heat treated at 700°C for 6, 12, 24, 48 hours, respectively.

for 6 hours gave the better characteristics. Further annealing caused the specimens to show the double transition with onset temperatures at $\sim 17^{\circ}K$ and $\sim 10^{\circ}K$, respectively, as can be seen from curves C and D on the figure. Prolonged annealing did not improve the characteristics of the specimen.

Figure 16 shows the measured electrical resistivities of the $Cu_{82.5}(V_3Si)_{17.5}$ specimens annealed at $900^{\circ}C$ for various lengths of time. It can be seen that the specimen which has been annealed for one day showed the best characteristics. This is in agreement with the results obtained for $Cu_{85}(V_3Si)_{15}$ specimens. But the choice of annealing time also seems important, as shown by curve E in Figure 16 for a specimen annealed for 36 hours at $900^{\circ}C$.

1.3 Alloys Containing 20 at. % of V_3Si. Figure 17 shows the electrical resistivities for the $Cu_{80}(V_3Si)_{20}$ rods annealed at $600^{\circ}C$ for various lengths of time. The as-rolled specimen had a complete superconducting transition at $\sim 5.5^{\circ}K$, but the annealed specimens were not superconducting above $4.2^{\circ}K$. All specimens showed double transitions with onsets at $\sim 17^{\circ}K$ and at $\sim 10^{\circ}K$, respectively, indicating the formation of a superconducting compound other than V_3Si. Figure 18 shows the electrical resistivities for specimens annealed at $800^{\circ}C$. It can be seen that annealing at $800^{\circ}C$ did not improve the characteristics of the specimens; but specimens annealed at $900^{\circ}C$ showed pronounced improvement. As shown in Figure 19, on which the electrical resistivities of specimens annealed at $900^{\circ}C$ are shown, the characteristics of specimens improved as the annealing time was increased; until the annealing time of one day was reached (curve D on

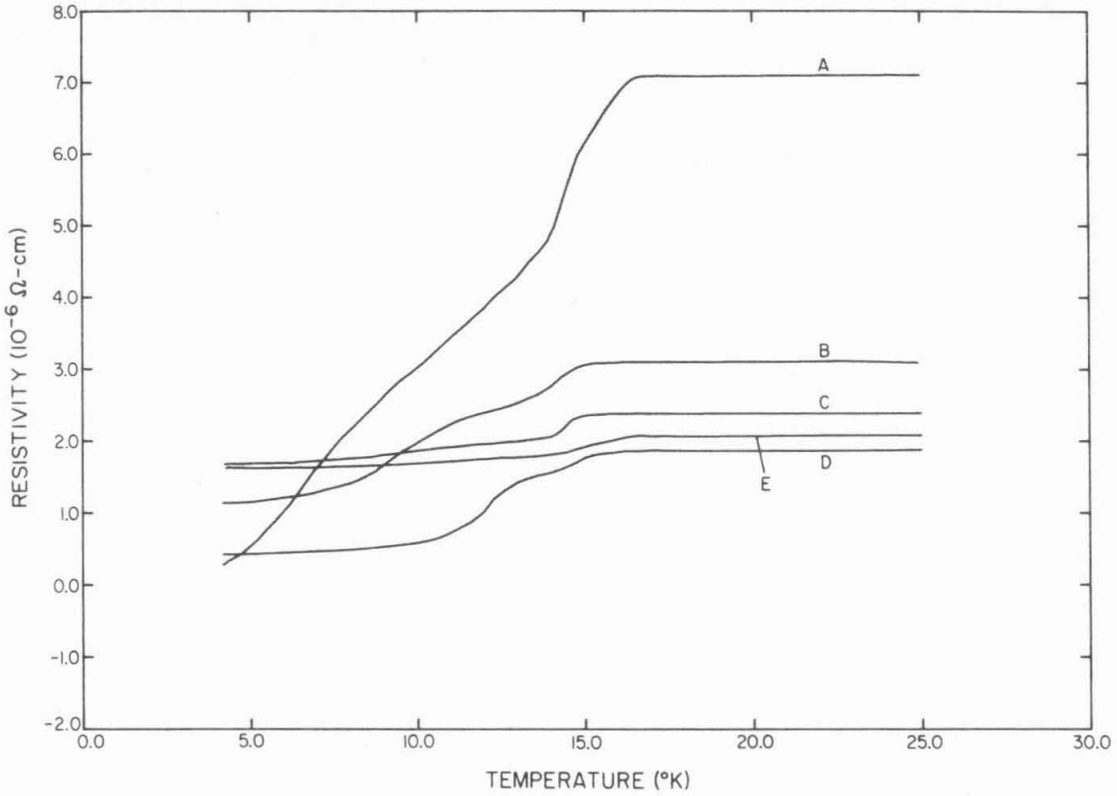

Figure 16. Electrical resistivities for $Cu_{82.5}(V_3Si)_{17.5}$ specimens. A: as rolled. B, C, D, E: heat treated at 900°C for 2.5, 12, 24, 36 hours, respectively.

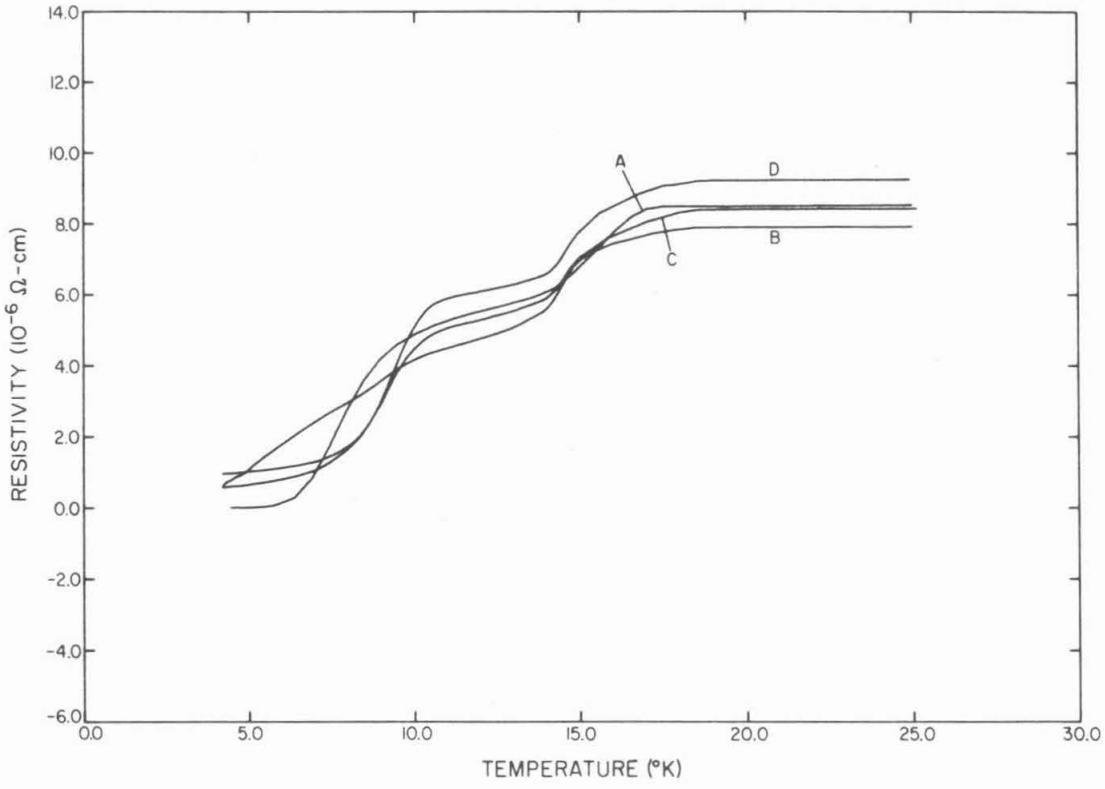

Figure 17. Electrical resistivities for $Cu_{80}(V_3Si)_{20}$ specimens. A: as rolled. B, C, D: heat treated at 600°C for 1, 2, 3 days, respectively.

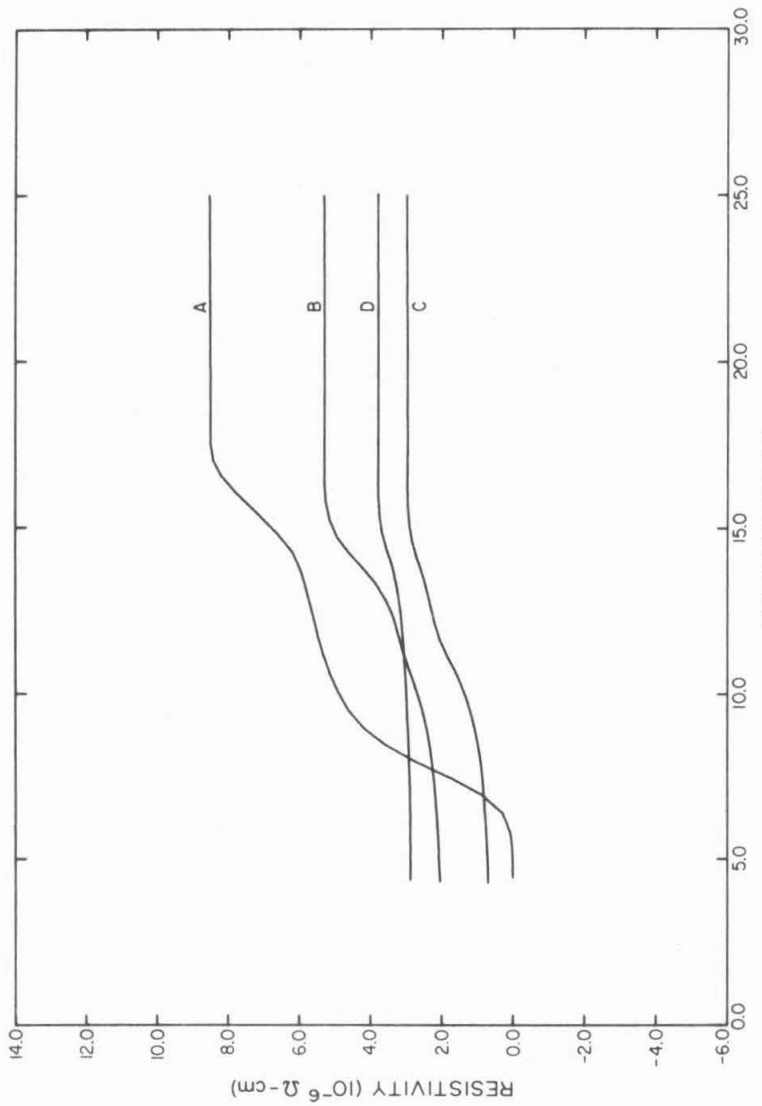

Figure 18. Electrical resistivities for $Cu_{80}(V_3Si)_{20}$ specimens. A: as rolled. B, C, D: heat treated at 800°C for 1, 2, 3 days, respectively.

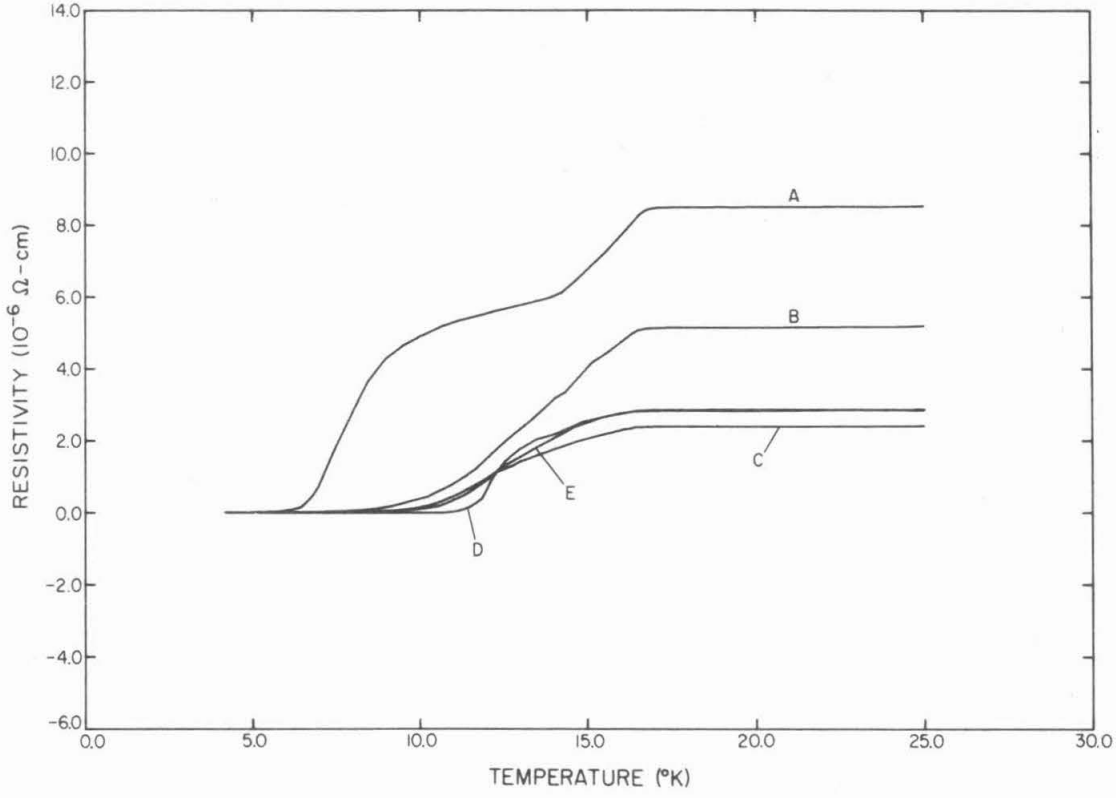

Figure 19. Electrical resistivities for $Cu_{80}(V_3Si)_{20}$ specimens. A: as rolled. B, C, D, E: heat treated at 900°C for 2, 9, 24, and 48 hours, respectively.

Figure 19), at which time the specimen exhibits the best characteristic achieved with the Cu-V-Si specimens. It showed the same onset temperature for the superconducting transition, but the temperature for complete transition to occur was $\sim 11.0^{\circ}K$. Further annealing tends to deteriorate the superconducting properties, as can be seen from curve **E** on the same figure, corresponding to a specimen which has been annealed for two days.

Thus, reinforcing our earlier remarks, we can arrive at the conclusions that, in order to obtain a Cu-V-Si specimen which has complete superconducting transition at relatively high temperature, the V_3Si content in the specimen has to be above a certain minimum, and the heat treatment must be done at a high temperature and with optimum annealing time.

1.4 Alloys with Other Compositions. Alloys containing more than 20 at. % of V_3Si have been made, but it was found that they were not ductile enough for proper cold working to be applied. Slight amounts of impurities such as Al or P have been added to some alloys hoping that they might reduce the oxidation and thus improve the bonding between the V_3Si phase and the Cu matrix, but not much improvement was observed.

Alloys with different atomic percent ratios of V to Si have also been tried. Figure 20 shows the measured electrical resistivities for $Cu_{85}V_{7.5}Si_{7.5}$ rods which have been annealed at $900^{\circ}C$ for various lengths of time. As can be seen from the figure, the annealing time of one day (curve B) seems to result in the best characteristic. But the specimen did not show a complete superconducting

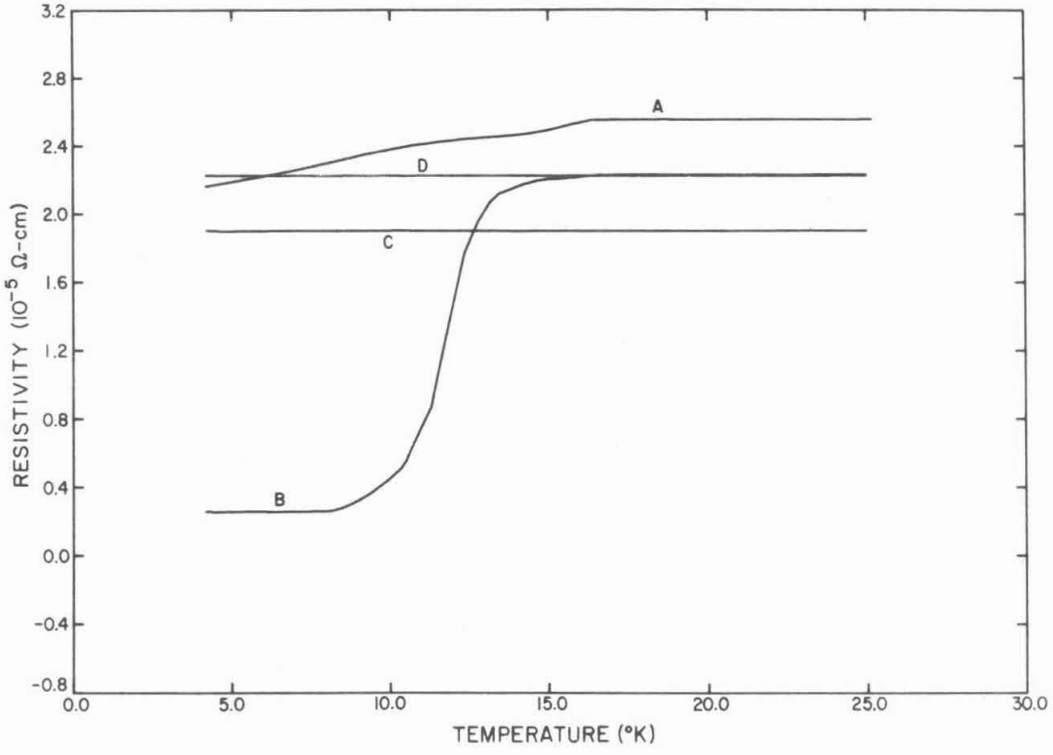

Figure 20. Electrical resistivities for $Cu_{85}V_{7.5}Si_{7.5}$ specimens. A: as rolled. B, C, D: heat treated at 900°C for 1, 2, 4 days, respectively.

transition.

2. Cu-V-Ga Specimens. The alloys studied can be grouped according to the atomic percentage of vanadium contained in them. There are five groups according to this classification, namely, those containing 5, 8, 10, 15, and 20 at. % of vanadium.

2.1 Alloys Containing 5 at. % Vanadium. Only one concentration has been studied in this group, with composition $Cu_{93}V_5Ga_2$. In the rods studied, no superconducting transition was observed in the as-rolled specimen or the annealed ones.

2.2 Alloys Containing 8 at. % Vanadium. Alloys with two different compositions have been studied, namely, $Cu_{82}V_8Ga_{10}$ and $Cu_{79.5}V_8Ga_{12.5}$.

Figure 21 shows the measured electrical resistivities as a function of temperature between 4.2°K and 25°K for rods rolled from a $Cu_{82}V_8Ga_{10}$ ingot and annealed at 650°C for different lengths of time up to 4 days. It can be seen from Figure 21 that the as-rolled specimen was not superconducting above 4.2°K, but the specimen which had been annealed for 27 hours had a non-complete superconducting transition with $T_c \sim 10.3$°K. Further annealing to 2 and 3 days caused the superconducting transition in the specimens to become complete at about the same T_c. But longer annealing times seem to cause the transition to become non-complete again, as can be seen from Curve E on the figure. By "non-complete" transition we mean that the specimen develops a finite potential drop across its potential leads even at temperatures below T_c.

This result indicates that annealing caused the formation of

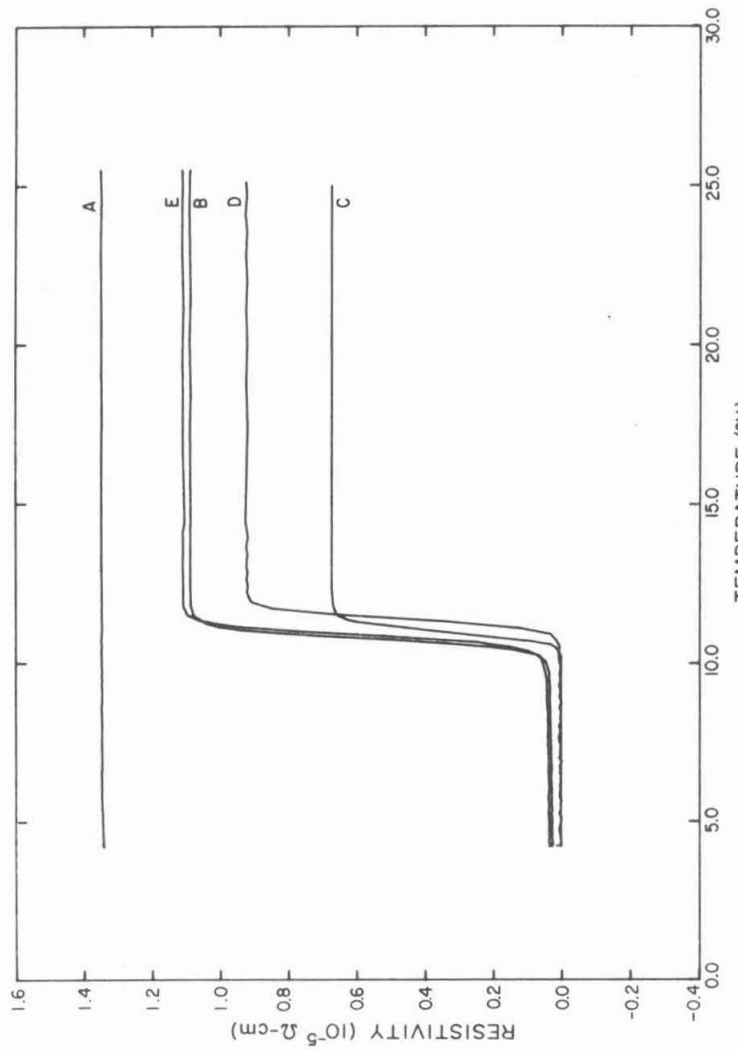

Figure 21. Electrical resistivities for $Cu_{82}V_8Ga_{10}$ specimens. A: as rolled. B, C, D, E: heat treated at 650°C for 27, 48, 72, 96 hours, respectively.

some compound with composition close to V_3Ga at the vanadium filaments. This agrees with the result of x-ray diffraction analysis made on the specimens.

Figure 22 shows the result of measured electrical resistivities for $Cu_{82}V_8Ga_{10}$ rods annealed at 800°C for 7.5 hours and 27 hours. The specimen annealed for 7.5 hours and 27 hours showed almost complete transitions at 9.1°K and 9.7°K, respectively. Thus, high-temperature annealing seems to cause the specimens to superconduct at a lower temperature.

Figure 23 shows the measured electrical resistivities for $Cu_{79.5}V_8Ga_{12.5}$ rods annealed at 650°C for 2 days, 3 days, and 4 days as well as the as-rolled specimen. It can be seen that the as-rolled specimen (curve A) started to superconduct at 8.0°K, which means that some V_3Ga-like compound has been formed in the process of casting the ingot. Specimens which have been annealed were all superconducting, with T_c of approximately 12.1°K, 12.6°K, and 12.4°K, corresponding to the annealing times of 2 days, 3 days, and 4 days, respectively. The onset of the transitions of the annealed specimens were all close to 14°K, which is higher than the onset temperature of 12°K for the superconducting transition in the $Cu_{82}V_8Ga_{10}$ specimens.

Figure 24 shows the measured electrical resistivities for $Cu_{79.5}V_8Ga_{12.5}$ specimens annealed at 800°C for 7.5 hours and 27 hours. They had complete superconducting transitions at 11.9°K and 12.1°K, corresponding to the annealing times of 7.5 hours and 27 hours, respectively. The onsets of the transitions were close to

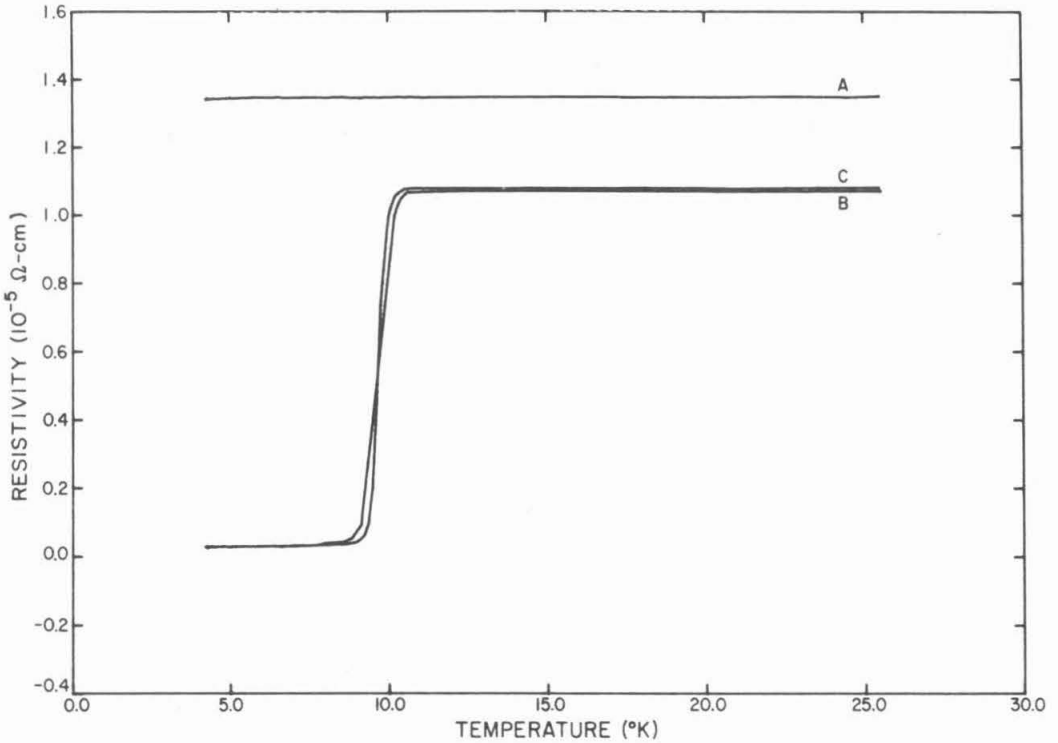

Figure 22. Electrical resistivities for $Cu_{82}V_8Ga_{10}$ specimens. A: as rolled. B, C: heat treated at 800°C for 7.5 and 27 hours, respectively.

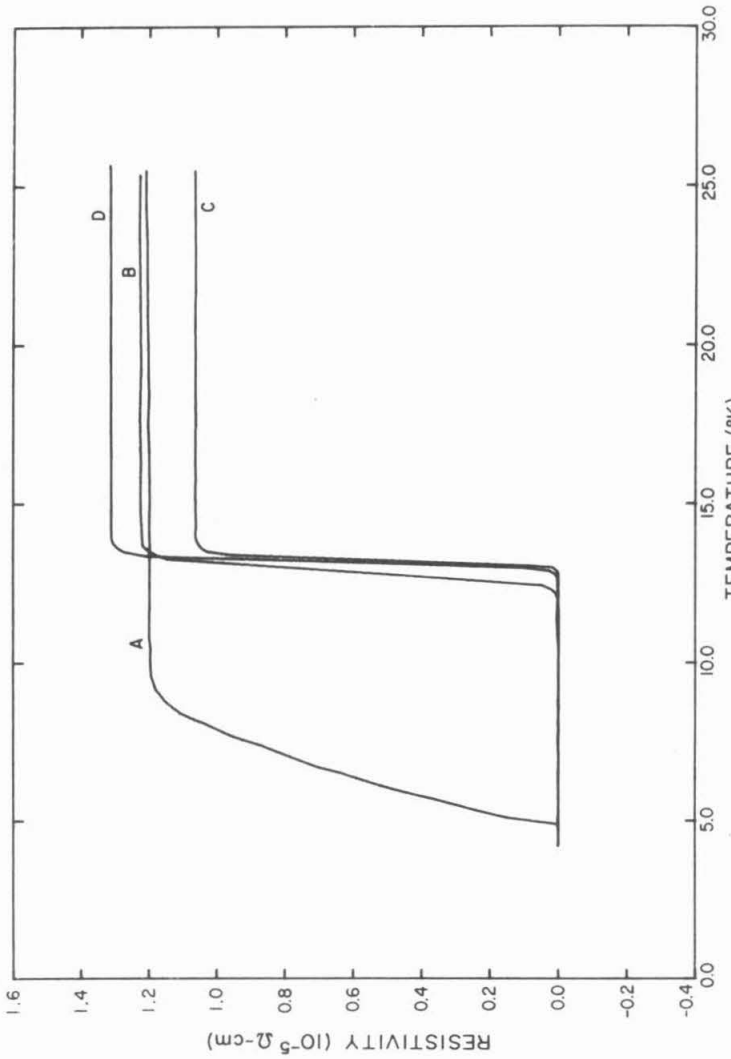

Figure 23. Electrical resistivities for $Cu_{79.5}V_{8}Ga_{12.5}$ specimens. A: as rolled. B, C, D: heat treated at 650°C for 2, 3, 4 days, respectively.

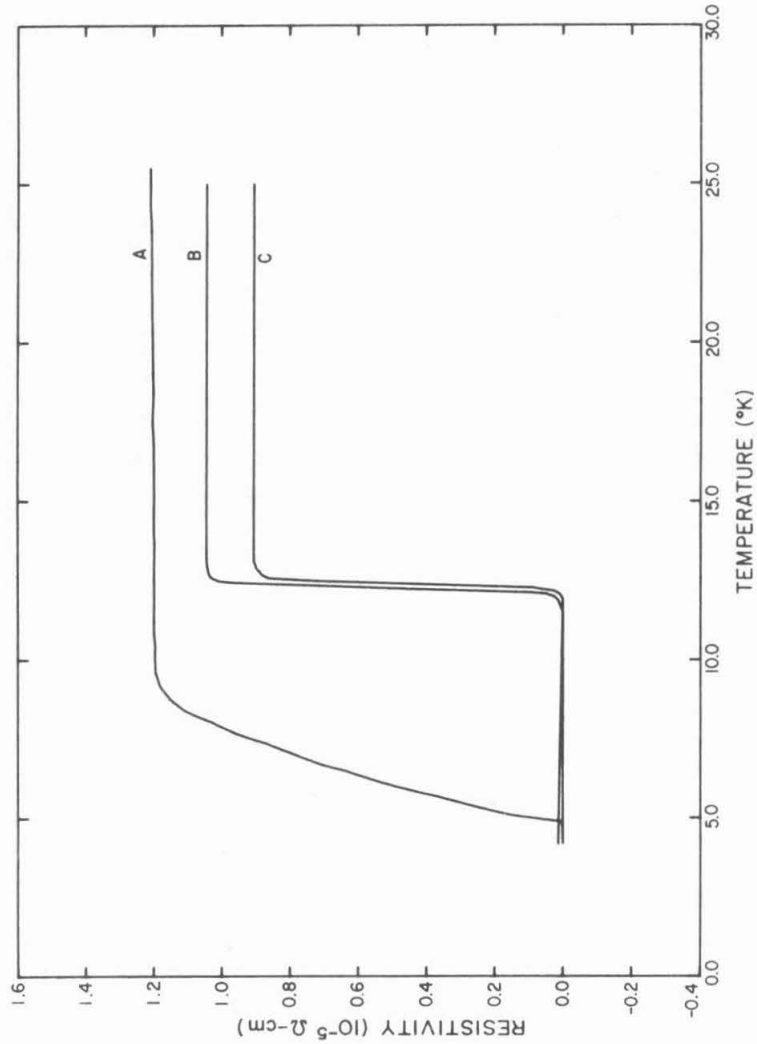

Figure 24. Electrical resistivities for $Cu_{79.5}V_8Ga_{12.5}$ specimens. A: as rolled. B, C: heat treated at 800°C for 7.5 and 27 hours, respectively.

13.0°K. Again, the results show that high-temperature annealing tends to lower the T_c.

The fact that $Cu_{79.5}V_8Ga_{12.5}$ specimens have higher T_c than the $Cu_{82}V_8Ga_{10}$ specimens tends to indicate that alloys with higher Ga content cause the formation of a compound closer to the stoichiometric composition of V_3Ga. But higher content of Ga in the alloy tends to make the matrix containing Cu-Ga solid solution brittle, and thus difficult to process.

2.3 Alloys Containing 10 at.% Vanadium. The necessity for the Ga concentration to be above a certain limit in order to obtain higher T_c is better demonstrated in alloys containing 10 at.% of vanadium. Figure 25 shows the measured electrical resistivities for $Cu_{85}V_{10}Ga_5$ rods which have been annealed at 650°C for 2 days and 4 days, respectively, as well as the as-rolled one. It can be seen that the as-rolled specimen was not superconducting above 4.2°K, but the annealed ones had complete superconducting transitions at 5.5°K and 6°K after being annealed for 2 days and 4 days, respectively. Annealing at 800°C did not cause the specimens of this composition to show any superconducting transition.

As expected, increasing the Ga content caused T_c to go up. Figure 26 shows the measured electrical resistivities for $Cu_{82}V_{10}Ga_8$ rods which have been annealed at 650°C for various lengths of time up to 4 days. The as-rolled specimen was again non-superconducting above 4.2°K, but the annealed specimens had complete superconducting transitions at 7.4°K (5 hours annealing time), 8.3°K (12 hours annealing), 8.7°K (1 day annealing), 8.8°K (52

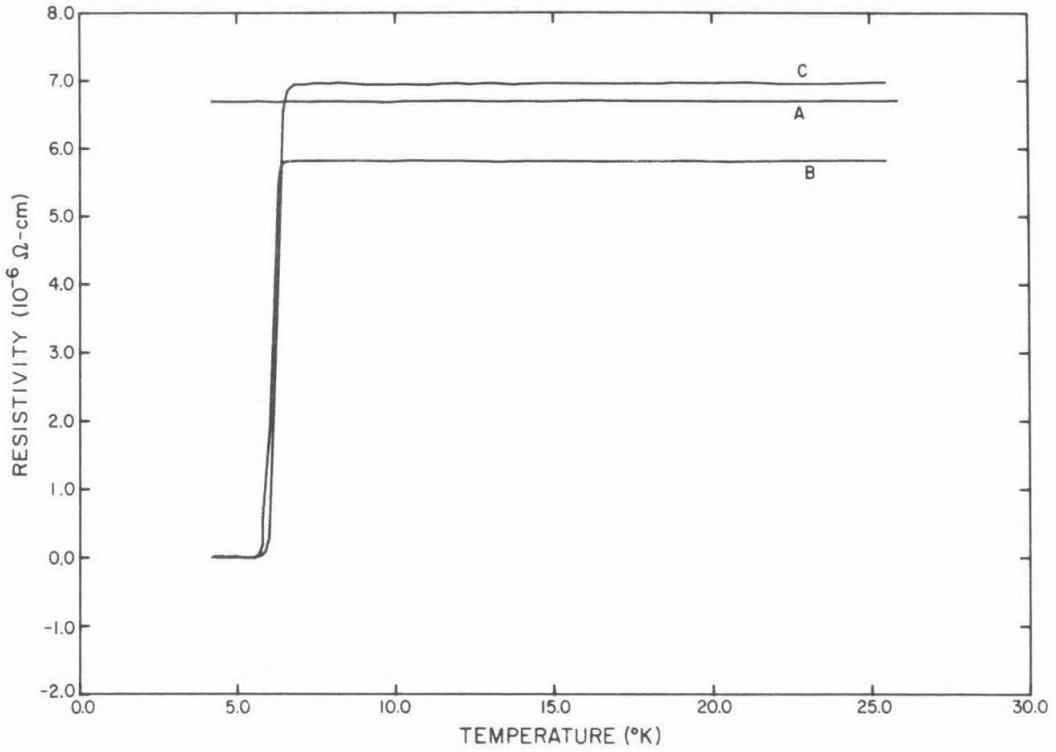

Figure 25. Electrical resistivities for $Cu_{85}V_{10}Ga_5$ specimens. A: as rolled. B, C: heat treated at 650°C for 2, 4 days, respectively.

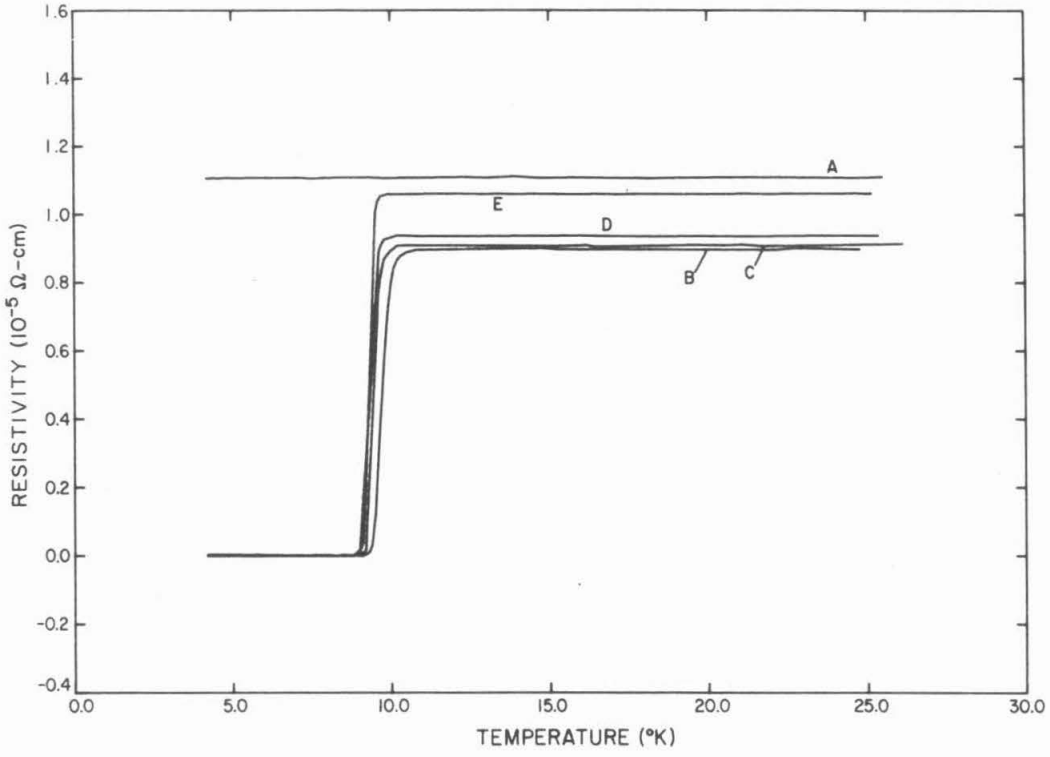

Figure 26. Electrical resistivities for $Cu_{82}V_{10}Ga_8$ specimens. A: as rolled. B, C, D, E: heat treated at 650°C for 5, 24, 52, 96 hours, respectively.

hours annealing), and 9.0°K (4 days annealing). Figure 27 shows the measured electrical resistivities for $Cu_{82}V_{10}Ga_8$ rods annealed at 800°C for 6 hours, 25 hours, and 2 days. They all have complete transitions at 7.3°K (6 hours annealing), 7.7°K (25 hours annealing), and 6.7°K (2 days annealing).

As the Ga concentration was raised above 10 at.%, T_c was pushed above 10°K. Figure 28 shows the measured electrical resistivities for $Cu_{80}V_{10}Ga_{10}$ rods annealed at 650°C for various lengths of time. The as-rolled specimen was not superconducting above 4.2°K, but the annealed ones had complete transitions at 10.6°K (12 hours annealing), 10.9°K (24 hours annealing), 11.0°K (49 hours annealing), and 11.2°K (4 days annealing). Figure 29 shows the measured resistivities for $Cu_{80}V_{10}Ga_{10}$ specimens which have been drawn into 0.4 mm wires and annealed at 650°C for various lengths of time. The as-drawn wire specimen was superconducting below 4.5°K, in contrast to the as-rolled specimen in rod form. The annealed specimens were all superconducting below about 10.5°K, which is comparable to that of rod specimens annealed at the same temperature.

Figure 30 shows the measured electrical resistivities for $Cu_{80}V_{10}Ga_{10}$ specimens annealed at 800°C for various lengths of time. They all have complete transitions at temperatures close to 9.7°K.

Alloys with higher Ga concentrations were studied. The composition was $Cu_{77.5}V_{10}Ga_{12.5}$. As expected from the results on alloys with 8 at.% vanadium, these specimens had higher T_c

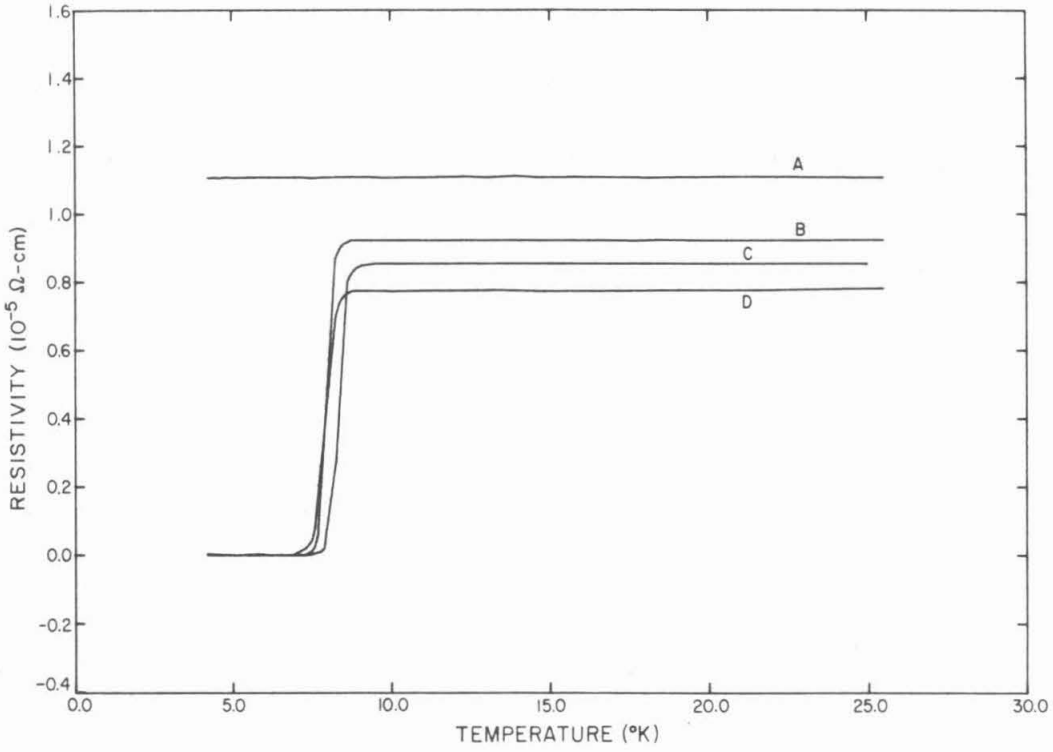

Figure 27. Electrical resistivities for $Cu_{82}V_{10}Ga_8$ specimens. A: as rolled. B, C, D: heat treated at 800°C for 6, 25, 48 hours, respectively.

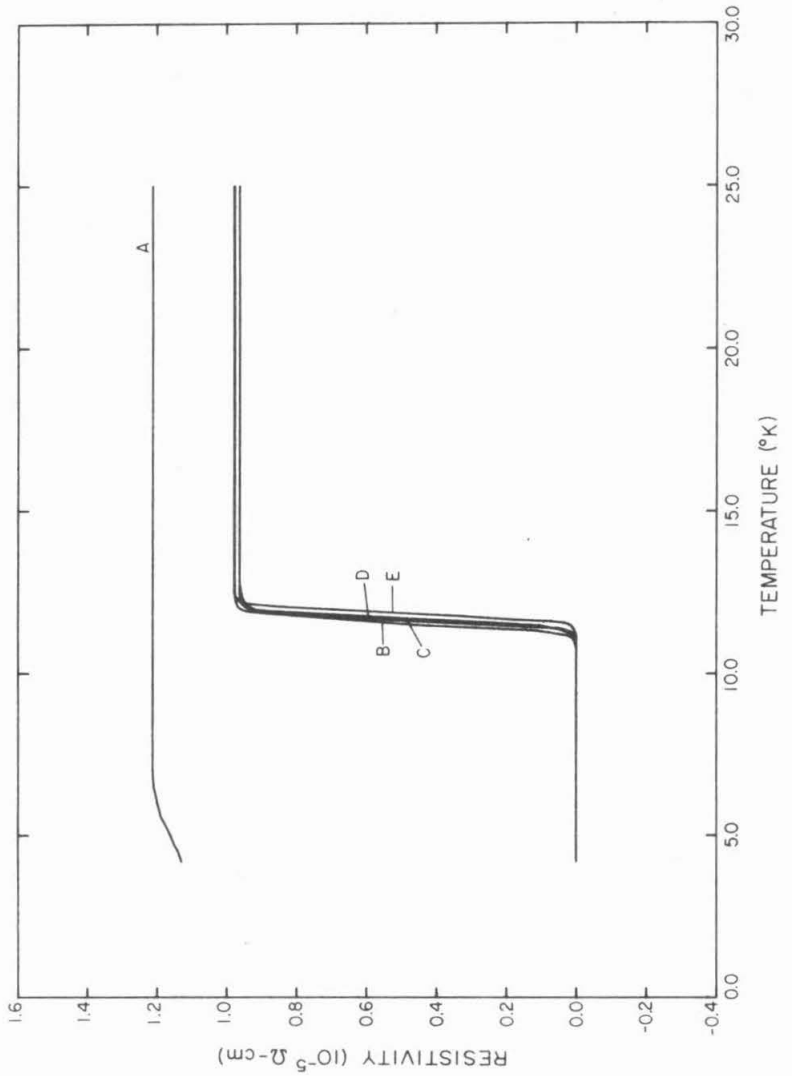

Figure 28. Electrical resistivities for $Cu_{80}V_{10}Ga_{10}$ specimens. A: as rolled. B, C, D, E: heat treated at 650°C for 12, 24, 49, 96 hours, respectively.

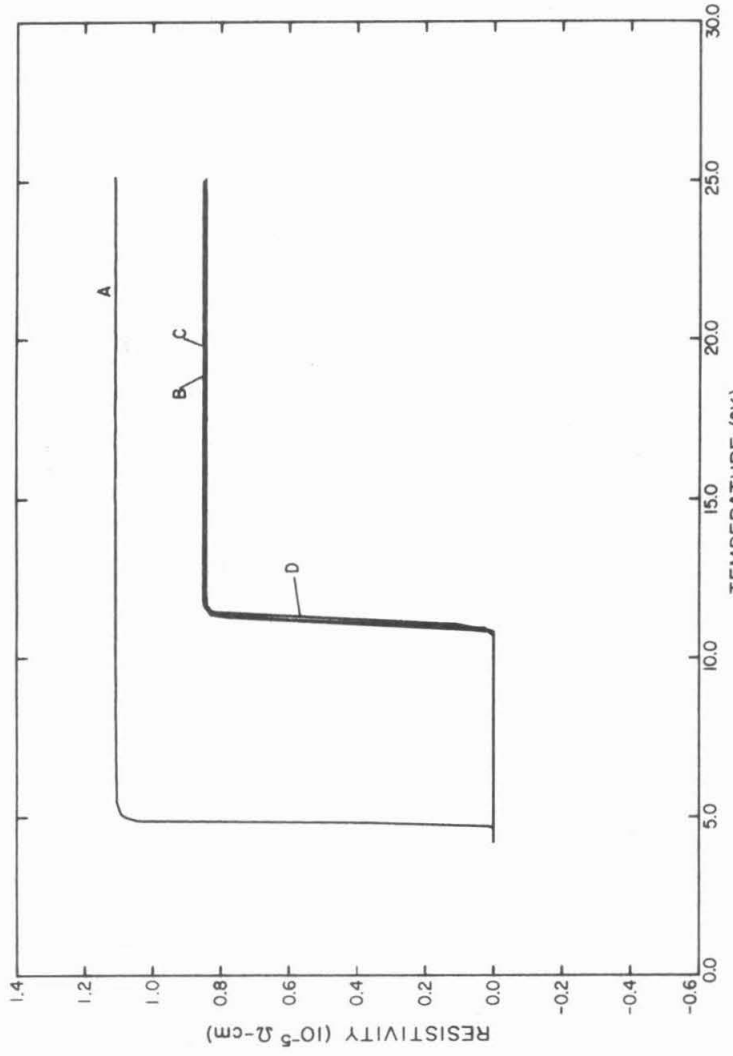

Figure 29. Electrical resistivities for 0.4 mm $Cu_{80}V_{10}Ga_{10}$ wire. A: as drawn. B, C, D: heat treated at 650°C for 12, 37, and 96 hours, respectively.

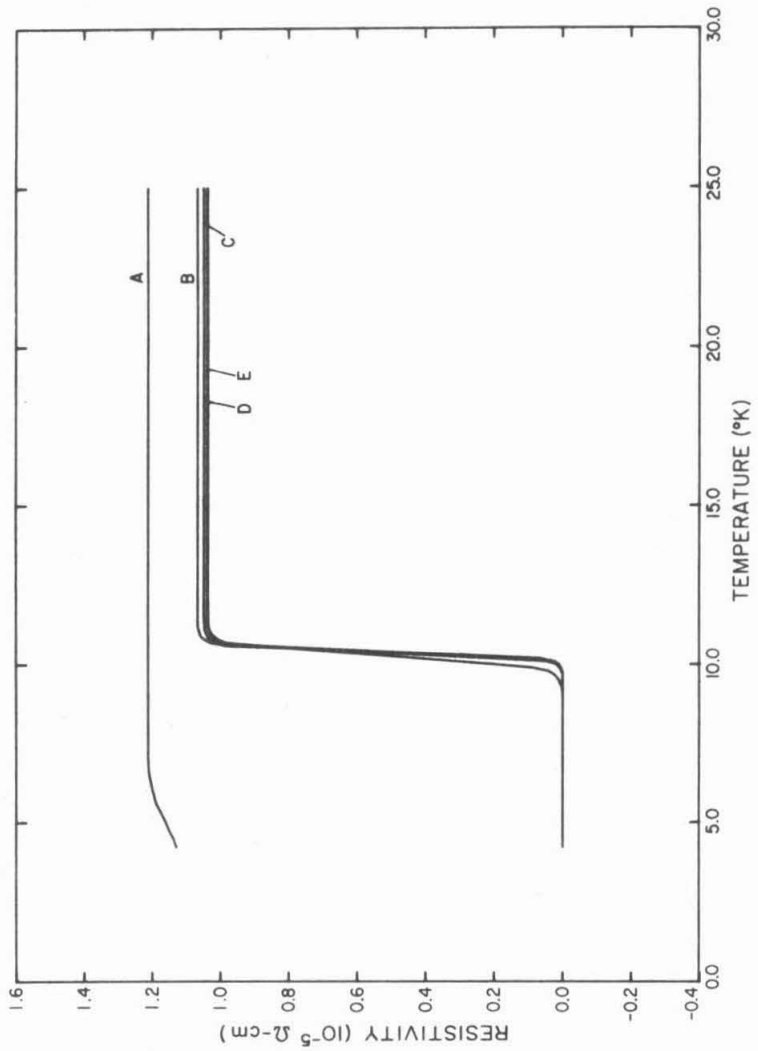

Figure 30. Electrical resistivities for $Cu_{80}V_{10}Ga_{10}$ specimens. A: as rolled. B, C, D, E: heat treated at 800°C for 4, 16, 36, 48 hours, respectively.

than other specimens with the same V concentration described above.

Figure 31 shows the measured electrical resistivities for $Cu_{77.5}V_{10}Ga_{12.5}$ rods annealed at 650°C for various lengths of time. The as-rolled specimen had a transition whose onset is about 9.0°K, but is not complete down to 4.2°K. The annealed specimens had complete transitions at 12.4°K (1 day annealing), 13.0°K (55 hours annealing), and 12.8°K (4 days annealing).

Figure 32 shows the measured electrical resistivities for $Cu_{77.5}V_{10}Ga_{12.5}$ rods annealed at 800°C for 6 hours and 1 day. They have complete transitions at 12.1°K (6 hours annealing) and 7.8°K (1 day annealing). Thus, it seems that prolonged annealing at high temperature tends to decrease the T_c.

Alloys with Ga concentrations higher than 13 at.% have been tried, but were found to be brittle, as mentioned before. Specimens in sheet form generally have the same T_c as specimens with the same composition but in rod or wire forms.

2.4 Alloys Containing 15 at.% and 20 at.% Vanadium. Figure 33 shows the measured electrical resistivities for $Cu_{75}V_{15}Ga_{10}$ rods annealed at 650°C or 800°C. The as-rolled specimen was not superconducting, but the annealed ones have complete transitions between 10.6°K and 12.0°K, depending on the annealing time and temperature. The specimens annealed at 800°C had lower T_c than those annealed at 650°C.

Figure 34 shows the electrical resistivities for $Cu_{70}V_{20}Ga_{10}$ rods annealed at 650°C. The annealed specimens have complete transitions at 11.8°K (1 day annealing), 12.0°K (2 days annealing),

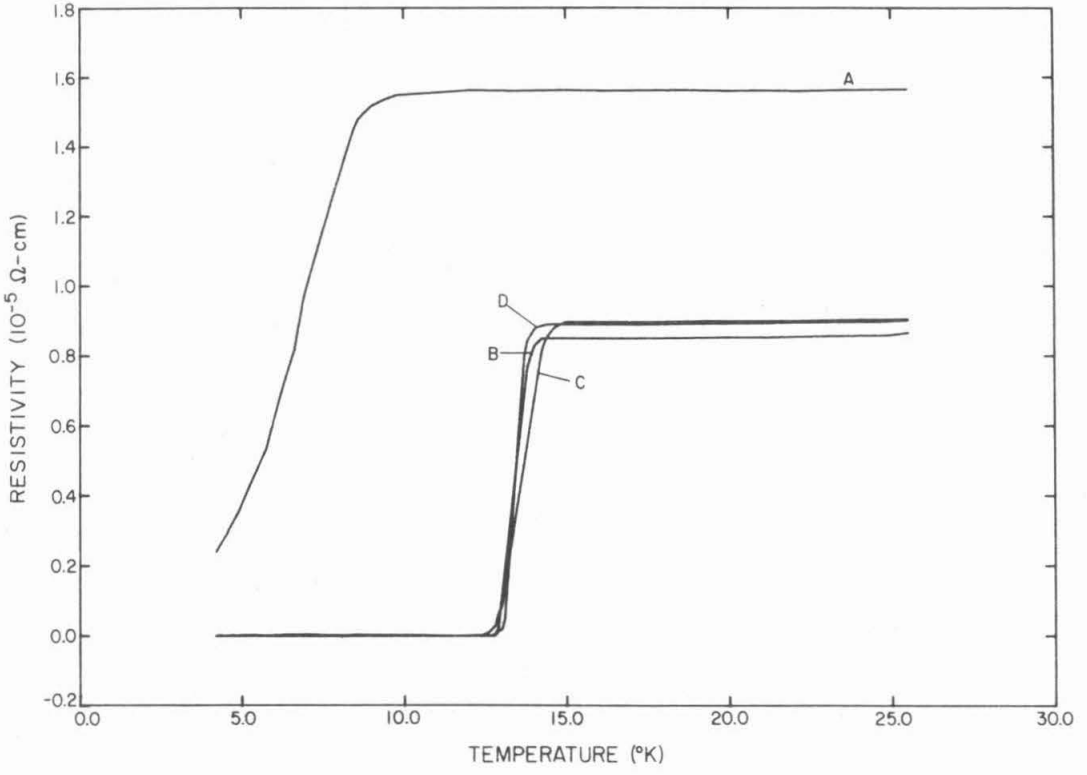

Figure 31. Electrical resistivities for $Cu_{77.5}V_{10}Ga_{12.5}$ specimens. A: as rolled. B, C, D: heat treated at 650°C for 24, 55, 96 hours, respectively.

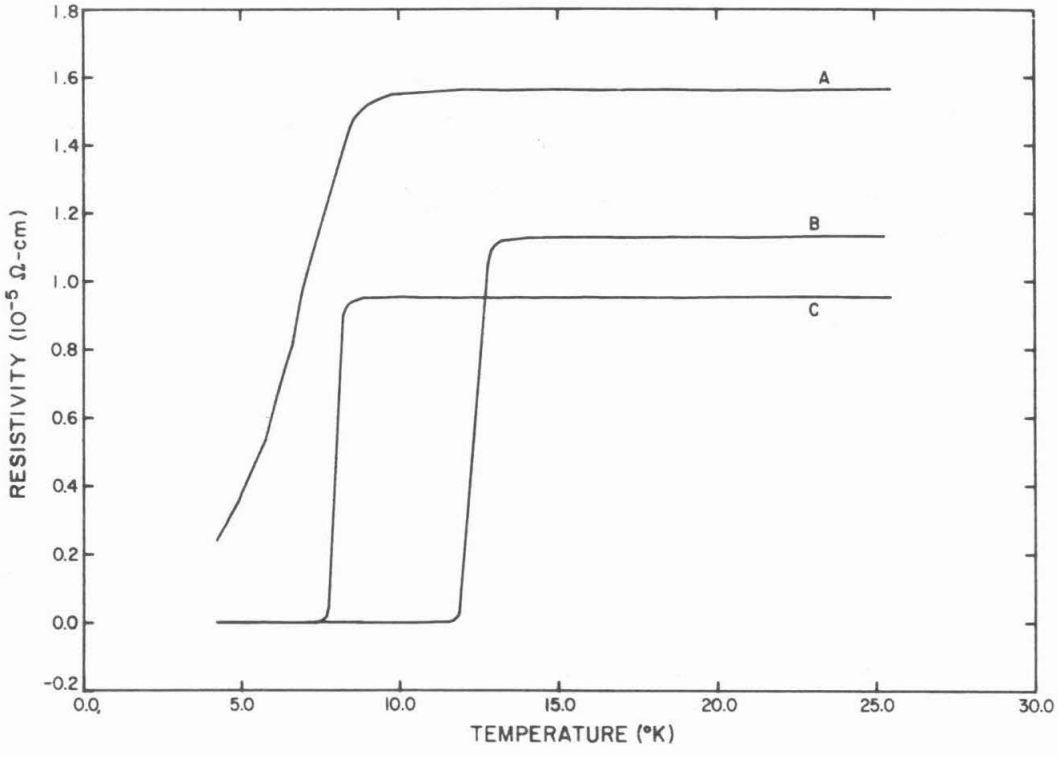

Figure 32. Electrical resistivities for $Cu_{77.5}V_{10}Ga_{12.5}$ specimens. A: as rolled. B, C: heat treated at 800°C for 6, 24 hours, respectively.

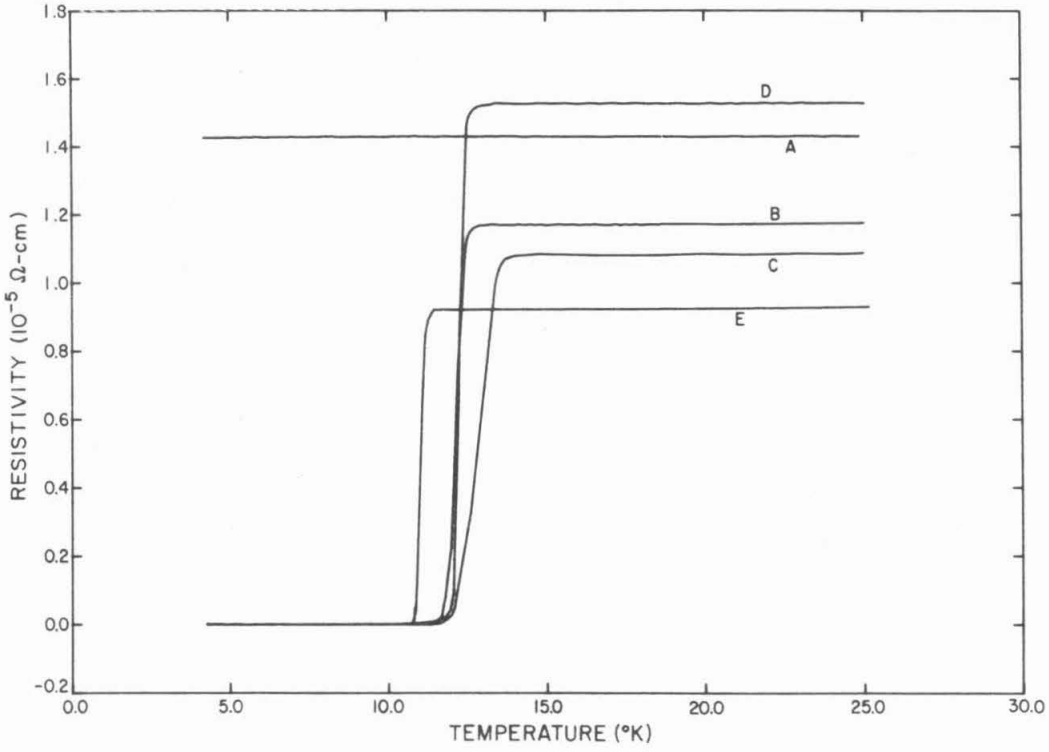

Figure 33. Electrical resistivities for $Cu_{75}V_{15}Ga_{10}$ specimens. A: as rolled. B, D, C: heat treated at 650°C for 1, 2, 4 days, respectively. E: heat treated at 800°C for 0.25 day.

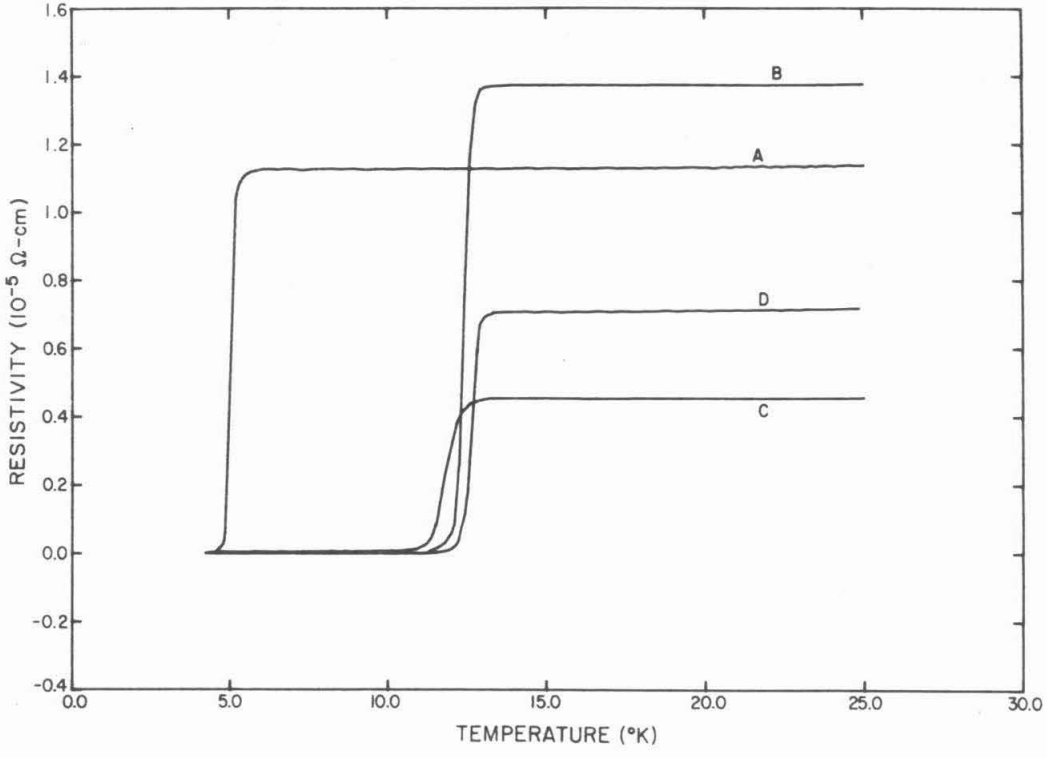

Figure 34. Electrical resistivities for $Cu_{70}V_{20}Ga_{10}$ specimens. A: as rolled. B, C, D: heat treated at 650°C for 1, 2, 4 days, respectively.

and 12.5°K (4 days annealing). There are significant variations of residual resistivities (the electrical resistivity above T_c), probably due to the fact that the rolled rod was not homogeneous and thus the actual composition of each specimen varies.

Figure 35 shows the electrical resistivities for $Cu_{70}V_{20}Ga_{10}$ rods annealed at 800°C. The T_c for the annealed specimens are close to 11.3°K, but again, the properties vary from specimen to specimen due to the inhomogeneity in the rods.

B. X-Ray Diffraction

Since in this study, x-ray diffraction was used mainly for phase identification, no serious attempt was made to make accurate determination of lattice constants. Moreover, since most specimens have been subjected to severe cold work in the rolling process, the x-ray diffraction lines were not sharp enough for accurate calculation of lattice constants. In general, an accuracy of ~0.01 Å can be obtained in the calculations. More emphasis has been put on Cu-V-Ga alloys.

1. Cu-V-Si Alloys. In general, more than 8 x-ray diffraction lines coinciding with the diffraction pattern of V_3Si have been identified in every specimen studied even before heat treatment. A number of lines matching with the diffraction pattern of V or Si can be found in general, depending on the specimen. As expected, the lines matching with that of Cu were dominant in intensity.

Table 3 summarizes the x-ray diffraction analysis for some of the Cu-V-Si alloys studied. In the table, the number of lines belonging to V_3Si, V, and Si patterns is indicated. The last two columns a_{V_3Si} and a_{Cu} stand for the lattice constants of the V_3Si phase and

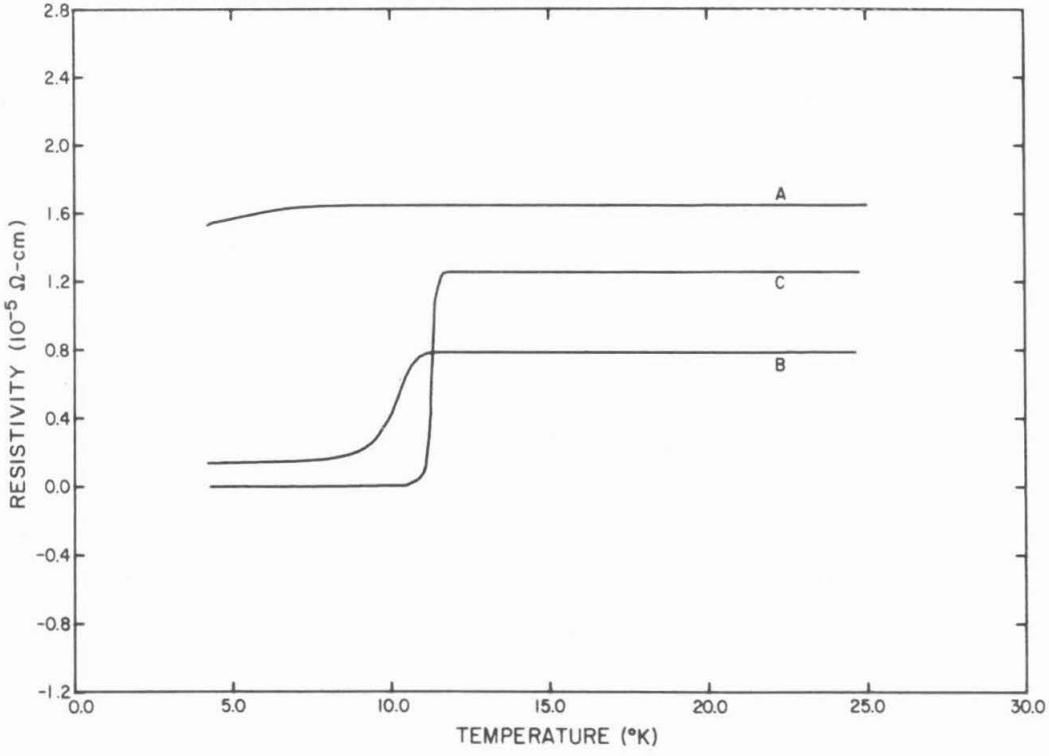

Figure 35. Electrical resistivities for $Cu_{70}V_{20}Ga_{10}$ specimens. A: as rolled. B, C: heat treated at 800°C for 5, 13 hours, respectively.

TABLE 3. X-Ray Diffraction Analysis of V-Si-Cu Alloys.

Composition	No. of V_3Si Lines	No. of V Lines	No. of Si Lines	a_{V_3Si} (Å)	a_{Cu} (Å)
$Cu_{95}V_{3.75}Si_{1.25}$	8	0	0	4.715	3.614
$Cu_{93}V_{5.25}Si_{1.75}$	8	2	5	4.727	3.616
$Cu_{90}V_{7.5}Si_{2.5}$	10	1	2	4.723	3.611
$Cu_{93.5}V_{3.75}Si_{1.25}Al_{1.5}$	9	1	1	4.728	3.625
$Cu_{88.5}V_{7.5}Si_{2.5}Al_{1.5}$	10	1	2	4.723	3.627

Cu phase in the alloy obtained by extrapolating the lattice constant derived from each line against the Nelson-Riley function. The lattice constants of V_3Si and Cu are 4.721 Å and 3.6150 Å, respectively[14,16].

From the results listed in Table 3, we can see that the compound V_3Si has been formed during the melting process. Some free V or Si can be found in some alloys.

2. Cu-V-Ga Alloys. X-ray diffraction analysis has been made on specimens containing more than 10 at.% vanadium. In contrast to the results for Cu-V-Si specimens, the as-rolled Cu-V-Ga specimens have no lines corresponding to V_3Ga phase in their diffraction pattern in general. But after annealing, lines with positions matching those of V_3Ga began to show up. In general, a few lines corresponding to vanadium are present in each specimen.

Table 4 summarizes the result of x-ray diffraction analysis of Cu-V-Ga alloys. The meanings of each column are similar to those in Table 3. The lattice parameters of the vanadium phase determined from films containing less than 4 vanadium lines are somewhat inaccurate. Also shown in the table are the conditions of heat treatment applied to the specimens before x-ray diffraction was taken.

From Table 4, we can see that V_3Ga phase has been formed in the process of annealing. The existence of vanadium lines indicates that the filaments might contain a vanadium core which has not reacted with gallium diffused from the matrix containing a solid solution of Cu and Ga. No lines corresponding to Ga have been identified, meaning that all the Ga in the alloy appears in the Cu-Ga solid solution and V-Ga solid solution before or after heat treatment.

TABLE 4. X-Ray Diffraction Analysis of V-Ga-Cu Specimens.

Composition	Heat Treatment (Temperature-Time)	No. of V_3Ga Lines	No. of V Lines	a_{V_3Ga} (Å)	a_V (Å)	a_{Cu} (Å)
$Cu_{80}V_{10}Ga_{10}$	as rolled	0	5	-	3.028	3.647
$Cu_{80}V_{10}Ga_{10}$	650°C - 48 hours	5	3	4.825	3.050	3.645
$Cu_{80}V_{10}Ga_{10}$	650°C - 96 hours	6	6	4.815	3.010	3.646
$Cu_{80}V_{10}Ga_{10}$	800°C - 27 hours	7	5	4.804	3.029	3.642
$Cu_{80}V_{10}Ga_{10}$	800°C - 48 hours	4	2	4.815	3.036	3.644
$Cu_{77.5}V_{10}Ga_{12.5}$	as rolled	0	2	-	3.029	3.654
$Cu_{77.5}V_{10}Ga_{12.5}$	650°C - 48 hours	6	4	4.836	3.037	3.650
$Cu_{77.5}V_{10}Ga_{12.5}$	800°C - 24 hours	4	1	4.810	3.637	3.642
$Cu_{75}V_{15}Ga_{10}$	as rolled	0	4	-	3.030	3.650
$Cu_{75}V_{15}Ga_{10}$	650°C - 48 hours	6	5	4.811	3.032	3.647
$Cu_{75}V_{15}Ga_{10}$	800°C - 11 hours	5	2	4.843	3.036	3.646
$Cu_{70}V_{20}Ga_{10}$	as rolled	0	5	-	3.029	3.647
$Cu_{70}V_{20}Ga_{10}$	650°C - 48 hours	8	4	4.840	3.034	3.651
$Cu_{70}V_{20}Ga_{10}$	650°C - 60 hours	6	3	4.878	3.03	3.652

C. Metallographic Studies

Cu-V-Si alloys have been studied by optical metallography only. Cu-V-Ga alloys have been studied more thoroughly; both optical metallography and scanning electron microscopy studies have been made on them. Some specimens have been examined with EDAX for the process of identifying their microstructure. Electron microprobe has also been used to study the distribution of various elements in some specimens.

1. Cu-V-Si Alloys. Figure 36 is the optical micrograph of the as-cast $Cu_{95}V_{3.75}Si_{1.25}$ specimen. The dendrites which precipitate out of the matrix are believed to be mostly V_3Si formed in the melting process. Their average dimension is about 15 μm. They were formed when the ingot was cooled from the melt on the silver boat.

Figure 37 shows the optical micrograph of the as-rolled $Cu_{95}V_{3.75}Si_{1.25}$ specimen in rod form. It can be seen that as the result of rolling, the dendrites were crushed and dispersed in the rolling direction. No continuous filament was formed in the rolled rod, in contrast to the Cu-V-Ga specimens in which relatively continuous filaments were formed as the result of rolling the ingot.

Figure 38 is the optical micrograph of the as-cast $Cu_{93.5}V_{3.75}Si_{1.25}Al_{1.5}$ alloy. The dendritic structure is more pronounced in this alloy than that in the as-cast $Cu_{95}V_{3.75}Si_{1.25}$ alloy.

Figure 39 is the optical micrograph of the as-rolled $Cu_{93.5}V_{3.75}Si_{1.25}Al_{1.5}$ specimen. Its microstructure is similar

Figure 36. Photomicrograph of an as-cast $Cu_{95}(V_3Si)_5$ specimen (750 ×).

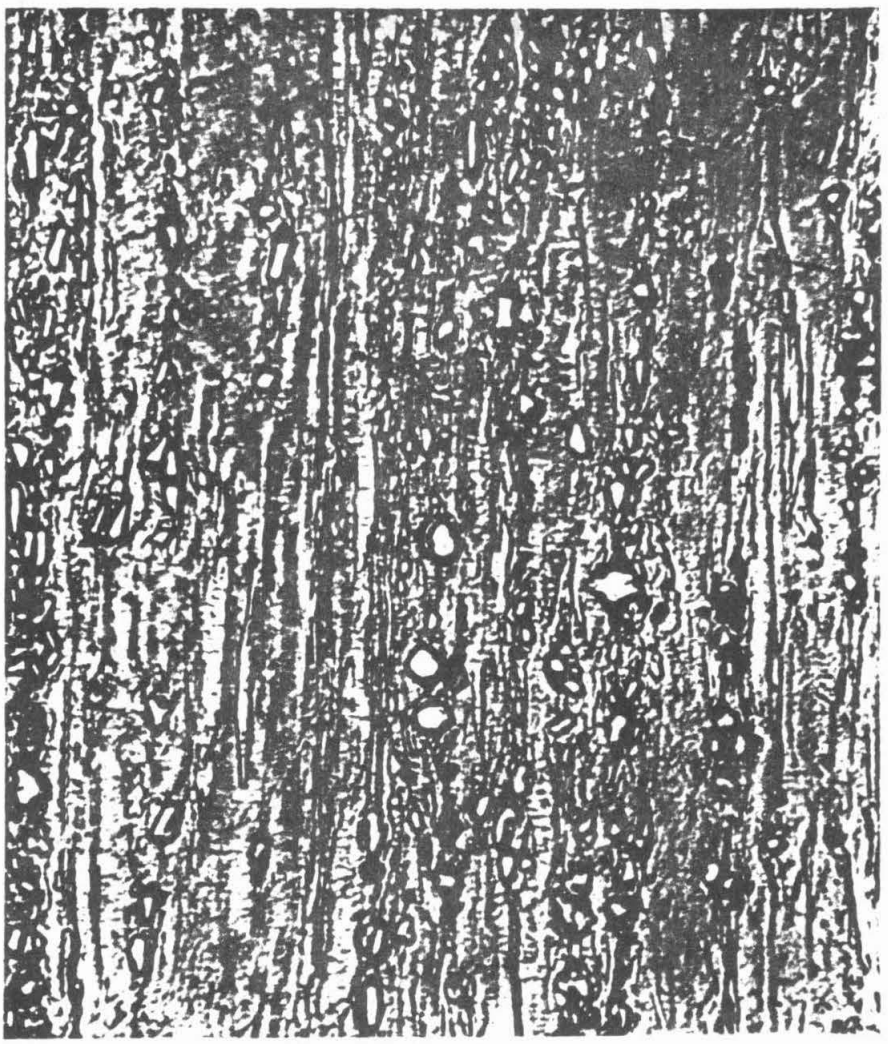

Figure 37. Photomicrograph of an as-rolled $Cu_{95}(V_3Si)_5$ specimen (750 ×).

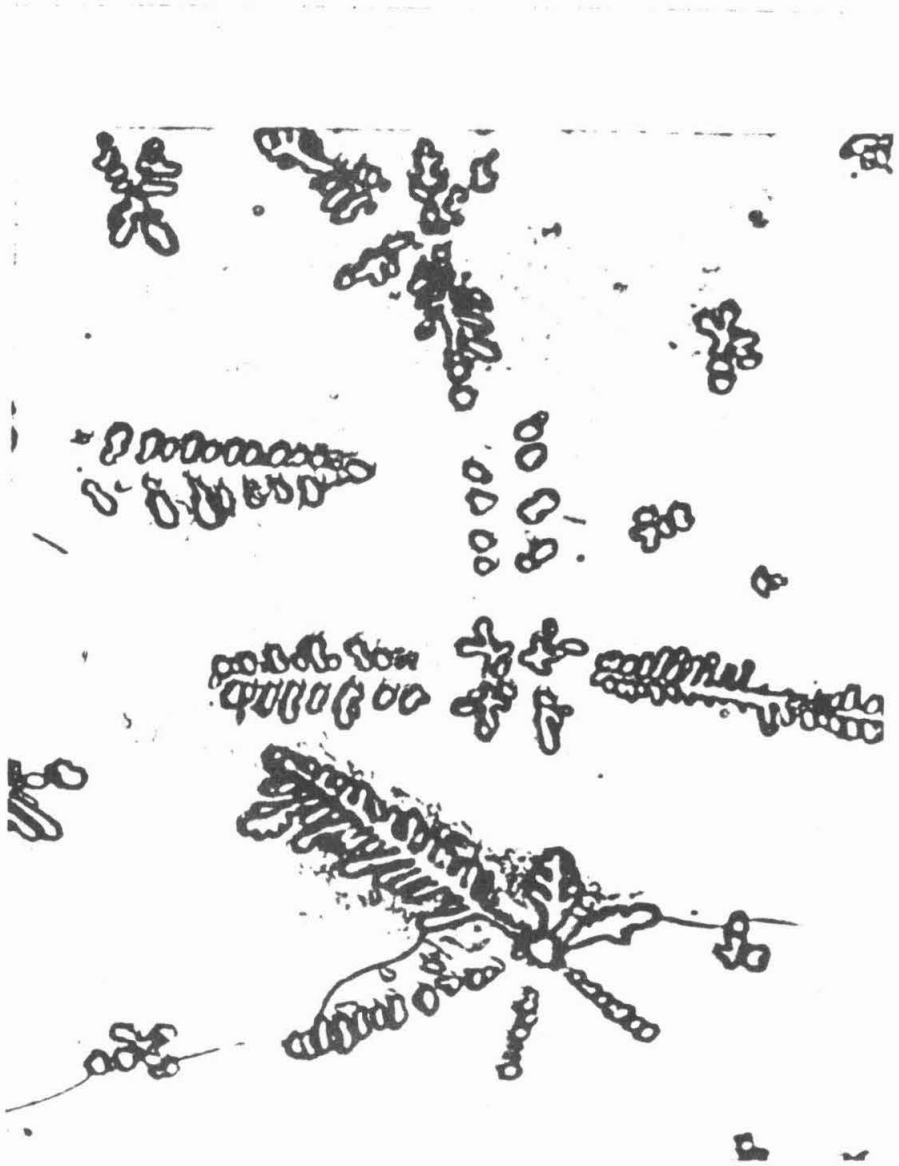

Figure 38. Photomicrograph of an as-cast $Cu_{93.5}(V_3Si)_5Al_{1.5}$ specimen (750 ×).

to that of the as-rolled $Cu_{95}V_{3.75}Si_{1.25}$ specimen. No continuous filament was formed as the result of rolling.

Metallographic studies made on specimens containing more V and Si have been made, and they were found to have similar microstructures. Thus, we can conclude that although V_3Si has been formed in the as-cast Cu-V-Si specimens, we cannot obtain continuous filaments by means of rolling the as-cast ingots into rods. This is due to the brittleness of the V_3Si dendrites formed in the matrix, and these dendrites are crushed into small particles during rolling.

2. Cu-V-Ga Alloys. Most of the effort was spent on alloys containing more than 10 at. % vanadium, since it was felt that they carry more current and thus are more important than alloys of other compositions.

Figure 40 is the optical micrograph for the as-cast $Cu_{80}V_{10}Ga_{10}$ specimen. The dendritic precipitates are composed mostly of vanadium, as can be identified with either the EDAX facility on the scanning electron microscope or by conventional x-ray diffraction studies. The average size of the dendrites is about 40 μm. The dendritic structure is similar to that in Cu-V-Si alloys.

Figure 41 is the optical micrograph of a $Cu_{80}V_{10}Ga_{10}$ rod annealed at 650°C for 2 days. It can be seen that the dendrites which were present in the as-cast specimen were ductile enough to be elongated into filaments in the rolling direction as the result of rolling the as-cast ingot into a rod. The cross-section reduction ratio obtained by the rolling process was about 50. The diameter of the filaments is about 3 μm. The filaments appear to be relatively continuous. This

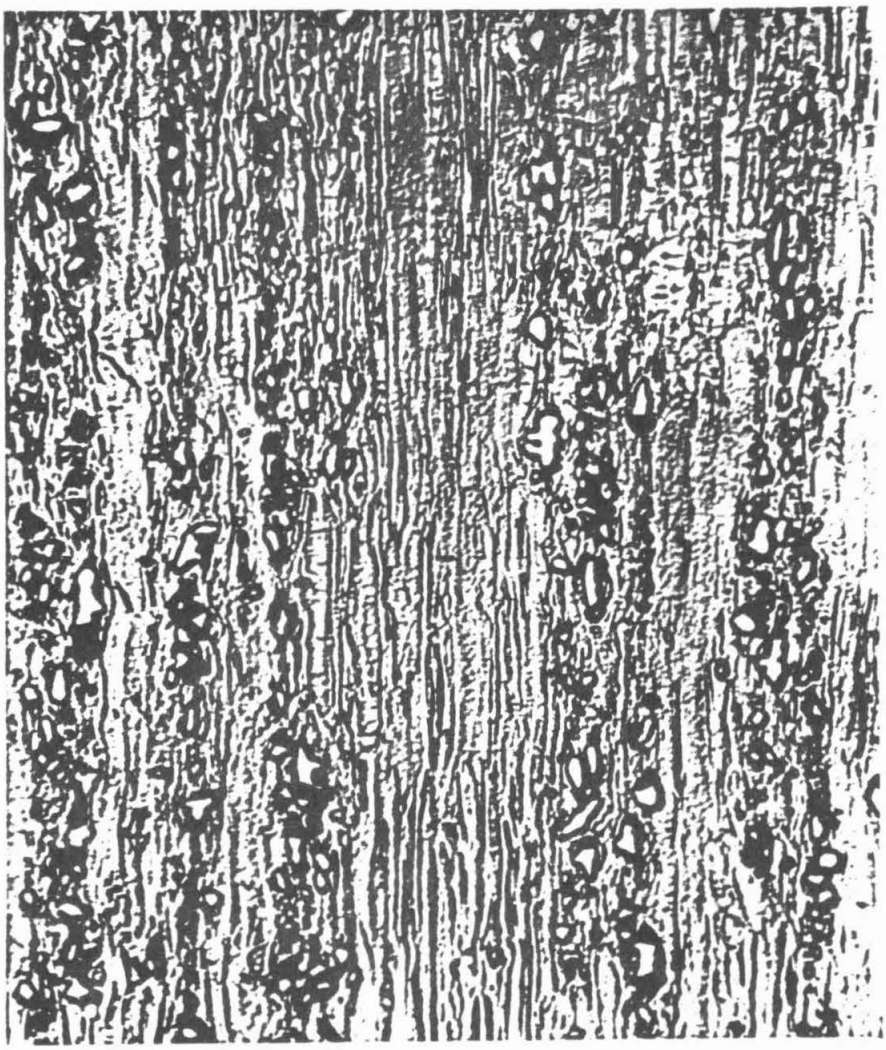

Figure 39. Photomicrograph of an as-rolled $Cu_{93.5}(V_3Si)_5Al_{1.5}$ specimen (750 ×).

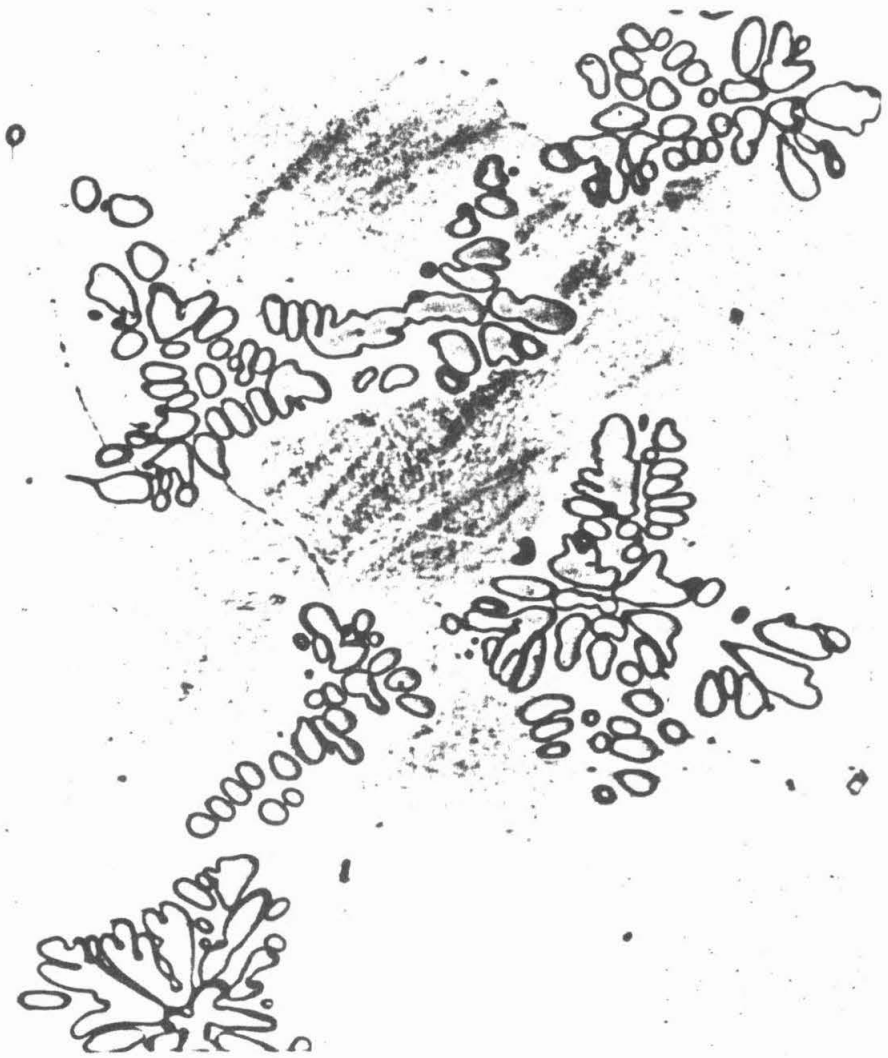

Figure 40. Photomicrograph of an as-cast $Cu_{80}V_{10}Ga_{10}$ specimen (750 ×).

Figure 41. Photomicrograph of a $Cu_{80}V_{10}Ga_{10}$ rod, heat treated at 650°C for 2 days (750 X).

agrees with the results of the electrical resistivity measurements in which sharp superconducting transitions were observed.

Figure 42 is a scanning electron micrograph of the as-cast $Cu_{80}V_{10}Ga_{10}$ specimen. EDAX was made on various parts of the specimen, and the dendrites were found to be mostly vanadium. The distribution of Ga in the specimen was difficult to determine even with the EDAX facility, since the secondary emission x-ray spectrum of Ga has peaks close to those of Cu, which is the dominant phase in the specimen. Furthermore, an accelerating voltage of 10 kV had to be used to examine the Ga distribution via the EDAX facility, but then the electron beam would penetrate to a depth of a few μm beneath the specimen surface, which is the typical dimension of the dendrites or filaments. Thus, the observed secondary emission spectrum may arise partly from the matrix under the structure to be studied. This fact further increased the difficulty in the determination of the Ga distribution with the EDAX facility; but the result of the microprobe analysis indicates that the Ga contained in the specimen appears to be uniformly distributed throughout the specimen. Figure 43 is the enlarged view of one of the dendrites obtained with the scanning electron microscope.

Figure 44 is a scanning electron micrograph of a $Cu_{80}V_{10}Ga_{10}$ rod which has been annealed at 650°C for 2 days. The excellent contrast of the scanning electron micrograph more clearly reveals the filamentary structure in the specimen. When attempts were made to follow the propagation of a group of filaments along the rolling direction, it was found that instead of abruptly terminating, the filaments

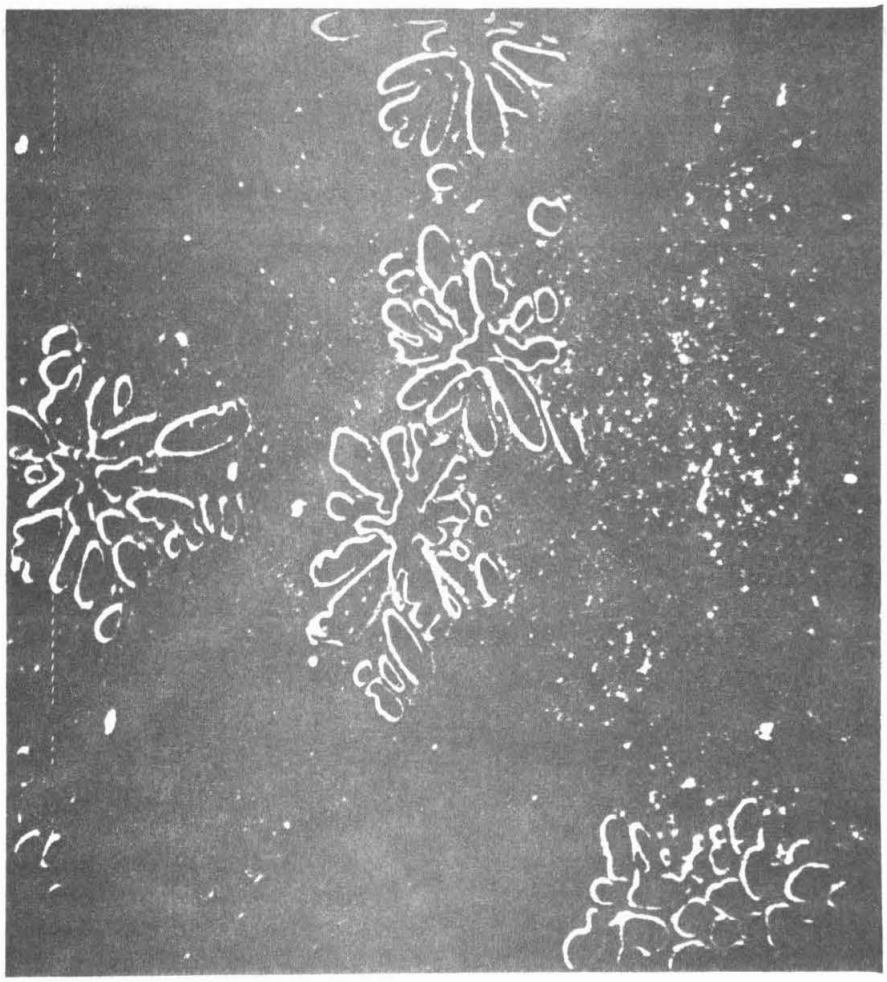

Figure 42. Scanning electron micrograph of an as-cast $Cu_{80}V_{10}Ga_{10}$ specimen (970 ×).

Figure 43. Scanning electron micrograph of an as-cast $Cu_{80}V_{10}Ga_{10}$ specimen, showing an enlarged view of a vanadium-rich dendrite (4800 ×).

Figure 44. Scanning electron micrograph of a $Cu_{80}V_{10}Ga_{10}$ rod heat treated at 650°C for 2 days (2050 X).

tended to terminate at locations where some globular structure is present. The typical size of these globules is about 10 μm in diameter, and sometimes they are ellipsoidal. Figure 45 is the scanning electron micrograph of the as-rolled $Cu_{80}V_{10}Ga_{10}$ specimen in which one of the globules can be seen. Some of the filaments are bent and bypass the globule while remaining continuous, but some are terminated at the globule itself. EDAX analysis indicates that these globules contain mostly vanadium. The actual determination of the compositions of the globules is quite difficult, but it is believed that they are compounds of V-Ga formed in the process of melting the ingot. These globules, which are not deformed during rolling, have a distinctive hardness when compared with the matrix or the V-Ga solid solution, which is quite soft and is elongated easily by rolling.

Figure 46 is a scanning electron micrograph of the $Cu_{80}V_{10}Ga_{10}$ rod showing the enlarged view of a typical globule. It can be seen that its surface consists of a shell of a few μm in thickness, which has a different texture from its center part.

Figure 47 is a scanning electron micrograph of the $Cu_{80}V_{10}Ga_{10}$ specimen in the form of wires of about 0.4 mm in diameter. Since the cross-section reduction ratio obtained by the drawing process for this wire is about 300, it is expected that the filaments in the wire would appear to be more continuous than those in the rod specimen, for which the cross-section reduction ratio is only about 50. This can be seen clearly from the micrograph. Typical diameter of the filaments is about 2 μm, which is also smaller than the filaments in the rod specimens.

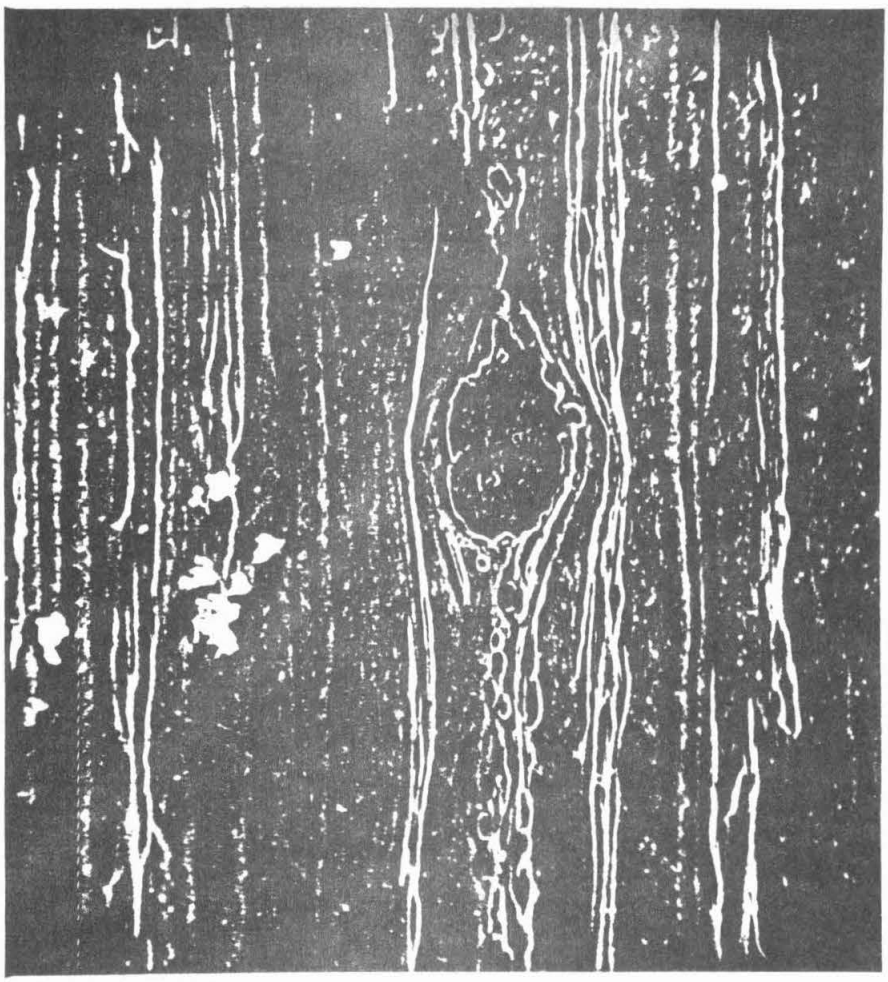

Figure 45. Scanning electron micrograph of an as-rolled $Cu_{80}V_{10}Ga_{10}$ rod, showing one of the vanadium-rich globules (1050 ×).

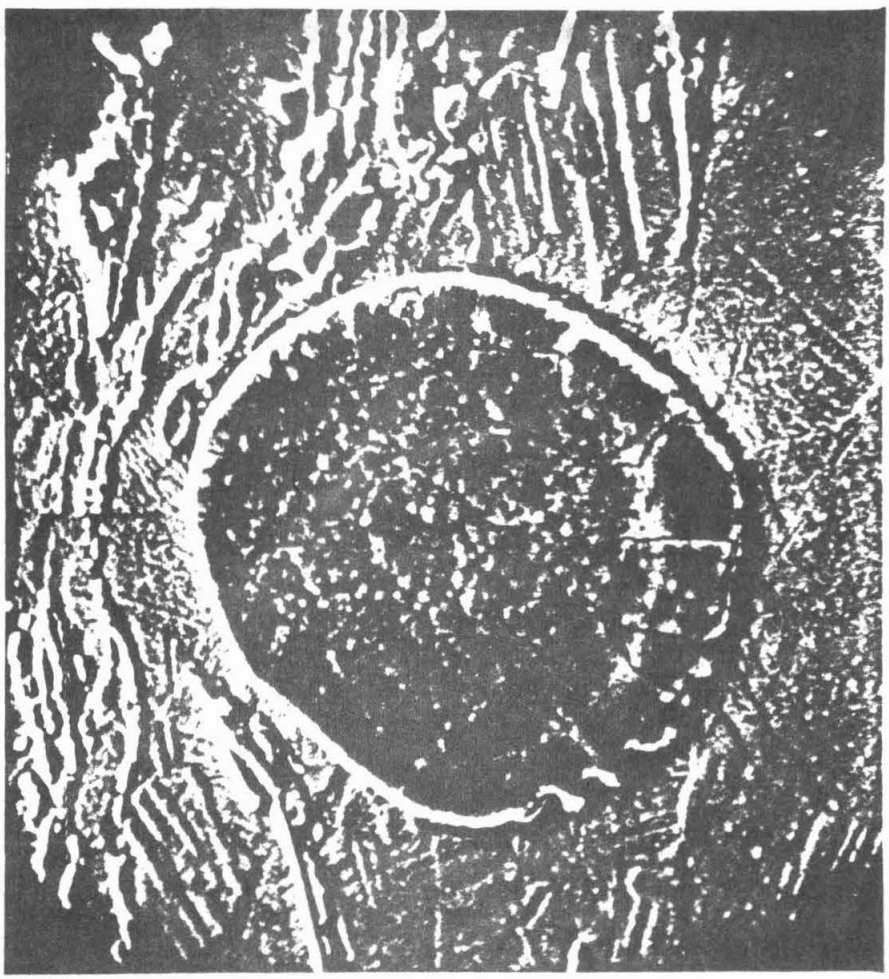

Figure 46. Scanning electron micrograph of a $Cu_{80}V_{10}Ga_{10}$ rod heat treated at 650°C for 2 days, showing an enlarged view of a globule (2050 ×).

Figure 47. Scanning electron micrograph of an as-drawn 0.4 mm $Cu_{80}V_{10}Ga_{10}$ wire (2350 ×).

Attempts to follow the propagation of these filaments were also made, and the filamentary structure was found to be similar to that in the rod specimen. There are also vanadium-rich globules present in the wire specimens, and groups of filaments also tend to terminate at these globules. Figure 48 is a scanning electron micrograph for the same wire specimen showing one of the globules, and the way filaments either terminate at or bend and bypass it.

Besides the large number of filaments, there are sometimes vanadium domains much larger in size present in the specimens. These domains are believed to arise from the fact that vanadium has a low solubility in Cu ,[15, 20, 21] and thus, in the process of melting the ingot, some vanadium may segregate into relatively large domains and remain so after the ingot has cooled down. After rolling, these domains were also elongated in the rolling direction and produced filaments of diameter much larger than those discussed previously. Figure 49 is an optical micrograph of the $Cu_{80}V_{10}Ga_{10}$ wire specimen (0.4 mm in diameter) in which one of the large vanadium filaments can be seen. The diameter of the filament is about 40 μm, and it extends a very long distance, nearly the entire length of the specimen which is about 2 cm.

Microstructures of specimens with different compositions have also been made. Figure 50 is a scanning electron micrograph of the as-cast $Cu_{77.5}V_{10}Ga_{12.5}$ specimen, showing dendritic structures similar to those in the $Cu_{80}V_{10}Ga_{10}$ specimens. Figure 51 is a scanning electron micrograph of the $Cu_{77.5}V_{10}Ga_{12.5}$ specimen which was annealed at 650°C for 2 days. The filamentary structure

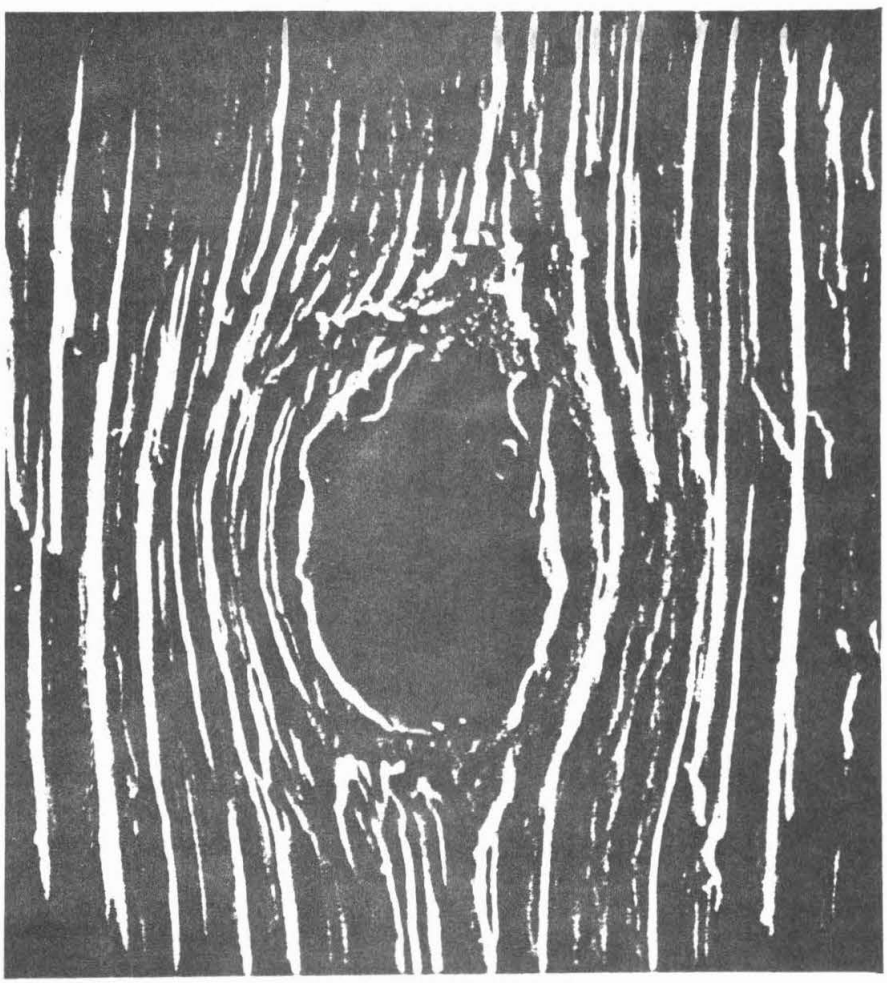

Figure 48. Scanning electron micrograph of an as-drawn 0.4 mm $Cu_{80}V_{10}Ga_{10}$ wire, showing a globule (2350 ×).

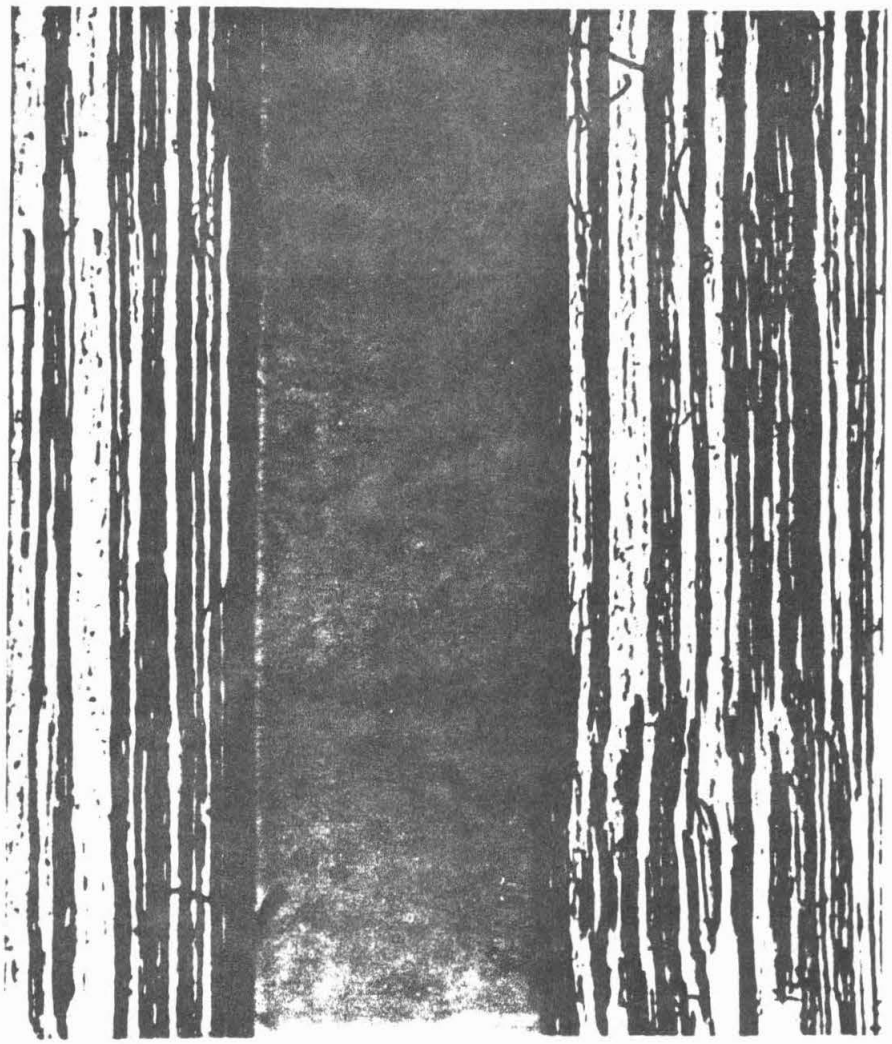

Figure 49. Photomicrograph of an as-drawn 0.4 mm $Cu_{80}V_{10}Ga_{10}$ wire, showing a vanadium-rich domain (750 x).

Figure 50. Scanning electron micrograph of an as-cast $Cu_{77.5}V_{10}Ga_{12.5}$ specimen (950 ×).

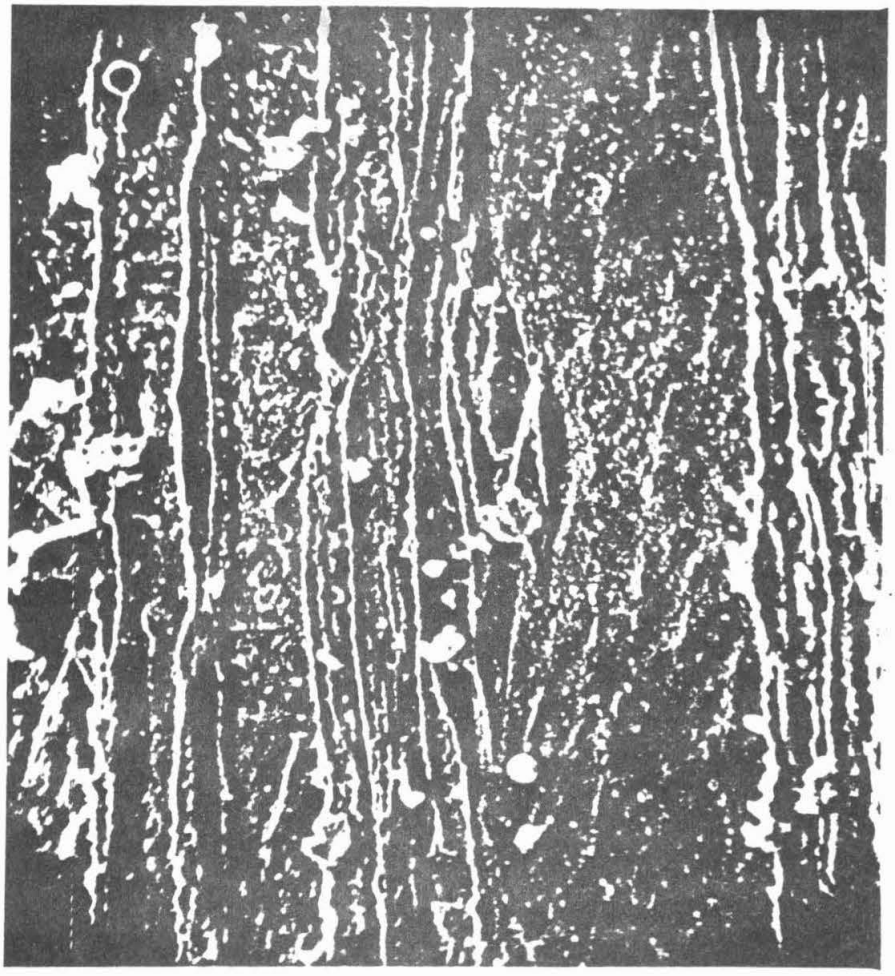

Figure 51. Scanning electron micrograph of a $Cu_{77.5}V_{10}Ga_{12.5}$ rod, heat treated at 650°C for 2 days (2000 x).

is also similar to that in the $Cu_{80}V_{10}Ga_{10}$ specimens; but microprobe analysis made on $Cu_{77.5}V_{10}Ga_{12.5}$ rods indicates that there have been variations in the Ga distribution before and after the annealing. In the as-rolled specimen, the Ga contained in the alloy appears to be uniformly distributed, whereas in the rod specimen which has been annealed at 650°C for 2 days, the Ga concentration at the location of the filaments appears to be higher, meaning that annealing caused some Ga to be extracted from the Cu-Ga matrix and diffused into the filaments, where it reacts with the vanadium to form V_3Ga. No quantitative analysis of the exact Ga distribution has been made, but presumably, with the electron microprobe this could be done.

Figure 52 is a scanning electron micrograph of a $Cu_{75}V_{15}Ga_{10}$ sheet which has been annealed at 650°C for 4 days. It can be seen that although the vanadium content in the specimen is high, there is no improvement on the continuity of the filaments. The filaments are relatively shorter than those in the specimens described previously. This may be due to the fact that the distribution of Ga among the Cu and V phases is that the V phase has higher hardness than the Cu phase; thus, the V dendrites are not elongated as the result of rolling.

Figure 53 is a scanning electron micrograph of a sheet $Cu_{70}V_{20}Ga_{10}$ specimen which has been annealed at 650°C for 4 days. The filaments are more continuous than those in $Cu_{75}V_{15}Ga_{10}$ specimens. Generally speaking, there are more globules and shorter filaments present in those specimens containing more than 10 at. % V than in specimens such as $Cu_{80}V_{10}Ga_{10}$. This is in agreement with the results of critical current measurements which will be discussed later.

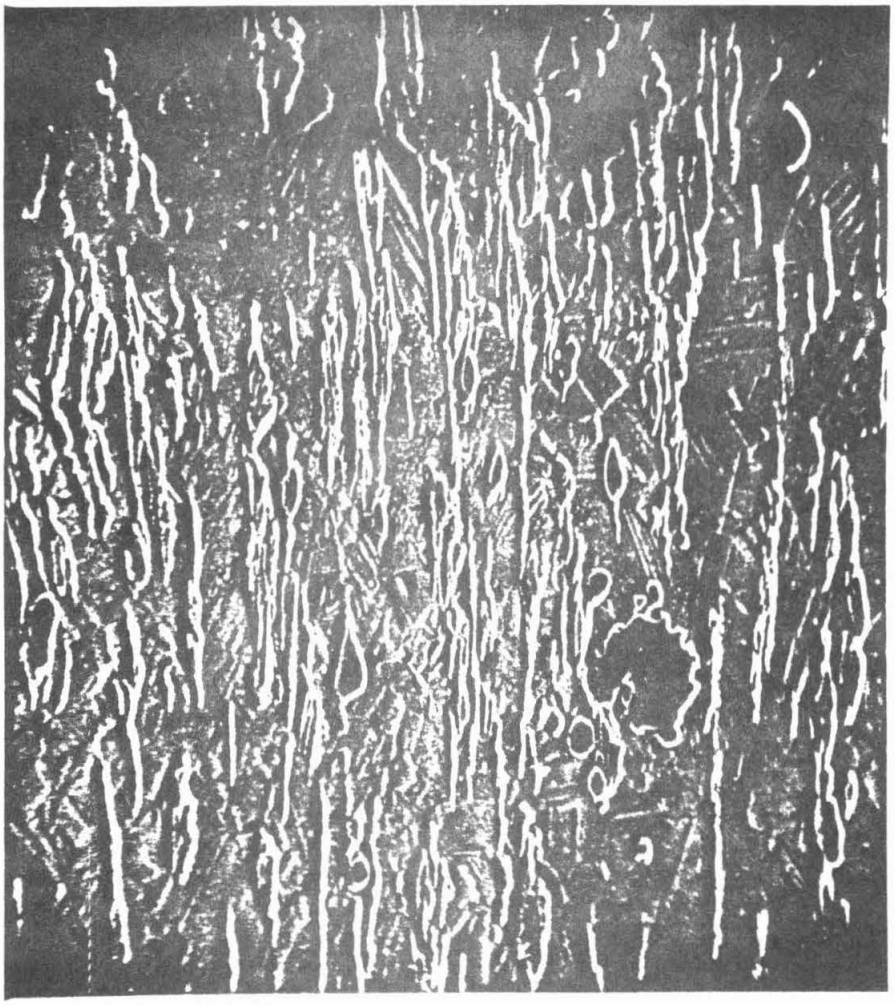

Figure 52. Scanning electron micrograph of a 0.25 mm $Cu_{75}V_{15}Ga_{10}$ sheet, heat treated at 650° for 4 days (600 ×).

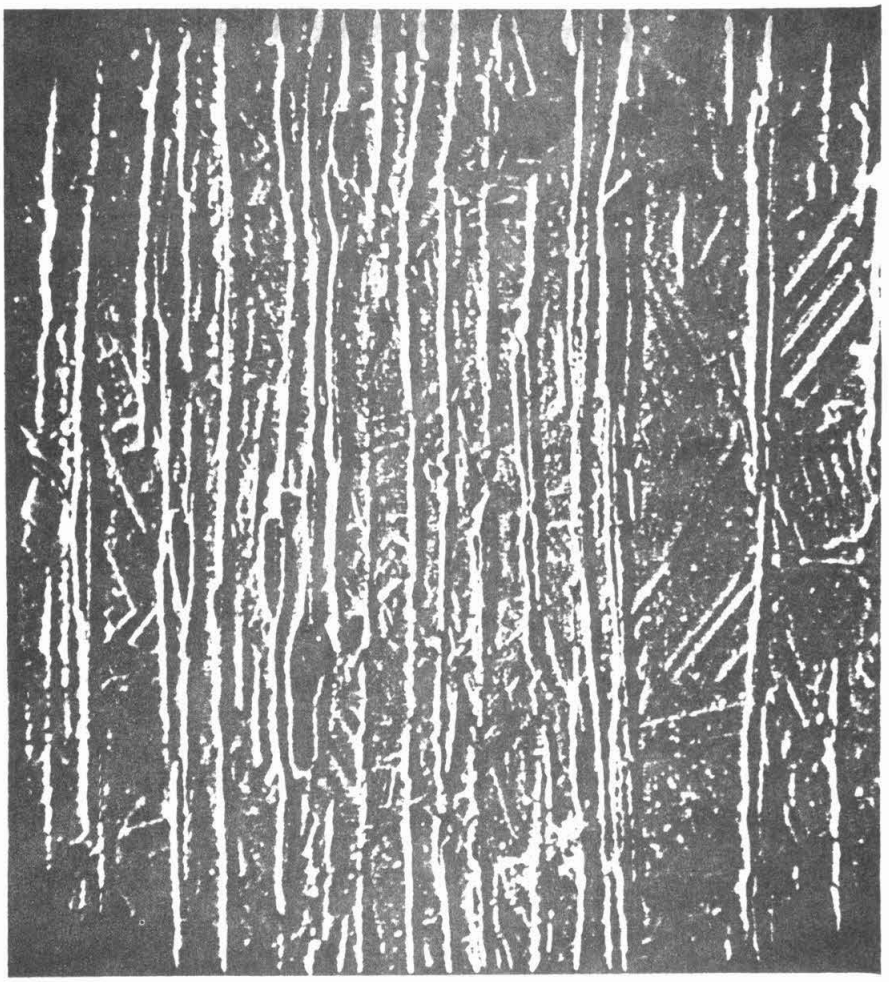

Figure 53. Scanning electron micrograph of a 0.25 mm $Cu_{70}V_{20}Ga_{10}$ sheet, heat treated at 650°C for 4 days (1130×).

D. Critical Current Density Measurements

The critical current densities of Cu-V-Ga specimens have been extensively studied. The critical current densities of Cu-V-Si specimens have not been measured; but some test for critical field was made, and it was found that the rod specimen $Cu_{80}(V_3Si)_{20}$, which was annealed at 900°C for 1 day and has the highest T_c for complete transition among all Cu-V-Si specimens studied, has a critical field exceeding 55 kG.

1. Critical Current Densities at Zero Field and Liquid Helium Temperature. The composition which has been studied most thoroughly is $Cu_{80}V_{10}Ga_{10}$, as early results indicated that specimens of this composition tend to have higher critical current densities than specimens of other compositions. Furthermore, it was found during the fabrication process that specimens of this composition had higher ductility, and thus seemed to be more promising for obtaining fine wires. Critical current densities of specimens with other compositions have also been measured. Compositions such as $Cu_{77.5}V_{10}Ga_{12.5}$, $Cu_{75}V_{15}Ga_{10}$, and $Cu_{70}V_{20}Ga_{10}$ have also been studied quite extensively.

Measurements have been made on specimens of various forms. These include wires, sheets, and rods. Since it is believed that the higher the degree of deformation applied to the specimen in the rolling or drawing process (meaning a larger reduction in cross section), the more the vanadium filaments are elongated; and thus, as a whole, the more continuous these filaments appear to be. As a consequence, the specimen is expected to be able to carry more super-current. Among

the three forms, wire specimens have the highest cross-section reduction ratio, which is about 300 for 0.4 mm wires, and 900 for 0.13 mm wires; thus, they are expected to have the best characteristic as far as current-carrying capacity is concerned. Next come the sheet specimens (cross-section reduction ratio about 100), and the rod specimens (cross-section reduction ratio about 50).

Table 5 lists some of the results of the critical current density J_c measurements made at 4.2°K and zero transverse magnetic field for some of the $Cu_{80}V_{10}Ga_{10}$ specimens. Also shown on the table are the form of the specimens, the annealing time, and annealing temperature at which the specimens have been heat treated prior to the measurements. The annealing temperature which has been used mostly in the heat treatment was 650°C. High-temperature annealing for prolonged periods of time was not applied, since it is believed that such heat treatment will reduce the current-carrying capacity[6, 17]. On the other hand, annealing at a temperature which is too low may reduce the reaction rate for the formation of V_3Ga. Thus, the three temperatures 600°C, 650°C, and 800°C were chosen. Only relatively short annealing time has been used for 800°C annealing.

It can be seen from Table 5 that one of the 0.4 mm wire specimens which has been annealed at 600°C for 2 days already has a critical current density as high as 8.18×10^3 A/cm^2. Annealing at 650°C for 4 days did not improve the critical current density. The same wire specimens annealed at 650°C for 1 day did not produce very high critical current density either. Also, as can be seen from Table 5, the variation in the magnitude of the critical current densities between

TABLE 5. Critical Current Densities Measured at 4.2°K and Zero Transverse Magnetic Field for Some of the $Cu_{80}V_{10}Ga_{10}$ Specimens.

Specimen Form	Cross-Section Reduction Ratio	Annealing Temperature (°C)	Annealing Time (hours)	J_c (10^3 A/cm^2)
rod	50	600	96	4.93
wire, 0.4 mm	300	600	48	3.77
"	300	600	48	3.53
"	300	600	48	8.18
"	300	600	48	4.09
wire, 0.4 mm	300	600	96	3.97
"	300	600	96	3.10
"	300	600	96	3.35
"	300	600	96	3.10
rod	50	650	24	2.15
wire, 0.4 mm	300	650	24	5.89
"	300	650	24	3.58
"	300	650	24	7.05
"	300	600	24	3.51
sheet	100	650	24	1.0
"	100	650	24	8.37
"	100	650	24	2.67
"	100	650	24	1.20
"	100	650	24	2.53
"	100	650	24	1.61
"	100	650	24	1.73
sheet	100	650	48	2.72
"	100	650	48	5.12
"	100	650	48	10.23
"	100	650	48	1.03
wire, 0.4 mm	300	650	48	3.09
"	300	650	48	2.75
"	300	650	48	7.49

TABLE 5. (Continued)

Specimen Form	Cross-Section Reduction Ratio	Annealing Temperature (°C)	Annealing Time (hours)	J_c (10^3 A/cm^2)
wire, 0.4mm	300	650	48	2.07
"	300	650	48	6.20
"	300	650	48	13.80
wire, 0.13 mm	900	650	48	9.69
"	900	650	48	13.00
"	900	650	48	13.80
"	900	650	48	8.78
"	900	650	48	16.90
"	900	650	48	5.13
"	900	650	48	3.11
"	900	650	48	1.44
sheet	100	650	96	1.18
wire, 0.4 mm	300	650	96	5.68
"	300	650	96	3.79
"	300	650	96	4.91
"	300	650	96	>28.5
"	300	650	96	>24.6
wire, 0.13 mm	900	650	96	4.30
"	900	650	96	3.15
"	900	650	96	5.22

different sheet specimens annealed at 650°C for 1 day can be as high as one order of magnitude.

From Table 5 it can be seen that as the annealing time has been increased to 2 days at 650°C, the critical current densities increased generally. Values exceeding 10^4 A/cm^2 can be obtained in many specimens. As expected, the 0.13 mm wire specimens produced higher values of J_c as a whole, which is in agreement with the reasoning that a high cross-section reduction ratio yields thinner but more continuous groups of filaments, and thus can produce specimens with higher critical current densities.

After the annealing time has been increased to 4 days at 650°C, the 0.4 mm wire specimens gave rise to much higher critical current densities than the 0.13 mm wire specimens. As can be seen in Table 5, J_c for 0.4 mm wires annealed at 650°C for 4 days can be as high as 2.9×10^4 A/cm^2, which is about the highest value ever obtained on Cu-V-Ga specimens so far. Possibly, this may be due to the fact that prolonged annealing caused Cu to diffuse into the very thin V_3Ga filaments (about 1 μm in diameter) in the 0.13 mm wire specimens and thus caused deterioration in its superconducting properties. On the other hand, vanadium filaments in the 0.4 mm wire specimens are larger in size, and it takes some extra time for the reaction of V_3Ga formation to be optimized.

Table 6 lists some of the results of the critical current density measurements made at 4.2°K and zero transverse magnetic field for specimens of compositions other than $Cu_{80}V_{10}Ga_{10}$. It can be seen from these two tables that the critical current densities for

TABLE 6. Critical Current Densities Measured at 4.2°K and Zero Transverse Magnetic Field for Some of the Specimens.

Specimen Composition	Specimen Form	Cross-Section Reduction Ratio	Annealing Temperature (°C)	Annealing Time (hours)	J_c (10^3 A/cm^2)
$Cu_{77.5}V_{10}Ga_{12.5}$	sheet	100	650	48	0.39
"	"	100	650	48	3.75
"	"	100	650	48	1.21
$Cu_{75}V_{15}Ga_{10}$	sheet	100	650	24	4.79
$Cu_{75}V_{15}Ga_{10}$	sheet	100	650	48	3.21
"	"	100	650	48	7.49
"	"	100	650	48	2.75
"	"	100	650	48	2.03
"	"	100	650	48	1.47
"	"	100	650	48	2.88
$Cu_{75}V_{15}Ga_{10}$	wire, 0.51 mm	230	650	48	1.80
"	"	230	650	48	2.30
"	"	230	650	48	3.20
"	"	230	650	48	2.50
"	"	230	650	48	4.35
$Cu_{75}V_{15}Ga_{10}$	sheet	100	650	96	0.46
"	"	100	650	96	2.44
"	"	100	650	96	2.89
"	"	100	650	96	1.99

TABLE 6. (Continued)

Specimen Composition	Specimen Form	Cross-Section Reduction Ratio	Annealing Temperature (°C)	Annealing Time (hours)	J_c (10^3 A/cm^2)
$Cu_{75}V_{15}Ga_{10}$	wire, 0.51 mm	230	650	120	1.50
"	"	230	650	120	0.77
"	"	230	650	120	2.60
"	"	230	650	120	0.86
$Cu_{75}V_{15}Ga_{10}$	sheet	100	800	7.5	1.55
$Cu_{75}V_{15}Ga_{10}$	sheet	100	800	11	2.37
"	"	100	800	11	1.08
"	"	100	800	11	0.42
"	"	100	800	11	2.09
$Cu_{70}V_{20}Ga_{10}$	sheet	100	650	24	1.81
"	"	100	650	24	3.56
$Cu_{70}V_{20}Ga_{10}$	sheet	100	650	48	1.82
"	"	100	650	48	3.82
"	"	100	650	48	2.76
"	"	100	650	48	3.65
"	"	100	650	48	2.42
"	"	100	650	48	3.47
"	"	100	650	48	0.47
"	"	100	650	48	0.45

TABLE 6. (Continued)

Specimen Composition	Specimen Form	Cross-Section Reduction Ratio	Annealing Temperature (°C)	Annealing Time (hours)	J_c (10^3 A/cm^2)
$Cu_{70}V_{20}Ga_{10}$	sheet	100	650	48	2.96
"	"	100	650	48	3.02
$Cu_{70}V_{20}Ga_{10}$	sheet	100	650	96	2.72
"	"	100	650	96	6.94
"	"	100	650	96	3.61
$Cu_{70}V_{20}Ga_{10}$	sheet	100	800	5	3.79
$Cu_{70}V_{20}Ga_{10}$	sheet	100	800	13	2.80
"	"	100	800	13	3.07
"	"	100	800	13	14.0

these specimens are generally not as high as those for the $Cu_{80}V_{10}Ga_{10}$ wire specimens. Except for occasional specimens, the critical current densities seldom exceeded 5.0×10^3 A/cm^2. It is believed that the change in the filamentary structure in these specimens discussed in Section C of this chapter may explain this result.

It can be noted from the results listed in Tables 5 and 6 that the specimen quality is not uniform as far as critical current density is concerned. Specimens taken from different sections of the same wire or sheet sometimes gave critical current densities differing by as high as a factor of 10. This may be due to the fact that in the process of melting the ingots and cooling them down, it is very difficult to achieve a uniform distribution in the local vanadium content in different regions of the ingot. Thus, after the rolling, different segments of the wire or sheet specimen may contain a different number of filaments. It is also hard to guarantee that the filamentary structure at different segments of the wire or rod is uniform.

From the results listed in Tables 5 and 6, we can see that the annealing temperature of 650°C and the annealing time of 2 to 4 days seem to be close to optimum. As expected, high-temperature annealing caused the critical current densities to go down. The reason why 650°C annealing caused the 0.13 mm wires to have relatively lower critical current densities than that of the 0.4 mm wires is not clear, but probably can be explained by the Cu-diffusion mentioned previously.

2. Critical Current Densities at Liquid Helium Temperature between 0 and 60 kG. Figures 54 and 55 show the measured critical

current densities J_c as a function of transverse magnetic field between 0 and 60 kG at 4.2°K. It can be seen that J_c for all the specimens decreased by about a factor of 10 when the magnetic field was increased from 0 to about 60 kG. It can be seen from both Figure 54 and Figure 55 that the 0.4 mm wires have better characteristics than the specimens of other forms. The value of J_c for sheet specimens tends to decrease faster with increasing field. One of the $Cu_{70}V_{20}Ga_{10}$ specimens in sheet form had a relatively high J_c at zero field, but its value decreased rapidly as the field was increased to 60 kG. The best characteristic ever achieved was from a 0.4 mm $Cu_{80}V_{10}Ga_{10}$ specimen which had been annealed at 650°C for 4 days.

Figures 56 and 57 show the measured voltage-current characteristics at different transverse magnetic fields for two of the specimens studied. The voltage can be interpreted as the potential drop created by the motion of flux vortex lines[1,23-25] or flux-flow resistivity. The specimen with higher critical current density which is shown in Figure 57 has much lower flux-flow resistivity than the specimen shown in Figure 56.

3. Critical Current Densities as a Function of Temperature. As mentioned previously, the critical current densities as a function of temperature were measured by the pulsed current method. Figure 58 shows the measured critical current densities as a function of temperature between 4.2°K and 13°K at two different values of transverse magnetic field (H = 0 kG and H = 8.4 kG) for a sheet specimen of $Cu_{80}V_{10}Ga_{10}$ annealed at 650°C for 1 day.

Figure 59 shows the measured J_c as a function of temperature

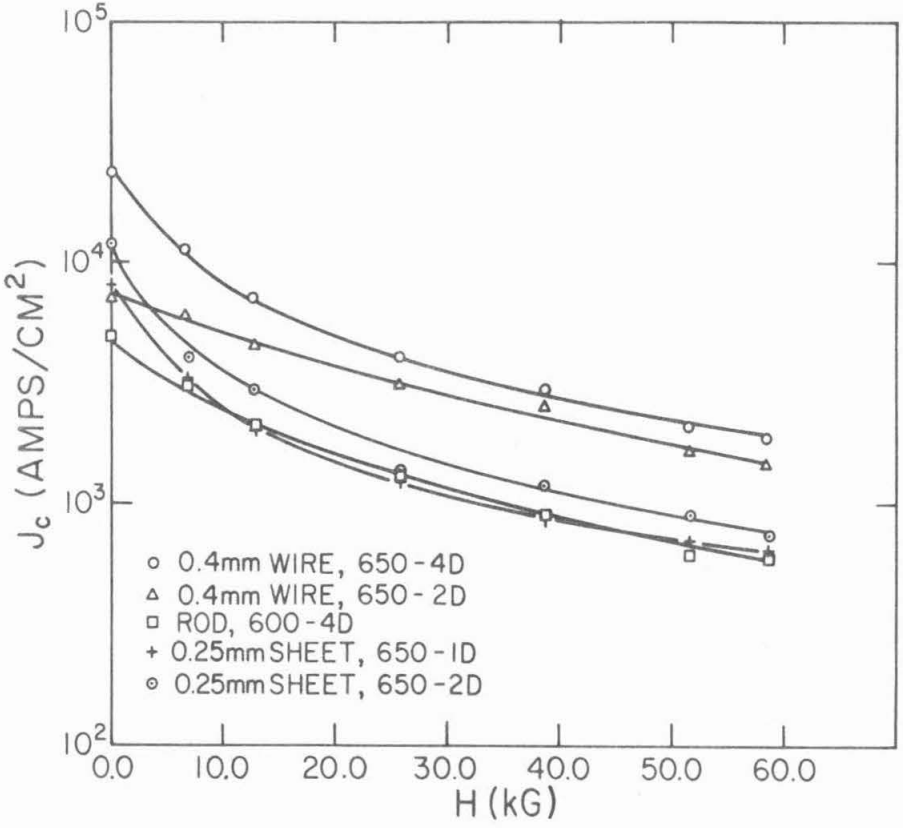

Figure 54. Critical current densities of some of the $Cu_{80}V_{10}Ga_{10}$ specimens as a function of transverse magnetic field.

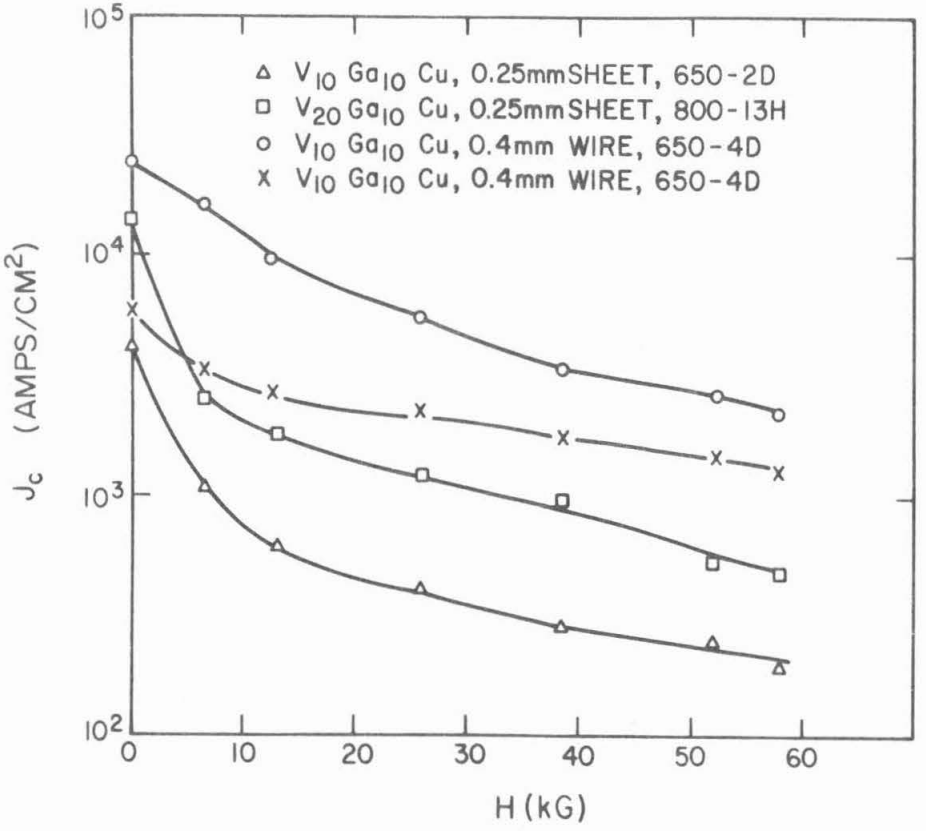

Figure 55. Critical current densities of some of the Cu-V-Ga specimens as a function of transverse magnetic field.

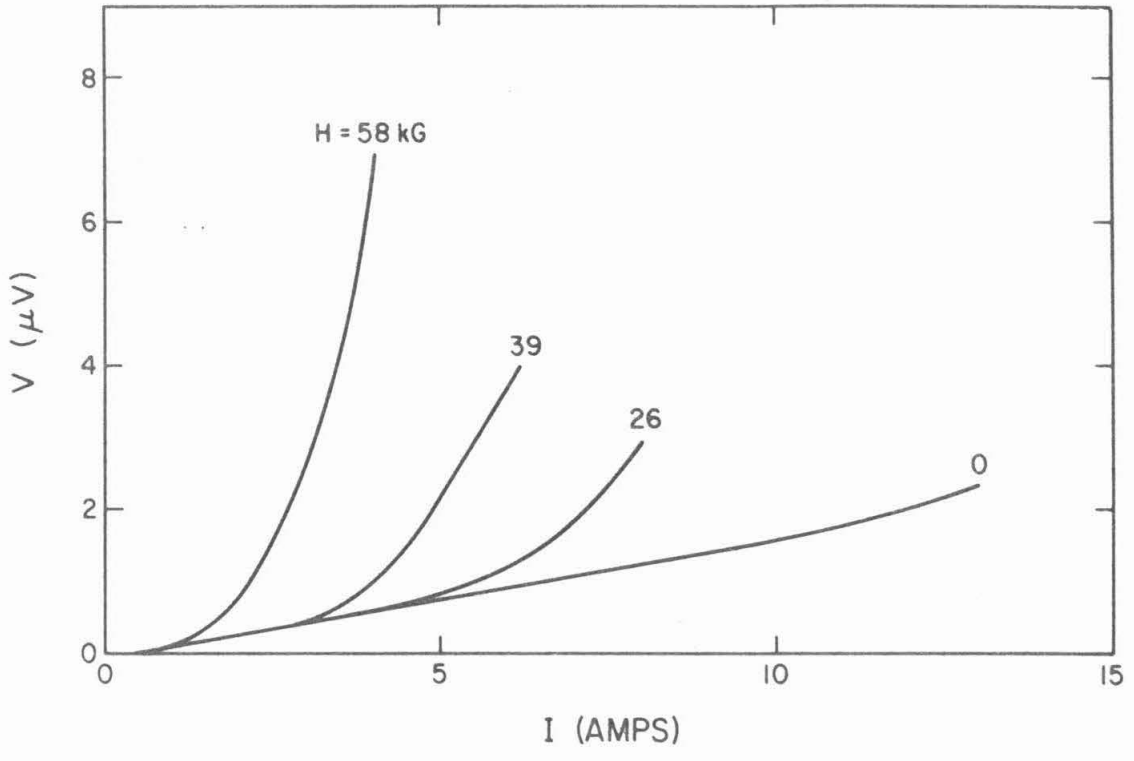

Figure 56. Current-voltage characteristic for a 0.4 mm $Cu_{80}V_{10}Ga_{10}$ wire, heat treated at 650°C for 2 days.

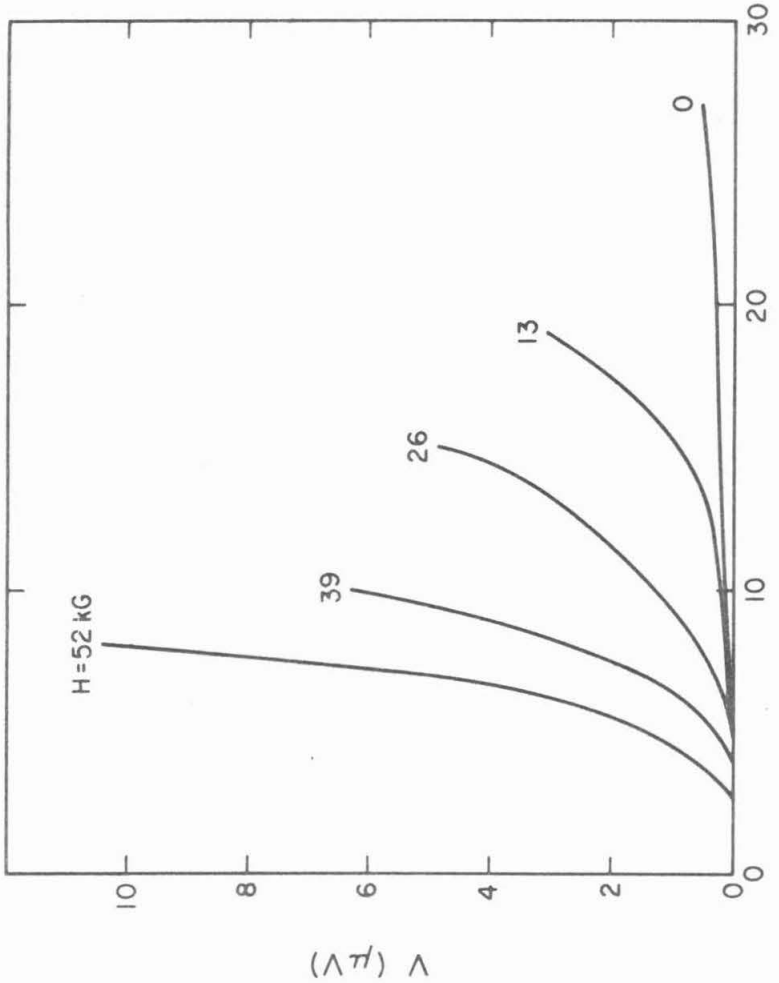

Figure 57. Current-voltage characteristic for a 0.4 mm $Cu_{80}V_{10}Ga_{10}$ wire, heat treated at 650^{0} for 4 days.

at three different values of transverse magnetic field for a 0.4 mm wire of $Cu_{80}V_{10}Ga_{10}$ which had been annealed at 600°C for 4 days. From Figures 58 and 59 we can see a steady decrease in J_c as the temperature or field was increased.

Figure 60 shows the results of the measured critical current densities as a function of temperature for some of the $Cu_{80}V_{10}Ga_{10}$ specimens. In agreement with the zero field measurements or the field dependence measurements made at 4.2°K, the best characteristic was obtained for a 0.4 mm wire of $Cu_{80}V_{10}Ga_{10}$ which had been annealed at 600°C for 4 days. All other specimens behaved similarly. As the temperature was increased, the critical current densities approached zero, while intersecting the $J_c = 0$ axis at temperature coinciding with the T_c of the specimen measured from their electrical resistivities.

One thing should be pointed out here. For specimens showing low flux-flow resistivities, the measured critical current densities by the pulsed current method may be higher than those measured with the DC current method at the same temperature. The criterion for the critical current in the DC method was that a voltage of 1 μV was developed across the potential leads of the specimen. However, for a low flux-flow resistivity specimen, the current required to produce a 1 μV signal may be lower than the current required to "quench" the specimen (i.e., to make the specimen transform into the normal state), which is the value of the critical current obtained with the pulsed current method.

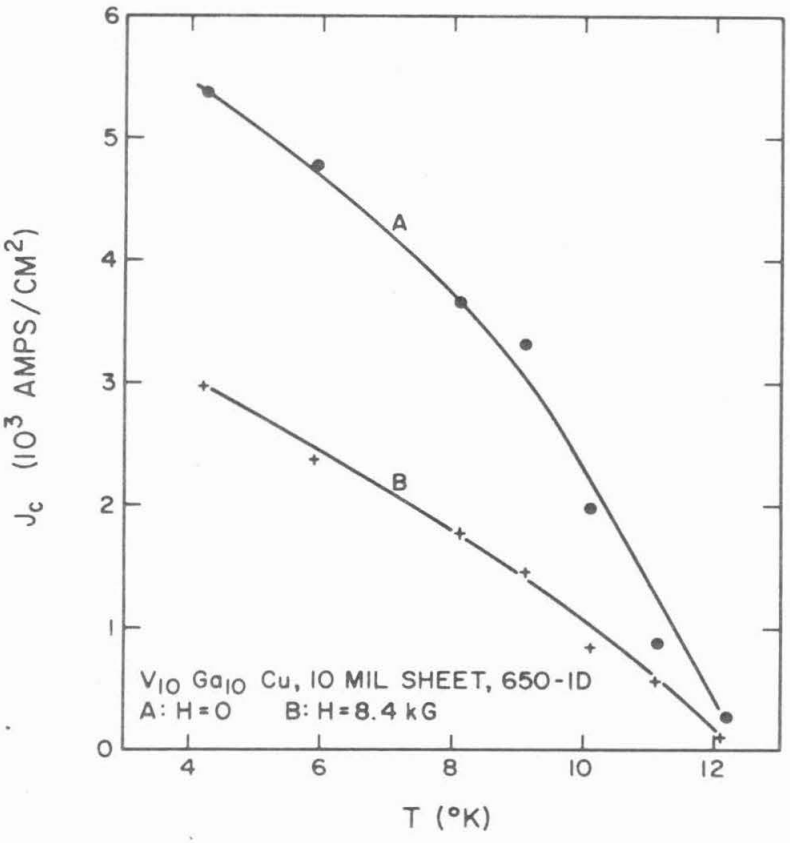

Figure 58. Critical current density as a function of temperature for a 0.25 mm $Cu_{80}V_{10}Ga_{10}$ sheet, heat treated at 650°C for 1 day. A: H = 0 kG, B: H = 8.4 kG.

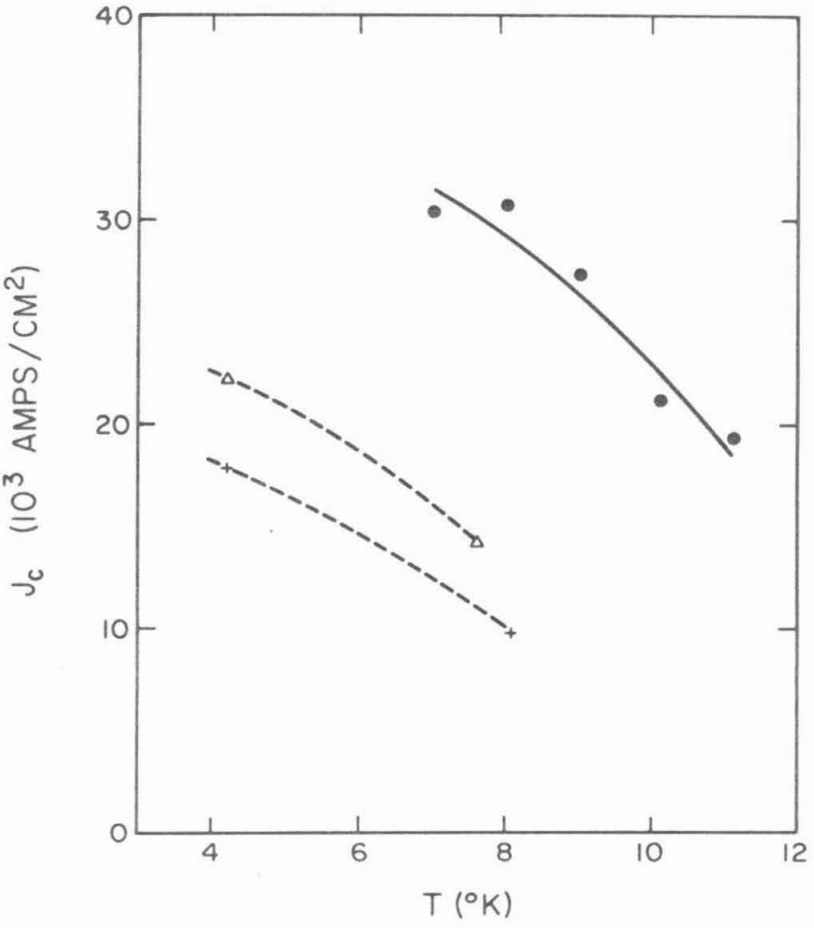

Figure 59. Critical current density as a function of temperature for a 0.4 mm $Cu_{80}V_{10}Ga_{10}$ wire, heat treated at 600°C for 4 days. Dot (·): H = 0 kG, triangle (△): H = 5 kG, cross (+): H = 8 kG.

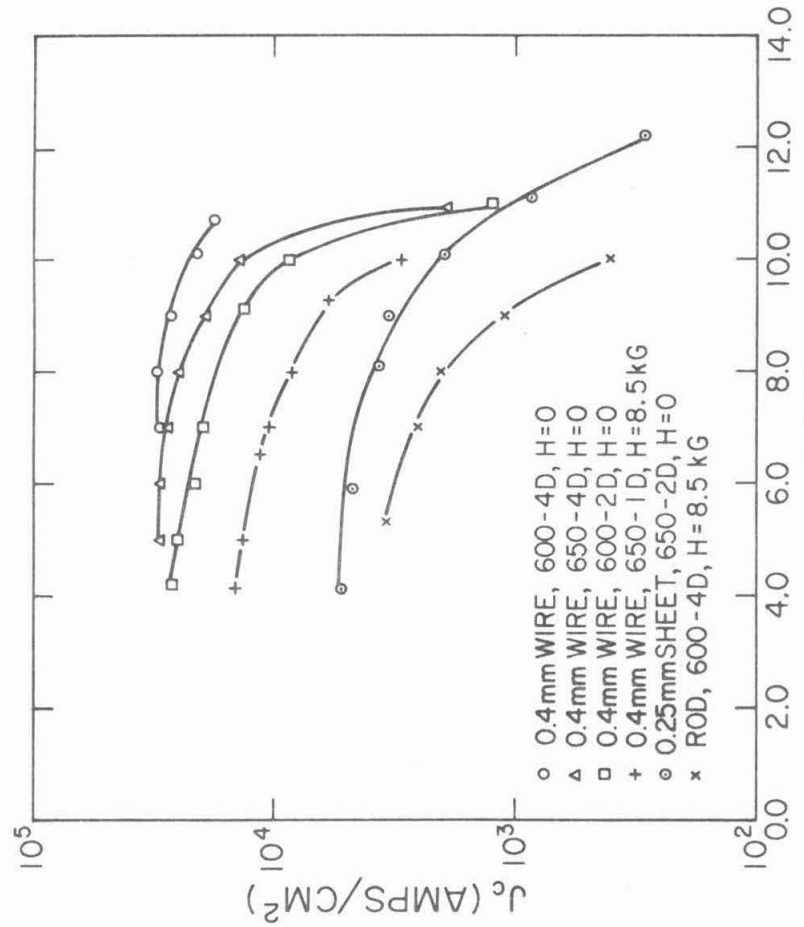

Figure 60. Critical current density as a function of temperature for some of the $Cu_{80}V_{10}Ga_{10}$ specimens.

E. Magnetization Measurements

Magnetization measurements have been made on a limited number of specimens only. Figure 61 shows the measured negative magnetization -M as a function of magnetic field from -6.0 kG to 6.0 kG. The measurement started at zero field, with field increasing in the positive direction until point A on Figure 61 was reached, where a sharp bending of the curve was observed corresponding to the H_{c1} of the specimen. As the magnetic field was further increased, the negative magnetization decreased steadily, showing the typical behavior of a type II superconductor[1, 22, 23], until point B was reached corresponding to the maximum available field with the Varian 6-inch magnet. As the field was decreased from point B, the negative magnetization changed sign and decreased rapidly, then followed a curve which looked like the mirror image of the curve AB until point C was reached; from here on, the negative magnetization started to return to the origin. When the field was increased in the reversed direction, the negative magnetization decreased steadily to point D, where the H_{c1} transition was again observed. The rest of the curve is similar to the inversion with respect to the origin of the part with field greater than zero.

The Faraday magnetometer may not be the ideal instrument for measuring the magnetization of the specimens studied in this work. As a result, the sections of the curve from C to D and from E to A are probably not reliable. This is because the electrobalance can only measure finite force, while the force acting on a specimen of volume V and magnetic susceptibility χ is[26]

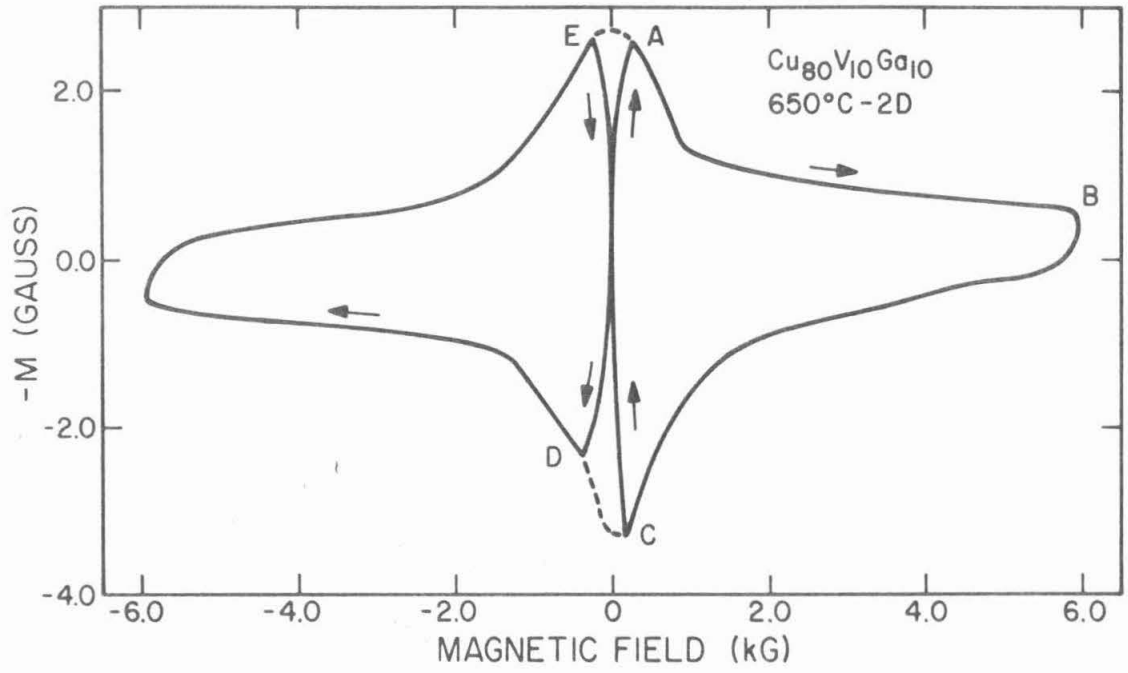

Figure 61. Magnetization as a function of field for a 0.25 mm $Cu_{80}V_{10}Ga_{10}$ sheet, heat treated at 650°C for 2 days.

$$F = \chi VH(dH/dx) \quad , \qquad (1)$$

where H is the magnetic field produced by the magnet, and (dH/dx) the gradient of H along the direction in which the force is measured. Since $M = \chi H$, we can see that the measured M is proportional to (dH/dx) , which goes to zero as H is decreased to zero. Thus, for zero applied magnetic field, the measured M is always zero, regardless of the real magnetization of the specimen. A more realistic picture can be obtained by joining points C - D and points E - A together; this type of behavior is to be expected for a type II superconductor with strong flux vortex pinning[1, 23, 24], in which category the $Cu_{80}V_{10}Ga_{10}$ specimens should belong.

A more revealing technique for measuring the magnetization for such materials is the integrating method[27, 28, 41], in which the output of a search coil containing the specimen is compared with the output of a matching empty coil, with both coils in the same magnetic field. The difference in the two signals is integrated with respect to time, resulting in a signal proportional to the magnetization in the specimen. No magnetization measurement has been made with the integrating method yet, but will be carried out in the near future.

IV. DISCUSSION

A. The Cu-V-Si Alloys

1. Phases present in the alloys. Before discussing the results of the present investigation, a brief review of the phase relationships in Cu-V-Si alloys is in order. The ternary phase diagram is, unfortunately, not known, but the three binaries V-Cu, Cu-Si, and V-Si have been investigated. These are reproduced in Figures 62, 63, and 64, respectively. Since Cu is the main constituent of the alloys studied, the important factors are the solubilities of Si and V in Cu, and then the possible formation of the superconducting phase V_3Si. The solubility of Si in Cu is relatively high (10 at. % at 600°C), but that of V is rather low (below 0.5 at. % at 900°C). After melting, it is therefore logical to expect that the Si will be in solid solution, but, at least in alloys containing V, the V will be present as a second phase. From the results described in Chapter III, it is also found that a certain amount of the V_3Si phase exists after melting.

As mentioned in Chapter III, although there are evidences that V_3Si has been formed in the process of casting the Cu-V-Si ingots, complete superconducting transitions have been observed for a limited number of specimens only. This can be explained by the results obtained from microstructure studies made on some of the specimens (Figures 37 and 39), which show clearly that no continuous filaments have been formed as the result of rolling the ingots into rods. Thus, although there is a superconducting phase with high transition temperature in the specimen, the superconducting phase exists either in the form of dendritic particles about 20 μm in size for the as-cast speci-

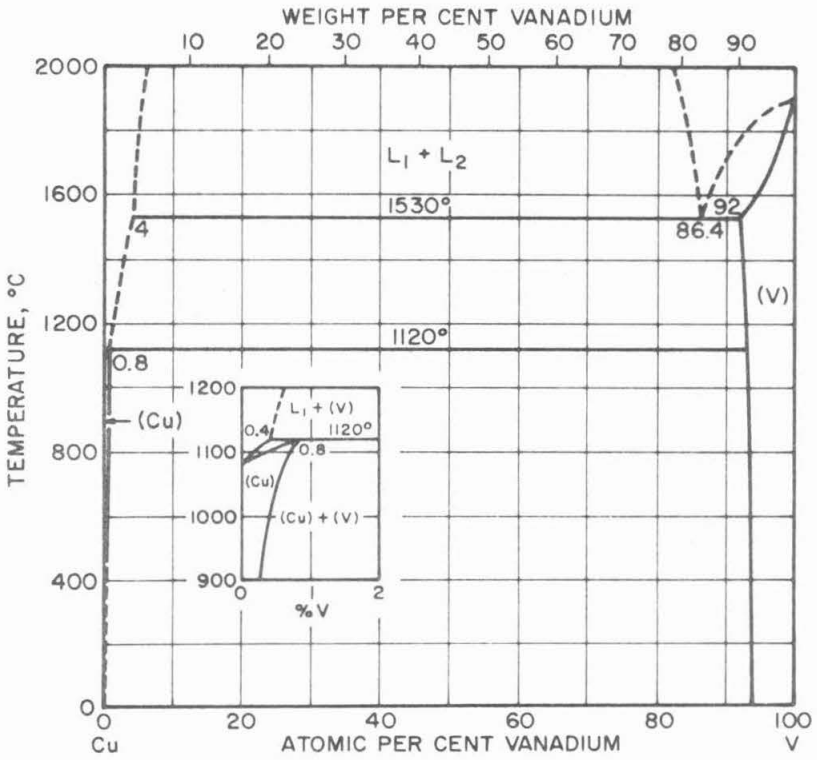

Figure 62. Equilibrium phase diagram for the Cu-V binary system.

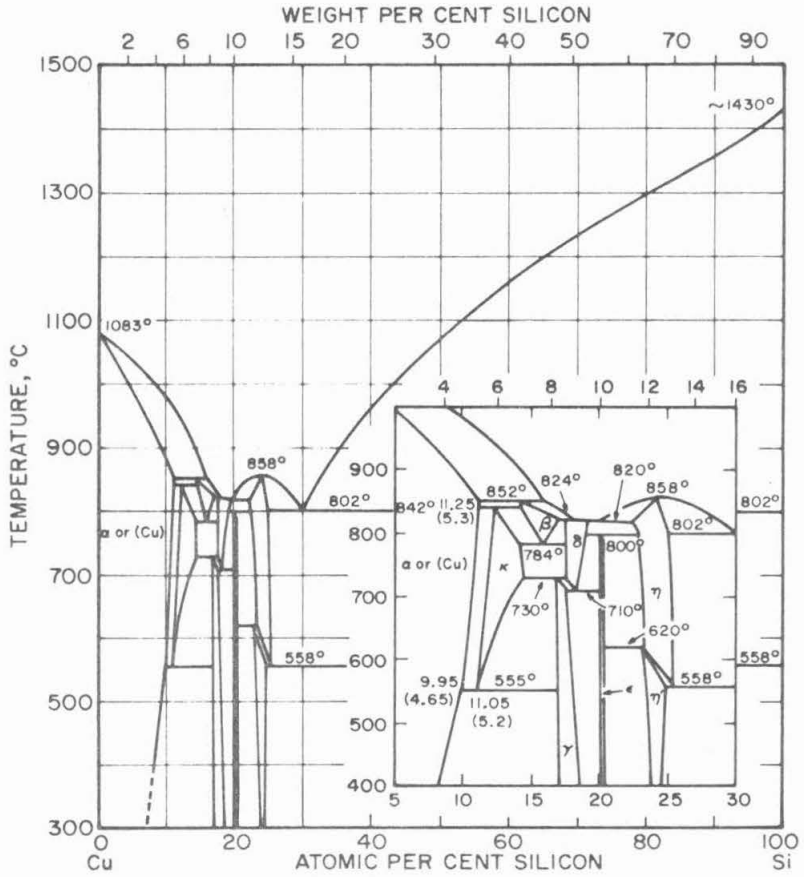

Figure 63. Equilibrium phase diagram for the Cu-Si binary system.

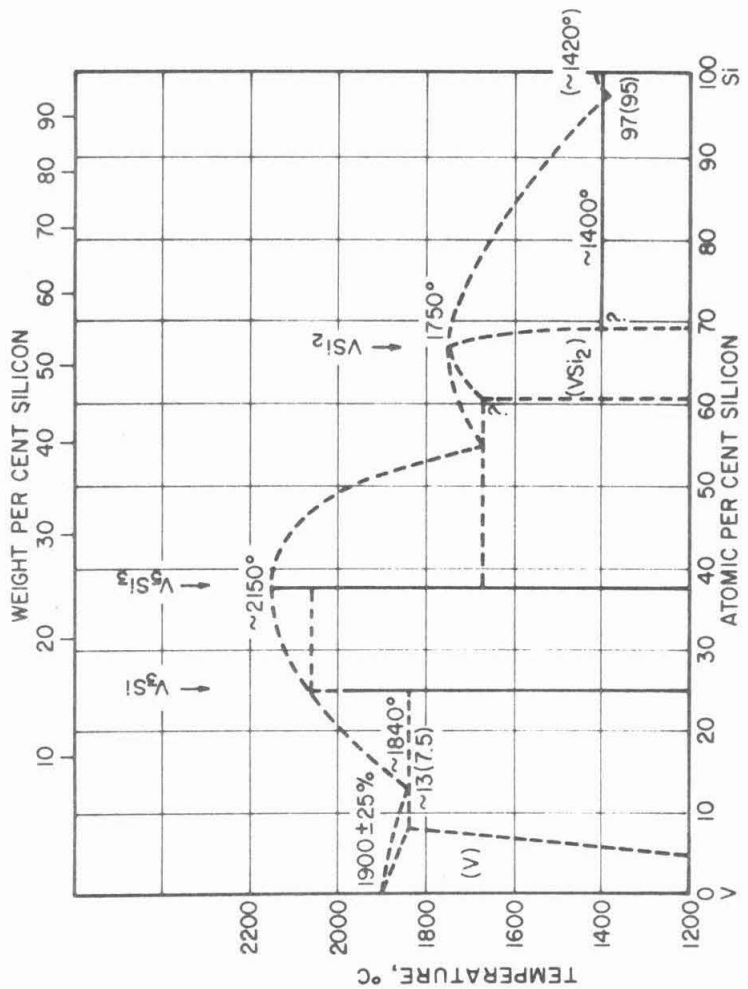

Figure 64. Equilibrium phase diagram for the V-Si binary system.

mens, or in the form of crushed particles about 2 to 5 μm in size for the rolled specimens.

In general, these superconducting particles are separated from each other by a distance of at least 1 μm; thus, no direct superconducting path can be established via these particles. Their distances from each other are even too large for a proximity effect[22, 32] to take place, which requires a characteristic "tunneling" distance of[32]

$$\xi_N = (\hbar v_N \ell_N / 6\pi k_B T)^{\frac{1}{2}} \qquad (2)$$

for a dirty superconductor-normal metal interface. In (2), v_N is the Fermi velocity, ℓ_N the electronic mean free path, and k_B is the Boltzmann constant. The estimated ξ_N for the present system is about 10^3 Å, which is much smaller than the inter-particle distance observed for most specimens. Only under certain conditions in which microparticles are present in the specimen in between the larger particles can the specimen exhibit complete superconducting transitions via the action of the proximity effect. This explains why most electrical resistivity measurements made on Cu-V-Si specimens showed broad superconducting transitions with onset temperatures of about 17°K, and broad tails extending all the way down to 4.2°K (Figures 7 through 20). Some of the specimens may be superconducting above 4.2°K due to the proximity effect, but the mechanism causing the $Cu_{80}(V_3Si)_{20}$ rod, which has been annealed at 900°C for 1 day and was the specimen with the best characteristics among all Cu-V-Si specimens studied, to have complete superconducting transitions at about 11°K is probably due to the formation of continuous superconducting paths. This will be discussed in the next paragraph.

2. Superconducting transitions in $Cu_{80}(V_3Si)_{20}$ specimens. As mentioned in Chapter III, measurements for critical field were made on a $Cu_{80}(V_3Si)_{20}$ specimen annealed at 900°C for 1 day. It was found that the specimen was superconducting up to a transverse field of 55 kG. Since the tunneling of Cooper pairs which gives rise to the proximity effect is quenched easily by applied magnetic field[32, 45], it is believed that the complete superconducting transition is caused by the existence of continuous superconducting paths. Since there is 15 at. % of vanadium and 5 at. % of silicon present in the alloy, the situation shown in Figures 37 and 39 in which only crushed V_3Si particles are present in the rolled specimens may be improved to such an extent that continuous superconducting paths can be established in the rolled $Cu_{80}(V_3Si)_{20}$ specimens if a suitable heat treatment is applied. Another possibility is that there may be large vanadium domains in these high V_3Si-content alloys, and as a result of rolling these domains elongated into large filaments which, after suitable heat treatment, reacted with the silicon present in the specimen to form a large V_3Si filament. In fact, during the specimen preparation for the measurement of their electrical resistivities, after part of the specimens were etched away by the nitric acid, some filaments of this sort were indeed observed.

3. Optimum conditions for heat treatment. Figure 62 is the binary phase diagram for the V-Cu system. It can be seen that the solubility of V in Cu is negligible at room temperature at the Cu-rich side. Even at temperatures as high as 900°C, the solubility of V in Cu is still below 0.5 at. %.[15, 20, 21] There are no intermetallic

phases in the V-Cu binary system. On the other hand, the solubility of Cu in V at the V-rich side is about 7 at. % at 600°C, and varies only slightly with the change in temperature. Figure 63 is the binary phase diagram for the Cu-Si system. Although there are a number of equilibrium phases present in between the composition range of 10 at. % Si to 25 at. %Si, we can neglect this complex region in the phase diagram, since the maximum Si content in the Cu-V-Si alloys studied was only 7.5 at. %. From the Cu-Si phase diagram, we can see that only the α phase is likely to exist in all the alloys studied.

Figure 64 is the binary phase diagram for the V-Si system. There are several intermediate phases, namely, V_3Si, V_5Si_3, and VSi_2. Since the maximum relative atomic per cent ratio of Si to V in all Cu-V-Si alloys studied was 1 to 1, only the first two intermediate compounds are likely to be present in the alloys. V_3Si has the A-15 ("β-W") structure with lattice parameter 4.721 ± 0.003 Å. The compound V_5Si_3 has the hexagonal $Mn_5Si_3(D_8)$ type structure, with A = 7.13 Å, C = 4.84 Å, C/A = 0.678.[15, 20, 21] The phase V_5Si_3 is not superconducting down to 0.35°K.[33]

Based on the information obtained from the relevant binary phase diagrams, we can reasonably assume that there are three phases in the alloy system in the composition range covered by the present study. The normal metal matrix consists of a solid solution of Si in Cu, and the superconducting phase consists of a solid solution of Si in V, and also V_3Si. The results of x-ray diffraction analysis indicate that V_3Si is the dominant superconducting phase. The

presence of Si lines in the diffraction patterns of some specimens might be fictitious, since all those lines were extremely weak in intensity and might have arisen from the cameras or erroneous film reading.

In the process of melting,the ingots were heated up to above 2000°C. It is believed that before the ingots were cooled down to room temperature, a significant portion of V in the alloy reacted with Si and formed V_3Si. This is a reasonable conjecture based on the V-Si binary phase diagram, and is also supported by results of x-ray diffraction analysis. As explained earlier in Chapter III, after the rolling process, the V_3Si which existed in the as-cast ingot in the form of dendritic particles (Figures 37 and 39) were crushed and dispersed along the rolling direction. The question of how to achieve the best characteristics is equivalent to the question of how to heat treat the specimen so as to form as much V_3Si as possible.

In previous studies on fabricating V_3Si-Cu composites made by K. Tachikawa, et al., it was found that V_3Si tends to form only by high temperature annealing[6]. In their study, the composite was made by rolling the composite rod consisting of a vanadium core and a Cu-Si alloy outer tube, followed by subsequent annealing. Their result indicated that the phase V_5Si_3 was formed dominantly even with high temperature (950°C) heat treatment, and that V_3Si was hardly formed by treatments below 700°C. In a similar study on fabricating multifilamentary V_3Si-Cu wires made by M. Suenaga and W. Sampson, it was also found that in order to get specimens with high T_c, high annealing temperature (850°C and above) and long annealing time (300

hours) were required[8].

Similar conclusions have been arrived at from the results obtained from the present study. Of course, the specimens have to contain enough amounts of both V and Si to start with. In all specimens containing more than 15 at. % of V_3Si studied, 900°C was found to be the best annealing temperature. As mentioned before, specimens containing 20 at. % of V_3Si produced the best characteristic; but it was found that there is an optimum annealing time. Over-annealing caused the superconducting properties of specimens to deteriorate. For $Cu_{80}(V_3Si)_{20}$ specimens, the annealing time of 1 day seems to be close to optimum for the annealing temperature of 900°C. This is in contrast with the results discussed in refs. 6 and 8, in which the transition temperature of specimens was not decreased as a result of long time annealing, although the critical current densities were observed to decrease slightly as the annealing time was increased to a few hundred hours. But this may be caused by the effect of over-grown V_3Si grain size, which affects the pinning strength of the material[6] to the flux vortex lines. This point will be discussed later.

The reason the superconducting properties of specimens studied in this work were more sensitive to the effect of over-annealing can probably be explained in the following way. The size of the superconducting phase in the specimens is of the order of a few μm, which is much smaller than the size of the vanadium layer in ref. 6 or the size of the vanadium filaments in ref. 8. Thus, although the diffusion rate of Cu in V is lower than that of Si in V, it is still much easier for Cu atoms to diffuse into the superconducting phase in the specimens

studied in this work as a result of prolonged annealing, since the equilibrium solubility of Cu in V is high at the V-rich side (Figure 62). But in refs. 6 and 8, because of the immense size of the vanadium-rich region, the superconducting properties are determined by the V_3Si layer formed at the interior of the vanadium regions, which is not affected by the Cu-diffusion near the surface.

B. The Cu-V-Ga Alloys

1. Phases present in the alloys. Before discussing the results of the studies made on Cu-V-Ga alloys, a brief review of the phase relationships seems in order. The ternary phase diagram is also not known, but the relevant binary phase diagrams for the Ga-V and Cu-Ga systems are known and are reproduced in Figures 65 and 66, respectively. The solubility of Ga in Cu is high (20 at. % at 600°C). The compound of interest V_3Ga does not form directly from the melt, according to Figure 65. Thus, after melting, it is expected that most of the V will be present as a second phase. The Ga will be in solid solution with both Cu and V.

Based on the experimental evidence discussed in Chapter III, we can conclude that the compound V_3Ga has been formed in most Cu-V-Ga specimens which have been heat treated. In comparison to the Cu-V-Si alloys, there is no evidence of V_3Ga formation in the process of casting the alloy ingots except for specimens containing more than 10 at. % of Ga. For most compositions studied, suitable heat treatment must be applied to cause the formation of V_3Ga.

In strong contrast to the case of Cu-V-Si alloys, rolling and drawing of Cu-V-Ga alloy ingots changed the microstructures of the

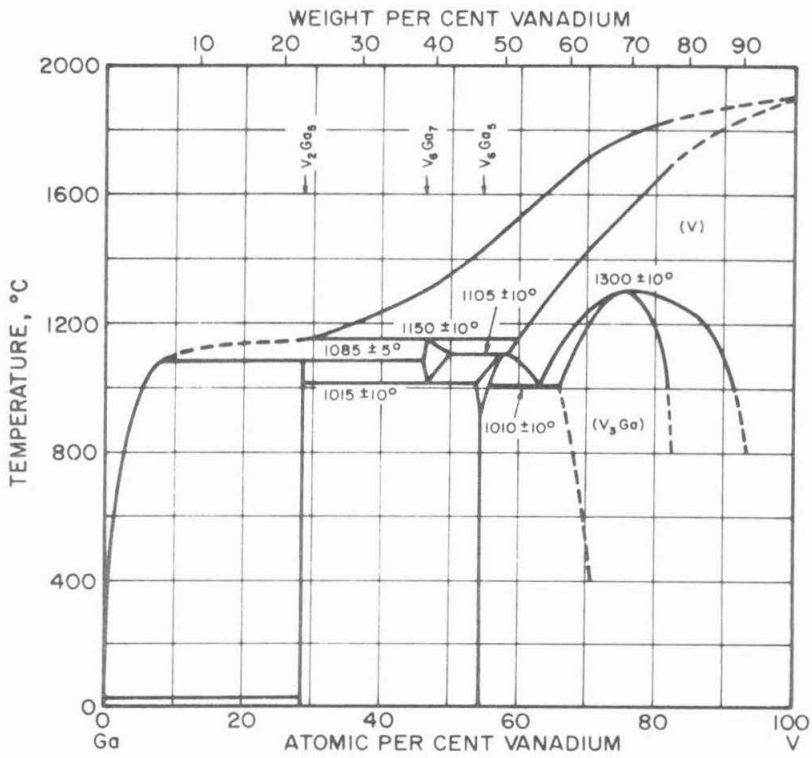

Figure 65. Equilibrium phase diagram for the Ga-V binary system.

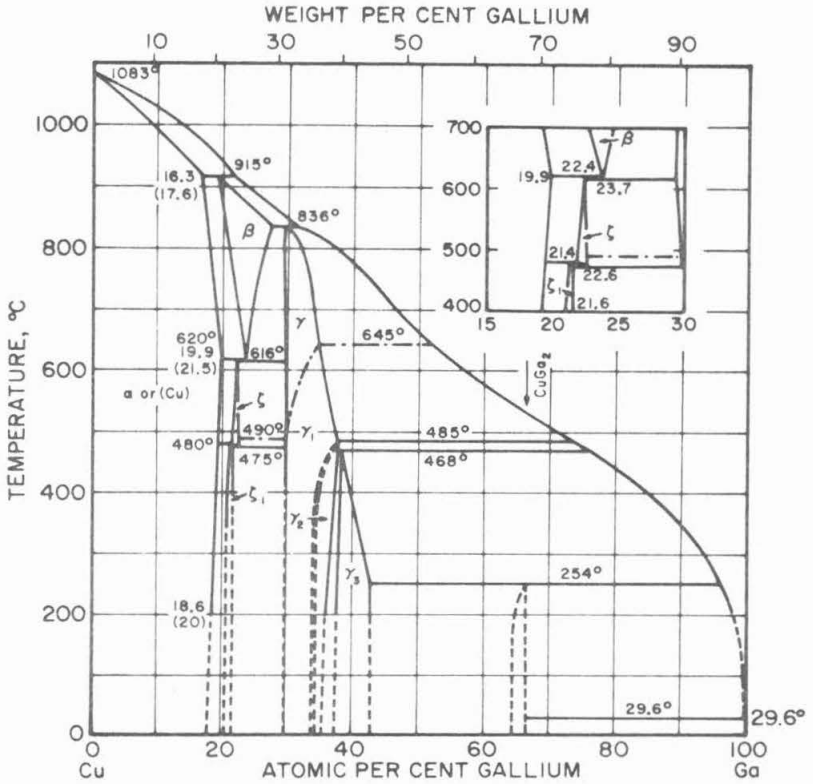

Figure 66. Equilibrium phase diagram for the Cu-Ga binary system.

materials so that relatively continuous filaments containing mostly vanadium were formed in the matrix. This is believed to be due to the fact that no brittle V-Ga compound has been formed during the process of casting the alloy ingots; only ductile V-Ga solid solution dendrites are formed. These dendrites can be elongated easily into long filaments as the result of rolling. This point is vital in the success of applying the Tsuei process to Cu-V-Ga alloys.

There are four experimental evidences indicating the formation of V_3Ga, namely: (1) X-ray diffraction analysis established the diffraction pattern of V_3Ga in most specimens which have been subjected to heat treatments; but the as-rolled specimens showed no such diffraction patterns. (2) Sharp superconducting transitions, which are also complete, in general, have been observed from the results of electrical resistivity measurements. The transition temperatures depend on the compositions of the specimens. But for a number of specimens containing enough V (say, 10 at. %) and Ga (say, 12.5 at. %), an onset temperature of $14^{\circ}K$ and a complete transition at $13^{\circ}K$ can be reached. Since $14.8^{\circ}K$ is the superconducting transition temperature of V_3Ga obtained in most studies[18, 29, 30, 35, 38], it is likely that the compound formed is close to the stoichiometric composition of V_3Ga. (3) Results of critical current measurements indicate that the critical field of most specimens studied is higher than 60 kG at $4.2^{\circ}K$. Of all the V-Ga intermediate compounds, only V_3Ga is known to be superconducting with high critical field. (4) Results of magnetization measurements also indicate that the H_{c2} of some of the specimens are above 6 kG at $4.2^{\circ}K$, which is high com-

pared with the H_{c2} of vanadium at 4.2°K.

It is generally known that the superconducting transition temperatures of A-15 compounds are very sensitive to the metallurgical state of the sample, such as the amount and nature of impurities, defect concentrations, lattice imperfections, stoichiometricity, and the degree of long range order[18, 19]. Thus, it is not surprising that the transition temperatures observed in most specimens are below that of the perfect V_3Ga phase. In fact, although it has been reported that a T_c of 16.5°K has been found for V_3Ga,[36] in most studies only 14.8°K has been obtained. Also, similar reduction in T_c has been observed in studies made by Tsuei on Cu-Nb-Sn specimens by the same process[9, 10], in which a T_c of about 16°K was obtained from the composite, while the T_c for Nb_3Sn should be 18.1°K.[37]

The reason the T_c for some specimens, in particular those containing less amounts of Ga, is lower than 13°K can be understood as the result of the formation of V-Ga compounds with compositions off from stoichiometricity. This explains why the T_c goes up with increasing Ga concentration while keeping the V concentration fixed in the alloys, since all evidence indicates that it needs high Ga concentration in the alloy to form V-Ga compounds close to stoichiometricity in these specimens.

2. <u>The role of the Cu phase in the V_3Ga formation process.</u> Figure 65 shows the equilibrium phase diagram for the Ga-V binary system. It can be seen that there are several intermediate compounds present in the system, namely, V_3Ga, V_6Ga_5, V_6Ga_7, and V_2Ga_5; although a revised V-Ga phase diagram[21] indicates that the

compounds VGa, V_2Ga_5 and V_3Ga_5, and V_3Ga are present in the composition range of more than 50 at. % of vanadium.

Figure 66 is the phase diagram of the Cu-Ga binary system. The structure is quite complex at compositions above 17 at. % of Ga in Cu, but in the present study, the maximum concentration used was 12.5 at. % of Ga. Thus, only the α phase is important for consideration.

Early studies made by Y. Tanaka, et al.[39] and K. Tachikawa, et al.[6] indicate that the selective diffusion of gallium from the Cu-Ga alloy to the vanadium phase resulted in the formation of V_3Ga in the system consisting of a vanadium phase in close bonding to a Cu-Ga solid solution. Moreover, V_3Ga is the only compound formed effectively, in comparison to the similar system of vanadium and Cu-Si solution, in which Cu is not effective for enhancing the formation of V_3Si.

It was also found that by the diffusion between Ga and V only at temperatures below 800°C, instead of forming V_3Ga, the compounds formed predominantly are richer in Ga content, namely, VGa_2 and V_3Ga_2. A very small amount of V_3Ga is formed by the diffusion between V_3Ga_2 and vanadium.[40] Cu dissolves in both VGa_2 and V_3Ga_2, as much as 7 at. % and 4 at. % respectively. Without the presence of Cu, only the grain boundaries of V_3Ga_2 are effective for the diffusion between V and V_3Ga_2 to proceed. But the addition of Cu changes the diffusion mode to a bulk one, and then the V_3Ga can be formed easily below 800°C. It is believed that the enhancement due to the presence of Cu is caused by the decrease of the melting point of V_3Ga_2 and the

introduction of vacancies into the V_3Ga_2 .

This agrees with the x-ray diffraction analysis made on the specimens in this work, in which only V_3Ga diffraction lines were visible for most annealed specimens. Also, it clarifies the question of why the Cu-V-Ga specimens have far better characteristics than the Cu-V-Si specimens, because V_3Ga is formed easily through the Cu enhancement in diffusion, while V_3Si is formed at a much slower rate at the same annealing temperature.

3. Optimum composition and optimum heat treatment. The results of superconducting transition temperature measurements made on Cu-V-Ga specimens are summarized in Figure 67, in which the dependence of T_c for complete transitions on the annealing time and temperature for specimens with various compositions are shown. The following points can be seen from Figure 67: (1) Specimens richer in gallium tend to have higher transition temperatures than the specimens containing the same amount of vanadium but less gallium. (2) Specimens which have been annealed at 650°C generally have higher T_c than the specimens of the same compositions but annealed at 800°C. (3) For 650°C annealing, the T_c for a specimen appears to be constant for the annealing time of more than two days. For 800°C annealing, the T_c for a specimen generally reaches a maximum as the annealing time increases and then is decreased again when the annealing time gets too long.

The dependence of the electrical resistivities of the specimens on their Ga concentrations can be further visualized from Figures 68 and 69. Figure 68 shows the electrical resistivities for the specimens

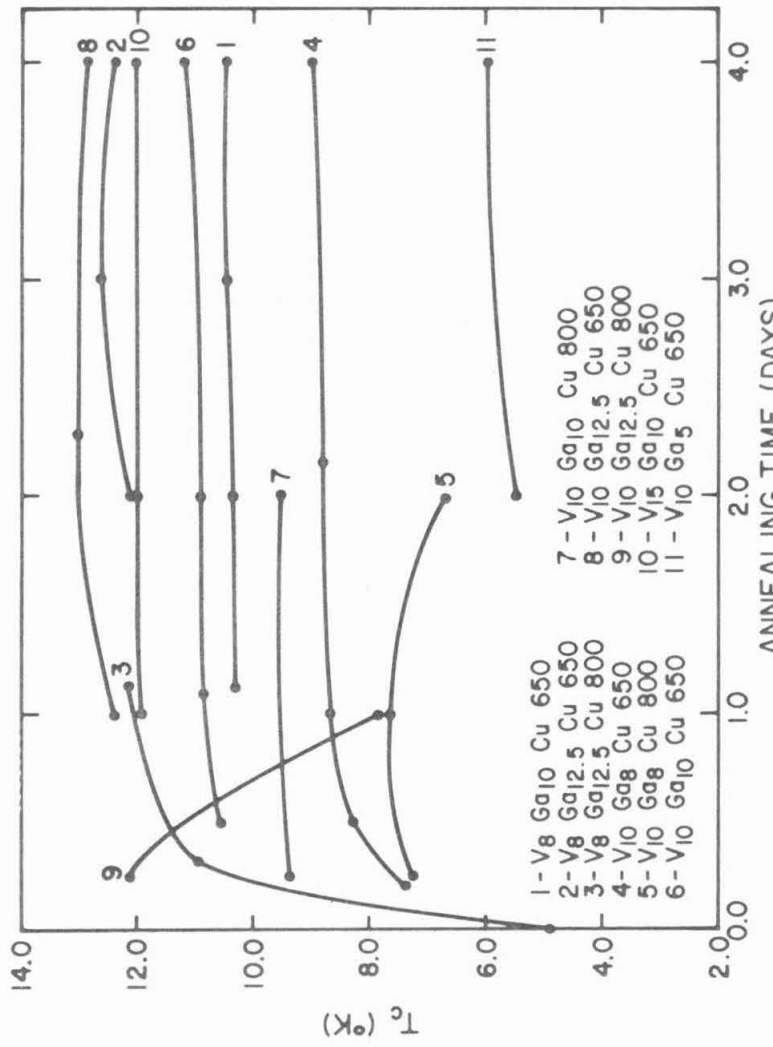

Figure 67. Superconducting transition temperature as a function of annealing time for some of the Cu-V-Ga specimens.

containing 10 at. % of vanadium but different amounts of gallium (5, 8, 10, and 12.5 at. %, respectively). All specimens have been annealed at 650°C for 2 days. The trend of the steady increase of T_c with increasing Ga concentration can be seen clearly. Also, it can be seen that the residual resistivities ρ_n of the specimens increase steadily with the Ga concentration and appear to be approaching saturation at the Ga concentration of 12.5 at. %. Figure 69 shows the electrical resistivities for the same group of specimens as in Figure 68, but annealed at 800°C for 6 hours. The transition of the specimens from non-superconducting at 5 at. % of Ga to superconducting at 8 at. % of Ga is quite dramatic. The same trend of increasing T_c with increasing Ga concentration can also be seen. In comparing Figure 68 with Figure 69, we can arrive at the conclusion that Ga tends to stay in the Cu-Ga solid solution rather than diffusing into the V regions to form V_3Ga as the annealing temperature is increased. This probably explains why V_3Ga is not formed in the process of casting the alloy ingots, because of the tendency for Ga to stay in the Cu-Ga solution at high temperatures.

As mentioned previously, the T_c that can be obtained in a Cu-V-Ga alloy tends to increase with increasing Ga concentration. But too much Ga in the alloy makes the Cu-Ga solid solution matrix brittle and thus limits the degree of cold working that can be applied to the alloy, or equivalently, the degree of elongation of the vanadium filaments.

Thus, although alloys with high Ga concentration (say, 12.5 at.%) may have higher transition temperature, their superconducting properties may not be better than alloys with the same vanadium concentration but lower in Ga content. That is because the most important charac-

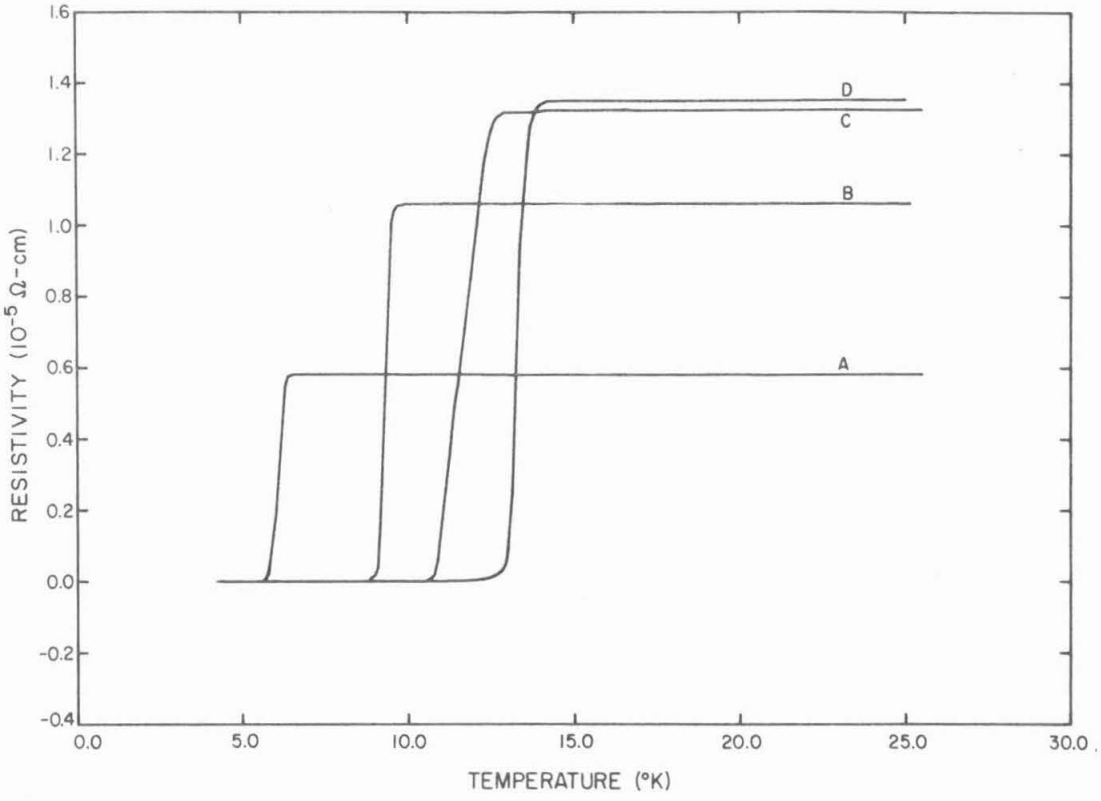

Figure 68. Electrical resistivities for the $Cu_{90-X}V_{10}Ga_X$ specimens, A: X = 5, B: X = 8, C: X = 10, D: X = 12.5. All specimens have been heat treated at 650°C for 2 days.

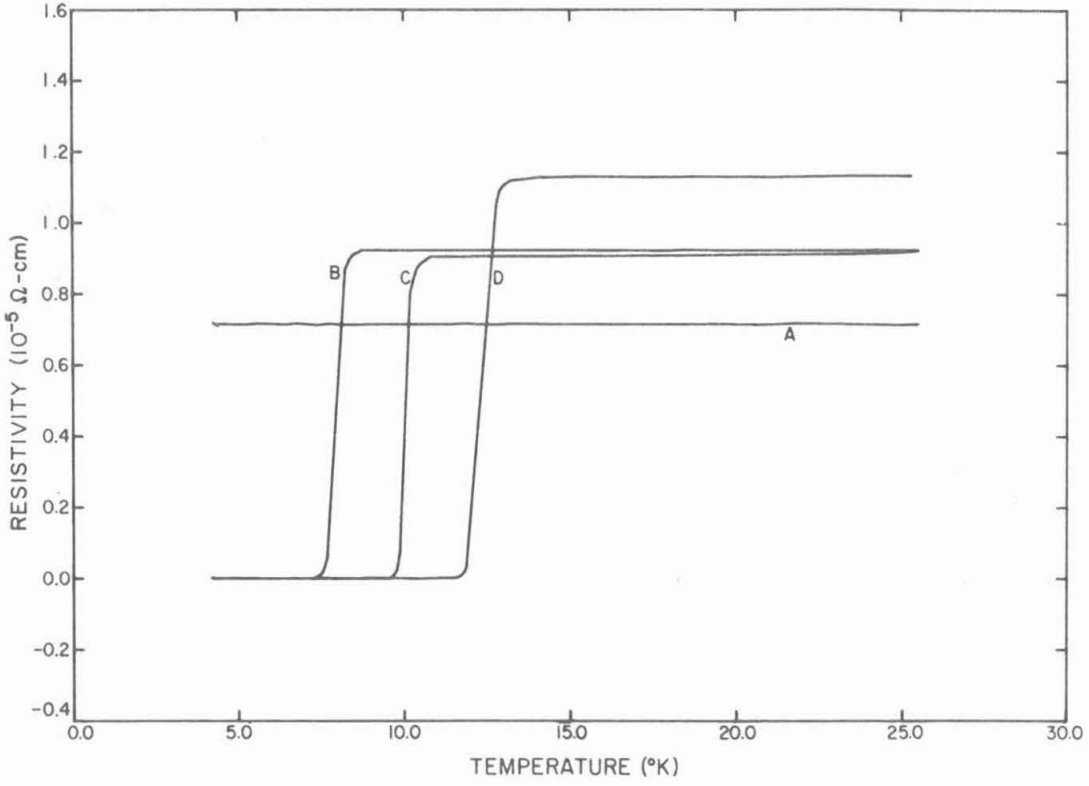

Figure 69. Electrical resistivities for the $Cu_{90-X}V_{10}Ga_X$ specimens. A: X = 5 , B: X = 8 , C: X = 10, D: X = 12.5. All specimens have been heat treated at 800°C for 6 hours.

teristic of a superconducting material, at least for the purpose of the present study, is its critical current density, while the critical current density of a material studied in this work seems to depend strongly on the degree of continuity of the vanadium filaments embedded in the Cu-Ga matrix. Of course, the V concentration has to be high enough so that enough filaments can be formed by the cold working.

This explains why the composition $Cu_{80}V_{10}Ga_{10}$ seems to yield the best characteristics so far. Its matrix is ductile enough that it can be drawn into wires ~ 0.13 mm in diameter. That will yield a cross section reduction ratio of ~ 900, with reasonably continuous filamentary structure produced.

As for the conditions of optimum heat treatment, the discussion has to be begun from the process of casting the alloy ingots. Since a number of V-rich globules, which are believed to be some V-Ga compound with high hardness formed in the melting process, have been observed in most rod or wire specimens, it is believed that the optimum procedure is to keep the temperature used in melting the various elements as low as possible, and also to keep the heating time as short as possible, in order to prevent the formation of any compound at high temperatures.

After the ingots were rolled into rods or sheets or drawn into wires, all evidences indicated that the annealing temperature of 650°C would be close to optimum. This agrees with the findings of some early works[3-8, 38]. High temperature annealings were found to be undesirable for achieving high transition temperatures, and also tended to reduce the critical current densities that can be obtained for speci-

mens studied in this work. Earlier studies made by E. Nembach, et al.[17] and by K. Tachikawa, et al.[6] also indicated similar results. The grain boundaries in V_3Ga are believed to be the most important flux-pinning centers, and thus the mean grain size is strongly related to the critical current densities that can be obtained from the material. High temperature annealing tends to result in large grain size, and is thus unfavorable for achieving high critical current density. On the other hand, annealing at a temperature which is too low will cause insufficient formation and growth of V_3Ga.

Another influencing factor against high temperature annealing in this work is the diffusion of Cu into the V_3Ga phase which has already formed, thus causing deterioration in its properties.

C. Effect of Discontinuity in the Superconducting Filaments

Some questions have been raised by Tinkham[42] whether the observed superconductivity in the Cu-V-Ga composites studied in the present work or in the Cu-Nb-Sn composites studied by Tsuei[9, 10] is largely due to a proximity effect, since it is not clear if the observed vanishing of electrical resistances of the specimens is due to the occurrence of a complete superconducting state in the specimens, or just because the current is carried by all the superconducting filaments embedded in the matrix in such a way that the electrical resistances of the specimens drop to a level below the sensitivity of the instrument used in the detection of voltage.

A simple model can be used to calculate the effective resistivity of a segment of specimen if the second case is true. Assume the

ideal case that each filament in the specimen has a length L, diameter a, and the separation between filaments is 2d. Also assume that there are N neighbors for each filament. If the current carried by a filament enters and leaves radially over a length L' at each end of the filament, then the effective resistivity of a segment of wire can be calculated in the following way. Since it is known that the problem of electrical current flow between two parallel cylindrical perfect conductors embedded in a conducting media is similar to the problem of the calculation of the electrical capacitance between two parallel cylindrical perfect conductors in a dielectric[43], the resistance per unit length R between the two conductors in the first problem can be shown to be related to the capacitance per unit length C between the two conductors in the second problem in the following way, if ρ is the resistivity of the conducting media:

$$R = \frac{\rho}{4\pi} \frac{1}{C} \quad , \tag{3}$$

whereas it can be shown[31] that

$$\frac{1}{C} = 2 \cosh^{-1}\{(2d^2 - a^2)/a^2\} \quad . \tag{4}$$

Assuming that all the voltage drop is due to this radial flow of the current in the normal metal between the superconducting filaments, then since there are N neighboring filaments acting in parallel in the current flow, the total resistance between a filament and all its neighbors is

$$R_{tot} = \frac{1}{N} \left(\frac{\rho}{2\pi L'} \right) \cosh^{-1}\{(2d^2 - a^2)/a^2\} \quad . \tag{5}$$

Thus, the effective resistivity of the specimen is

$$\rho_{eff} = \frac{\rho}{2\pi N} \frac{4\pi d^2}{LL'} \cosh^{-1}\{(2d^2-a^2)/a^2\}$$

$$= \frac{\rho}{N} \frac{2d^2}{LL'} \cosh^{-1}\{(2d^2-a^2)/a^2\} \quad . \qquad (6)$$

The inverse hyperbolic cosine factor is about 3.6 if the filaments form 10 per cent of the volume of the specimen. Assume N = 6, and L' = 1/3 L , then

$$\rho_{eff} \approx 3.6\, \rho \frac{d^2}{L^2} \quad . \qquad (7)$$

If r is the cross section reduction ratio after the drawing, then d^2/L^2 will be proportional to $1/r^3$. Thus, if r = 300 for the 0.4 mm wire specimens, then

$$\rho_{eff} \approx 3.6 \times \rho/2.7 \times 10^7 \approx 1.0 \times 10^{-13} \qquad \text{(ohm-cm)} \qquad (8)$$

if 10^{-6} ohm-cm is used as the resistivity ρ of the normal matrix.

From (8), we can see that the resistivity of the specimen can indeed be reduced to a level below the sensitivity of standard instruments ($\sim 10^{-11}$ ohm-cm) by the fact that the current is carried mostly by the superconducting filaments, and only in transferring from one filament to another does the current flow in the normal metal matrix.

A measurement was made using a superconducting voltmeter to measure the resistivity of Cu-Nb-Sn wires fabricated by Tsuei with the same kind of process, and it was found that the resistivity of the wire is below 3×10^{-17} ohm-cm. [44] Since the Cu-V-Ga wires are believed to have very similar properties to the Cu-Nb-Sn wires, we expect that the resistivity of the Cu-V-Ga wires must also be below the measurable limit of the SQUID voltmeter, i.e., 3×10^{-17} ohm-cm. This means that the wires are actually superconducting by the estab-

lishment of superconducting paths, or by means of the proximity effect in between filaments. The exact mechanism giving rise to the complete superconducting state in these wires is difficult to determine even with strong applied field, because, according to an argument made by Tinkham[42], the radial current density J_n in the normal metal is related to the current density in the filaments J_f by

$$J_n/J_f = a/2L \approx \tfrac{1}{2}(r)^{-3/2} \approx 10^{-4} , \qquad (9)$$

which is only a small fraction. Furthermore, since the radial current flows outwards from the filaments, a portion of it is always parallel to the applied transverse field and thus should not be sensitive to it. Thus, although the proximity effect itself is sensitive to applied magnetic field, and the superconducting state caused by it should not be able to sustain a field strength of above 10 kG, it is still difficult to say for sure that it is playing a dominant role in the superconductivity observed in these wires based only on the magnetic field dependence of their critical current densities.

D. Critical Current Densities

Before discussing the results of critical current measurements, a brief review of the existing theories on hard superconducting materials seems in order. The discussion will be limited to such aspects as flux pinning, magneto-thermal instabilities, and stabilization of hard superconductors.

1. Review of Relevant Theories. It has been known that the properties of type II superconductors under applied magnetic field can be described, at least qualitatively, by the GLAG (Ginzburg-

Landau-Abrikosov-Gorkov) theory. At fields above H_{c1}, which is about a few hundred gauss for most type II superconductors, flux starts to penetrate into the superconductor in the form of flux bundles of units of $\phi_o = hc/2e \approx 2 \times 10^{-7}$ gauss-cm^2. [1, 22-24, 46] These flux bundles (sometimes called fluxoids, fluxons, or vortices) are each cylindrical with radius of the order of the coherence length ξ of the superconductor, and they form lattice structures, which in the ideal case are hexagonal, with the lattice spacing determined by the field strength $\vec{B}$. Such a superconducting state is called the mixed state.

If a bulk current of density $\vec{J}$ transverse to the vortices is flowing in the superconductor, there is a Lorentz force $\vec{J} \times \vec{B}$ acting on each vortex. In a homogeneous specimen, vortices will move in response to this force producing losses and therefore electrical resistance. The electrical resistivity arising from this nature in the superconductor is called the flux flow resistivity. Thus, a homogeneous superconductor can carry no lossless bulk current in the mixed state. The flux flow resistivity ρ_f can be shown to be equal to

$$\rho_f = \frac{H_e}{H_{c2}} \rho_n \quad , \tag{10}$$

where H_e is the applied field, H_{c2} the upper critical field of the material, and ρ_n the normal resistivity of the material.

However, in some type II superconductors, the presence of lattice irregularities can "pin" the vortices against movement under the action of Lorentz forces, thus enabling the current to flow without dissipation. Pinning centers can be voids, normal inclusions,

local compositional variations, dislocations, etc. As an example, the grain boundaries of V_3Ga are believed to be the most important pinning centers against the vortex motion. Type II superconductors in which flux movement is inhibited by pinning are called hard superconductors.

It was found experimentally that there is a limit to the strength of the pinning force. Vortices are pinned as long as the current density J and field strength B satisfy the relation

$$J \times (B + B_o) \leq \alpha_c \quad , \tag{11}$$

where α_c is the value of the Lorentz force which overcomes the pinning strength at a given temperature, and B_o is a constant. Vortex motion and thus flux flow resistivity will occur as soon as the relation (11) is violated. The quantity α_c was found to depend on both the temperature and the field[52].

Assume that persistent currents whose magnitude satisfies the relation $J \times (B+B_o) = \alpha_c$ flow in a hard superconductor under applied magnetic field, in such a way as to shield the interior of the superconductor from further flux penetration, we arrive at the critical state model, or the Bean model, which is commonly used for describing the electrical and magnetic properties of hard superconductors[1, 47-51]. That portion of the superconductor carrying this limiting current density is said to be in the critical state. As the external field increases, the region of critical state penetrates further, until the equilibrium condition is reached and all vortices are pinned again. From the critical state model, quantities such as the hysteresis magnetization of a hard superconductor can be cal-

culated, and the results are in reasonable agreement with experimental measurements.

The rate of decrease of field strength in the mixed state region is given by

$$dH/dx = J_c \tag{12}$$

with

$$J_c \times (B+B_o) = \alpha_c \quad . \tag{13}$$

Thus, the thickness δ of the critical state region can be estimated from the following relation

$$\delta \approx H/J_c \quad . \tag{14}$$

So far, the discussion has been limited to situations in which no transport current is present. If a transport current is flowing in the superconductor while an external field is being applied, the field penetration profiles will be modified. For instance, consider a slab of hard superconductor which has been cooled to below T_c before a field H_o is applied parallel to the plane of the slab. Before the application of a transport current, the field strength in the slab decreases linearly according to (12) on both sides of the slab. For a sufficiently strong applied field, the flux penetration from the two sides meet. If a transport current is then applied, the external field on one side of the slab is increased while the external field on the other side is decreased, at the same time keeping the local current density to the maximum allowed locally by the pinning strength. The local current flow on one side of the slab is partly reversed in order to give rise to the net transport current. The limiting value of the

transport current is reached when all the current flow on one side of the slab has been reversed. Under such a condition the flux density in the slab decreases continuously from the higher value on one side of the slab to the lower value on the other side. If the transport current is further increased, then vortex motion will occur and thus give rise to electrical power loss in the superconductor, since the critical pinning strength of the material will inevitably be exceeded.

In reality, the current-carrying capacities of hard superconductors are also determined by some other factors. It has been found that most of the hard superconductors have poor thermal conductivity; thus, the magnetic flux can, under some conditions, diffuse through these materials much faster than the heat generated by the moving flux. Thus, these hard superconductors can be heated up appreciably if a sudden field change occurs[53, 54]. Such a temperature increase will decrease the pinning strength, and thus allow further flux penetration and movement. Hence, the penetration of flux is a regenerative process which may become catastrophic under some conditions.

The conditions under which a hard superconductor can recover from the disturbance of a small change in the applied field can be calculated, and the limit of stability can be shown to be

$$H_e^2 \leq J_c C \left(\mu_o \frac{\partial J_c}{\partial T} \right)^{-1} , \qquad (15)$$

where H_e is the applied field, C is the specific heat of the superconductor, and μ_o the permeability. In most cases, instability results directly from the negative value of $\partial J_c / \partial T$ displayed by most

hard superconductors. For some alloys, $\partial J_c / \partial T$ could be made positive, resulting in inherent stability. The condition (15) can be modified to be

$$d_s^2 \leq 2C\left(\mu_o J_c \frac{\partial J_c}{\partial T}\right)^{-1} , \tag{16}$$

where d_s is the maximum half-thickness of the hard superconductor in which instabilities will not occur. The condition (16) applies for a slab of hard superconductor, but a similar condition differing from (16) only by a multiplicative constant can be derived for a wire superconductor.

In actual use, a hard superconductor has to be "stabilized" by various methods. The principle of stabilization is to have a normal metal with high electrical and thermal conductivity in intimate contact with the hard superconductor. Such a conductor configuration is usually called a "superconducting composite." The composite is immersed in liquid helium in actual use. When the composite is carrying a transport current in a magnetic field, and if flux jumping occurs in some part of the superconductor, the heat generated can be conducted away through the normal metal, thus preventing the superconductor from going normal. If, in the worst condition, the superconductor did go normal by an excessive amount of heat generated, the normal metal then serves as the path for current flow for a short time, until the heat is dissipated into the helium bath and the superconductor recovers from the normal state back into the superconducting state; then the current flows again in the superconductor itself. Thus, stabilization is achieved at the sacrifice of a reduction in the

over-all current density that can be obtained from the composite[28, 55, 56].

The actual analysis involves some other factors, such as the mode of heat transfer between the helium bath and the surface of the composite changes from the nucleate boiling to film boiling as the temperature difference between the two exceeds $1^{o}K$, and is quite complicated. But the essential points are:

(i) The thermal bonding between the superconductor and the normal metal must be good.

(ii) The size of the superconductor must be under some limit in order for the heat generated in a flux jumping process to be efficiently removed. Also, there must be sufficient amounts of normal metal in the composite. In fact, the criterion for stability can be written as

$$J_c^2 d_s \leq 4 \frac{a_n}{a_s} \frac{\gamma}{\rho_n} J_c \left(\frac{\partial J_c}{\partial T} \right)^{-1} , \qquad (17)$$

where d_s is the diameter of the superconducting filament; γ is the heat transfer coefficient between the superconductor and the normal metal; a_n and a_s are the cross-sectional areas of the normal metal and the superconductor, respectively; and ρ_n is the resistivity of the normal metal.

(iii) The over-all size of the composite must not be too large in order to assure efficient heat dissipation into the liquid helium bath.

Further analysis indicates that appropriate configuration of the composite can actually prevent flux jumping from occurring. This is called "dynamic stabilization."[48, 57] For a flat composite which can be cooled from two faces, the stability criterion can be written as

$$J_c^2 d_s^2 < \frac{\pi}{4} \frac{K_s}{d_s} \left(\frac{d_n}{\rho_n} + \frac{d_s}{\rho_f} \right) J_c \left(\frac{\partial J_c}{\partial T} \right)^{-1} , \qquad (18)$$

where K_s is the thermal conductivity of the superconductor, d_s the thickness of the superconductor, and ρ_f its flux-flow resistivity. d_n and ρ_n are the thickness and resistivity of the normal metal, respectively.

Thus, it can be seen that the size of the superconductor in the composite must be small in order to achieve a high stability against flux jumping. For this reason, most composites are either composed of a thin layer of superconductor such as Nb_3Sn cladded with copper and stainless steel, or are in the form of wires containing a number of thin ($\sim$ 50 μm in diameter) superconducting filaments embedded in copper[58]. So far, most of the latter class of materials contains ductile Nb-Ti alloys as their superconducting filaments; thus, their T_c is only about 10°K. Only recently have multi-filamentary superconducting composites containing Nb_3Sn or V_3Ga been developed.

2. Stability of Cu-V-Ga Composites. From the previous discussions, we realize that the critical current density of a superconducting material is determined by quite a number of factors. First of all, the material itself must be a very good type II superconductor, and it must contain a high density of pinning centers to give rise to a high pinning strength to flux vortices. Then, the material must be fabricated into thin filaments or strips and stabilized with normal metals before it can be used in actual applications.

For composites fabricated by conventional processes, for example, multi-filamentary Nb-Ti-Cu composites, the conductor con-

figuration that can be achieved is limited. The smallest size of the superconducting filaments embedded in the Cu matrix that can be achieved is only $\sim$ 50 μm, whereas both the criterion for thermal stability (17) and the criterion for stability against flux jumping (18) require a small size for the superconducting filaments. In this sense, the Cu-V-Ga composites fabricated by the Tsuei process should provide a higher stability, since the size of a typical superconducting filament in them is only about 5 μm. The heat generated in these filaments can be easily dissipated through the Cu matrix. Furthermore, since the filaments are produced by elongation of the dendrites formed in the melting process, the contact of the filaments to the surrounding matrix is extremely clean and allows a very efficient heat conduction between them. Whereas in the conventional composites, the filaments are produced by repeatedly rolling and drawing rods composed of a Cu outer tube and a superconducting core, there is always the possibility of surface contamination and oxidation on the superconductor, which will create a thermal barrier between the superconducting filaments and the Cu matrix, and as a consequence decrease the stability of the composite.

Thus, from this point of view, the composites fabricated by the Tsuei process should have inherent advantages in their conductor configurations as far as magneto-thermal stability is concerned.

From the criterion for thermal stability (17) and the criterion for stability against flux jumping (18), we can see that the stability of a composite requires the normal metal to have low electrical resistivity ρ_n (or, equivalently, high electrical conductivity σ_n). Also,

from (17), we can see that high thermal stability also requires a large heat transfer coefficient between the superconductor and the normal metal γ . Since γ in turn is determined by the thermal conductivity K_n of the normal metal, we can say that a large K_n is in favor of a high stability.

It is known that both the thermal and electrical conductivities of a metal are determined by the purity and the perfectness of the crystalline state of the metal[26]. The higher the purity and the degree of perfection of its crystalline state, the higher are the electrical and thermal conductivities of the metal. For the case of the Cu-V-Ga composites studied in this work, the residual electrical resistivity of a typical specimen is about 10^{-5} ohm-cm. Since the Cu matrix provides the main path for current flow above the transition temperature, this value is expected to be close to the electrical resistivity of the Cu matrix alone. This high electrical resistivity is believed to be due partly to the amount of Ga dissolved in the Cu matrix, and partly to the high degree of structural damage caused by the mechanical deformation applied to the material but not completely removed in the process of annealing. Compared to the value of 10^{-7} to 10^{-8} ohm-cm which is the typical magnitude of electrical resistivity for pure Cu, the electrical resistivity of the Cu matrix in these composites is not very satisfactory. The thermal conductivity K_n is difficult to estimate, but from the Wiedemann-Franz law[26], it is expected that K_n is 2 to 3 orders of magnitude lower than the value for pure Cu. Hopefully, we can increase both the electrical and thermal conductivities of the Cu matrix by appropriate choice of the alloy composition and

the condition of heat treatment.

3. Optimum Composition and Heat Treatment. Figures 70 and 71 show the measured flux pinning parameters $\alpha = J_c \times H$ for some of the specimens studied. As can be seen, for most specimens, α remains constant up to a field of 60 kG. As mentioned previously, specimens of composition $Cu_{80}V_{10}Ga_{10}$ in the form of 0.4 mm wire and heat treated at 600 - 650°C for 2 - 4 days tend to give the best critical current or flux pinning characteristics. This means that such a heat treatment caused the formation of a layer of V_3Ga with optimum thickness and flux pinning center density in the filaments. As mentioned before, grain boundaries are the most important flux pinning centers for V_3Ga; thus, we can say that such a heat treatment caused the V_3Ga formed to have an optimum grain size. High temperature heat treatments tend to cause overgrown V_3Ga grains, and thus reduce the flux pinning center density. Also, as indicated from transition temperature measurements, high temperature heat treatments tend to cause the V_3Ga formed to be off stoichiometry; this can be seen from the low transition temperature of the specimens which have been heat treated at high temperature.

It is believed that the critical current densities of these specimens are limited by the fact that not all the V_3Ga filaments in them are continuous. Also, the globules present in most specimens effectively reduce the number of filaments available for carrying current. It is hoped that the situation for globule formation can be improved by developing an appropriate procedure of melting the ingots. As for the continuity of the filaments, it is hoped that a higher degree

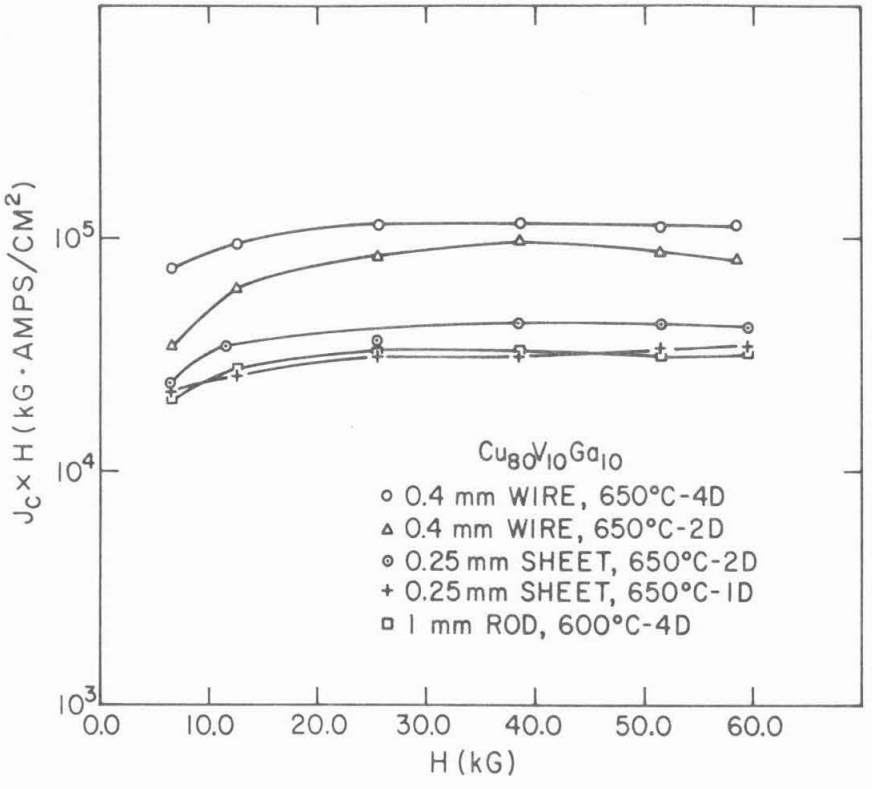

Figure 70. Pinning parameter $\alpha = J_c \times H$ as a function of field for some of the $Cu_{80}V_{10}Ga_{10}$ specimens.

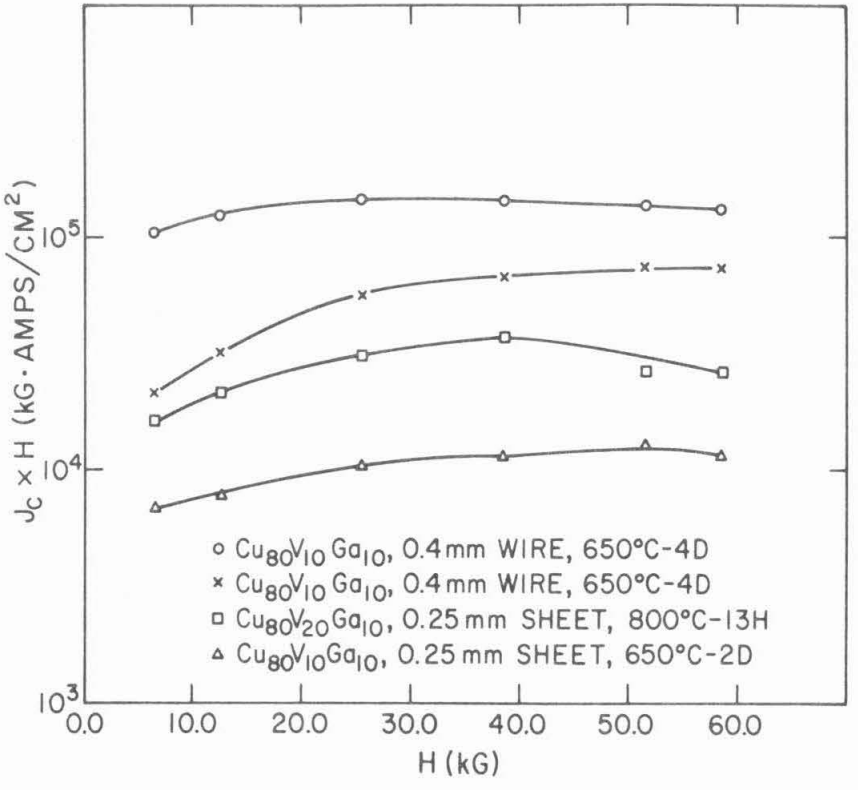

Figure 71. Pinning parameter $\alpha = J_c \times H$ as a function of field for some of the Cu-V-Ga specimens.

of deformation, i.e., a higher cross-section reduction ratio, can be obtained; effectively, this will improve the continuity of the filaments.

E. Suggestions for Further Studies

The properties of the Cu-V-Ga composites obtained in this work are not yet optimized. It is believed that with some further study, some optimum parameters such as the composition, the condition for heat treatment, etc., can be found so that composites with higher critical current densities can be fabricated. Some of the studies that are expected to be valuable in improving the understanding will be discussed in this section.

1. Ternary Phase Diagrams. Some studies on the Cu-V-Ga and the Cu-V-Si ternary phase diagrams, especially near the Cu-rich region, should be very valuable. This information can provide the direction for selecting the optimum compositions as well as the optimum heat treatment conditions. It can also be used to predict the amount of Ga or Si dissolved in the Cu matrix, and thus provide information about the mechanical properties of the composites. The problem of how to form stoichiometric V_3Ga or V_3Si compounds in the composite can also be resolved from information obtained from the ternary phase diagrams.

2. Optimum Fabrication Procedures. As mentioned in Chapters III and IV, in order to improve the critical current densities of the composites, we have to improve the continuity of the filaments, and reduce the number of V-rich globules. The important parameters are the melting temperature and time used, the cross-section reduction ratio, and intermediate annealing process.

3. Further Studies of Critical Current Densities. Further studies on the critical current density should be carried out based on the knowledge of the Cu-V-Ga ternary phase diagram. The main objectives are to increase the electrical and thermal conductivities of the Cu matrix by reducing the amount of dissolved Ga, and to maintain the stoichiometricity of the V_3Ga formed, so that higher magneto-thermal stability can be achieved. It is also desirable to study the means of improving the continuity of the filaments.

4. Effects of Additional Elements. It has been found that the addition of some elements such as Si, Ge, or Au will enhance the diffusion reaction for the formation of V_3Ga. The addition of some other elements such as Zr, Hf, or Ti will increase the critical current densities of the composites made by the composite process mentioned previously[7]. It is desirable that similar studies of the effects of these additional elements be made on the Cu-V-Ga composites made with the Tsuei process. This can proceed in conjunction with points 2and 3 mentioned in this section.

5. Studies of AC Properties. One of the more important properties of a superconducting material is its AC loss properties. Essentially, that is the energy loss dissipated in the material when it is in a time-varying magnetic field, or when it is carrying a time-varying transport current[59-61]. Judging from the results obtained so far, the Cu-V-Ga composites fabricated by the Tsuei process does not seem ideal for the construction of magnets, but may be perfect for the purpose of power transmission. Since it is more desirable to transmit AC rather than DC power, it is desirable to make studies on the

AC loss properties of the material. This will involve magnetization measurements of the hysteresis loops, and direct measurements of AC loss as a function of frequency and power level. The results of some theoretical calculations on the AC loss properties of composite materials such as those mentioned in references 61-62 may be used for comparison.

6. Other Studies. Besides the possible studies suggested above, some other studies may also be valuable in the further understanding of the Cu-V-Ga materials. One of these is the coil test; essentially that involves the winding of a superconducting coil with the Cu-V-Ga wires made with the Tsuei process and studying the decay of the persistent current set up in the coil. Such studies can help understanding the real mechanism of superconductivity in the material.

Also, results from specific heat or low field magnetization measurements would be useful for interpreting the role of the proximity effect in the superconductivity of the material.

V. SUMMARY AND CONCLUSIONS

The subject of this study is concerned with applying the Tsuei process to the fabrication of Cu-rich superconducting composites containing the A-15 compounds V_3Si or V_3Ga as the superconducting component. Some studies of the superconducting properties of the resulting composite materials have also been made.

The essence of the Tsuei process is to melt the constituent elements into ingots, keeping the A element in the A-15 compound A_3B ductile enough to be elongated into long filaments by subsequent rolling and drawing of the ingots. Also, it requires a low solubility of the element A in the Cu matrix. In the idealized case, the A-15 compounds will be formed during the heat treatment applied to the material after mechanical working.

During the course of this study, it was found that the Tsuei process does not apply very satisfactorily to the composites containing V_3Si. Electrical resistivity measurements and X-ray diffraction analysis indicate that V_3Si is indeed formed in the composite, but it is formed during the melting process and is crushed into small discontinuous particles during the cold rolling process, as indicated by microstructure analysis. Thus, we cannot obtain continuous V_3Si filaments in the composite by applying the Tsuei process to the composites containing V_3Si.

In the case of the composites containing V_3Ga, it has been found that materials with satisfactory properties can be obtained by the Tsuei process. Microstructure studies indicate that rolling and drawing of the ingots into rods or wires caused the vanadium den-

drites formed in the melting process to be elongated into fine filaments. The continuity of these filaments increases with increasing cross section reduction ratio used in the rolling process. Furthermore, both the electrical resistivity measurements and the X-ray diffraction analysis indicate that V_3Ga is formed in the material only after heat treatments have been applied. This explains why the Tsuei process works for the composites containing V_3Ga, because the ductility of the vanadium is not affected by the formation of brittle V-Ga compounds in the melting process.

The highest measured temperature for a complete superconducting transition for the Cu-V-Ga alloys studied was 13.0°K, which was obtained for a $Cu_{77.5}V_{10}Ga_{12.5}$ alloy heat treated at 650°C for 2.25 days. The highest measured critical current density at 4.2°K and zero transverse magnetic field was 2.9×10^4 A/cm^2, which was obtained from a 0.4 mm $Cu_{80}V_{10}Ga_{10}$ wire heat treated at 650°C for 4 days. The critical current density at 4.2°K for the same specimen decreased to 1.9×10^3 A/cm^2 when a transverse magnetic field of 60 kG was applied. So far, $Cu_{80}V_{10}Ga_{10}$ heat treated at 650°C for 2 to 4 days seems to give the best results for critical current densities.

There are some inherent difficulties with composites made by the Tsuei process, however. Under a careful study of the microstructures, it is revealed that the superconducting filaments are not entirely continuous, although the degree of continuity of the filaments improves with increasing cross-section reduction ratio of the wires. Nevertheless, high-sensitivity electrical resistance measurement using SQUID voltmeters indicated that the electrical resistivity of

Cu-Nb-Sn wires made by the Tsuei process is below 3×10^{-17} ohm-cm, or, equivalently, the wire is superconducting to within the measurable limit of the SQUID voltmeter. The implication of this finding is that there exist superconducting paths in the wire even though the superconducting filaments are not entirely continuous. It is expected that a similar situation exists for Cu-V-Ga materials. Even so, this discontinuity of filaments is believed to be the reason that the critical current densities of the material are still not very satisfactory. Also, it appears that the properties of different segments of a specimen are not very reproducible. But it is believed that an industrial process based on the Tsuei process can be set up to obtain highly homogeneous wires.

As compared to composite materials fabricated by conventional techniques such as the composite method or the vapor deposition method, the most important advantage of the present material is the economic factor. The Tsuei process offers a method for fabricating composite materials at a cost that is not much higher than the cost of fabricating copper wires.

Another advantage of the Tsuei composite materials over the conventional ones, according to existing theories on composite materials, is its inherent high magneto-thermal stability. As explained in Chapter IV, due to the small size of the superconducting filaments which are in intimate metallurgical contact to the surrounding Cu matrix, the Tsuei composite materials are expected to have higher magneto-thermal stability than the conventional ones.

However, an apparent disadvantage of the Tsuei composite

materials is that their critical current densities are not very high. Compared with conventional composites, their critical current densities are lower by one to two orders of magnitude. However, this drawback will only impair the applicability of these composites as materials for the construction of high-field magnets. For other less demanding types of applications, such as superconducting electrical motors and generators or power transmission lines, the Tsuei composites should be the more desirable material based on economical grounds.

The most immediate relevant study that should be made is the optimization of the various metallurgical factors involved, such as the concentration of the alloys, the cross-section reduction ratio, and the heat treatment, so as to produce a material with better characteristics. Some studies should be made on the basic mechanism of superconductivity in the Tsuei composites, such as the effect of the discontinuity of the superconducting filaments on the properties of the material, and the role of proximity effect in the observed properties. Studies on the AC loss properties of the material should also be done, since such properties are important to the application of the material in constructing power transmission lines or electrical machinery.

REFERENCES

1. J. E. C. Williams, Superconductivity and its Applications, Pion Limited, London, 1970.

2. R. B. Britton, Proceedings of the 1968 Summer Study on Superconducting Devices and Accelerators, Brookhaven National Laboratory Report BNL 50155 (C-55), 1968.

3. K. Tachikawa and Y. Tanaka, J. Appl. Phys. 44 (898), 1973.

4. K. Tachikawa and Y. Iwasa, Appl. Phys. Letters 16 (230), 1970.

5. K. Tachikawa and Y. Tanaka, Japan J. Appl. Phys. 6 (782), 1967.

6. K. Tachikawa, Y. Yoshida, and L. Rinderer, J. of Material Science 7 (1154), 1972.

7. K. Tachikawa, in Proceedings of the 1972 Applied Superconductivity Conference, IEEE, New York, 1972.

8. M. Suenaga and W. B. Sampson, in Proceedings of the 1972 Applied Superconductivity Conference, IEEE, New York, 1972.

9. C. C. Tsuei, Science 180 (57), 1973.

10. C. C. Tsuei, M. Suenaga, and W. B. Sampson, to be published.

11. C. C. Tsuei and L. R. Newkirk, J. of Materials Science 8, (1307), 1973.

12. H. F. Sterling and R. W. Warren, Metallurgia 67 (310), 1963.

13. B. D. Cullity, Elements of X-Ray Diffraction, Addison-Wesley, Reading, Mass., 1956.

14. ASTM X-Ray Powder Data File, ASTM, 1959 .

15. M. Hansen and K. Anderko, Constitution of Binary Alloys, McGraw-Hill, New York, 1958.

16. W. B. Pearson, Handbook of Lattice Spacings and Structures of Metals, Pergamon Press, New York. Vol. 1 (1957), and Vol. 2, (1967).

17. E. Nembach and T. Tachikawa, J. Less-Common Metals 19 (359), 1969.

18. B. W. Roberts, General Electric Research Laboratory Report No. 64-RL-3540 M, 1964.

19. A. K. Sinha , Progress in Materials Science 15 (81), 1972.

20. R. P. Elliot, Constitution of Binary Alloys, First Supplement, McGraw-Hill, New York, 1965.

21. F. A. Shunk, Constitution of Binary Alloys, Second Supplement, McGraw-Hill, New York, 1969.

22. P. G. de Genes, Superconductivity of Metals and Alloys, W. A. Benjamin, Inc., New York, 1966.

23. D. Saint-James, E. J. Thomas, and G. Sharma, Type II Superconductivity, Pergamon Press, London, 1969.

24. A. M. Campbell and J. T. Evetts, Advances in Physics 21 (199), 1972.

25. Y. B. Kim and M. J. Stephen, in Superconductivity, Vol. 2, ed. by R. D. Parks, Marcel Dekker, Inc., New York, 1969.

26. C. Kittel, Introduction to Solid State Physics, 3rd Edition, John Wiley and Sons, New York, 1966.

27. A. D. McInturff, in Proceedings of the 1968 Summer Study on Superconducting Devices and Accelerators, Brookhaven National Laboratory Report BNL 50155 (C-55), 1968.

28. M. N. Wilson and C. R. Walters, J. Phys. D : Appl. Phys. 3 (1547), 1970.

29. W. Kunz and E. Sour, in Proceedings of the IXth International Conference on Low Temperature Physics, edited by J. G. Dannt, D. O. Edwards, F. J. Milford and M. Yaqub, Plenum Press, New York, 1965.

30. G. Otto, E. Sour, and H. Wiggall, J. of Low Temperature Physics 1 (19), 1969.

31. L. D. Landau and E. M. Lifshitz, Electrodynamics of Continuous Media, Pergamon Press, New York, 1960.

32. G. Deutscher and P. G. de Genes, in Superconductivity, Vol. 2, edited by R. D. Parks, Marcel Dekker, Inc., New York, 1969.

33. B. T. Matthias, T. H. Geballe, and V. B. Compton, Rev. of Modern Physics 35 (1), 1963.

34. J. E. Crow and M. Suenaga, in Proceedings of the 1972 Applied Superconductivity Conference, IEEE, New York, 1972.

35. K. Hechler, G. Horn, G. Otto, and E. Sour, J. of Low Temperature Physics 1 (29), 1969.

36. W. E. Blumberg, J. Eisinger, V. Jaccarino, and B. T. Matthias, Phys. Rev. Letters 5 (149), 1960.

37. B. W. Roberts, NBS Technical Note 724, U. S. Department of Commerce Publication, 1972.

38. C. C. Koch, J. Phys. Chem. Solids 34 (1445), 1973.

39. Y. Tanaka, K. Tachikawa, and K. Sumiyama, J. Japan Inst. Metals 34 (835), 1970.

40. Y. Tanaka and K. Tachikawa, J. Japan Inst. Metals 34 (597), 1970.

41. W. A. Fietz, Rev. Scientific Instruments 36 (1621), 1970.

42. M. Tinkham, to be published.

43. J. D. Jackson, Classical Electrodynamics, John Wiley and Sons, New York, 1962.

44. Measurements made at Harvard University by M. Tinkham and A. Davidson.

45. P. G. de Genes and J. P. Hurault, Phys. Lett. 17 (181), 1965.

46. A. L. Fetter and P. C. Hohenberg, in Superconductivity, Vol. 2, ed. by R. D. Parks, Marcel Dekker, Inc., New York, 1969.

47. J. D. Livingston, in Proceedings of the 1968 Summer Study on Superconducting Devices and Accelerators, Brookhaven National Laboratory Report BNL 50155 (C-55), 1968.

48. H. R. Hart, Jr., in Proceedings of the 1968 Summer Study on Superconducting Devices and Accelerators, Brookhaven National Laboratory Report BNL 50155 (C-55), 1968.

49. C. P. Bean, Phys. Rev. Letters 8 (250), 1962.

50. C. P. Bean, Rev. Mod. Phys. 36 (31), 1964.

51. Y. B. Kim, C. F. Hempstead, and A. R. Strnod, Phys. Rev. Letters 9 (306), 1962.

52. P. W. Anderson and Y. B. Kim, Rev. Mod. Phys. 36 (39), 1964.

53. S. L. Wipf, Phys. Rev. 161 (404), 1967.

54. P. S. Swartz and C. P. Bean, J. Appl. Phys. 39 (4991), 1968.

55. A. El Bindari, J. Appl. Phys. 40 (2070), 1969.

56. A. El Bindari and R. E. Bernert, J. Appl. Phys. 39 (2529), 1968.

57. F. Lange, Cryogenics 6 (176), 1966.

58. P. A. Bottoms, Cryogenics 12 (356), 1972.

59. S. L. Wipf, in Proceedings of the 1968 Summer Study on Superconducting Devices and Accelerators, Brookhaven National Laboratory Report BNL 50155 (C-55), 1968.

60. J. P. Blenett, in Proceedings of the 1968 Summer Study on Superconducting Devices and Accelerators, Brookhaven National Laboratory Report BNL 50155 (C-55), 1968.

61. R. Hancox, Proc. IEE (London) 113 (1221), 1966.

62. G. H. Morgan, J. Appl. Phys. 41 (3673), 1970.

63. This notation of alloy composition is for convenience only, since the atomic per cent ratios of V to Si is 3 to 1 in most cases. It does not mean that all the V and Si exist in the alloys in the form of an A-15 V_3Si phase; such a case would be true if the V and Si present have reacted completely to form V_3Si.